SYNTHESIS, CHARACTERIZATION AND BIOLOGICAL ACTIVITIES OF PHOTOCORMS DERIVED FROM CYCLOPENTADIENYL IRON DIMER WITH ORGANOSULFUR AND ORGANOSELENIUM LIGANDS

GAN CHUN HAU

FACULTY OF SCIENCE
UNIVERSITI MALAYA
KUALA LUMPUR

2022

SYNTHESIS, CHARACTERIZATION AND BIOLOGICAL ACTIVITIES OF PHOTOCORMS DERIVED FROM CYCLOPENTADIENYL IRON DIMER WITH ORGANOSULFUR AND ORGANOSELENIUM LIGANDS

GAN CHUN HAU

DISSERTATION SUBMITTED IN FULFILMENT OF THE REQUIREMENTS FOR THE DEGREE OF MASTER OF SCIENCE

DEPARTMENT OF CHEMISTRY
FACULTY OF SCIENCE
UNIVERSITI MALAYA
KUALA LUMPUR

2022

UNIVERSITI MALAYA

ORIGINAL LITERARY WORK DECLARATION

Name of Candidate: **GAN CHUN HAU**

Matric No: **17021685/2 (NEW) / SMA180013 (OLD)**

Name of Degree: **MASTER OF SCIENCE**

Title of Dissertation:

SYNTHESIS, CHARACTERIZATION AND BIOLOGICAL ACTIVITIES OF PHOTOCORMS DERIVED FROM CYCLOPENTADIENYL IRON DIMER WITH ORGANOSULFUR AND ORGANOSELENIUM LIGANDS

Field of Study:

INORGANIC CHEMISTRY

I do solemnly and sincerely declare that:

(1) I am the sole author/writer of this Work;

(2) This Work is original;

(3) Any use of any work in which copyright exists was done by way of fair dealing and for permitted purposes and any excerpt or extract from, or reference to or reproduction of any copyright work has been disclosed expressly and sufficiently and the title of the Work and its authorship have been acknowledged in this Work;

(4) I do not have any actual knowledge nor do I ought reasonably to know that the making of this work constitutes an infringement of any copyright work;

(5) I hereby assign all and every rights in the copyright to this Work to the University of Malaya ("UM"), who henceforth shall be owner of the copyright in this Work and that any reproduction or use in any form or by any means whatsoever is prohibited without the written consent of UM having been first had and obtained;

(6) I am fully aware that if in the course of making this work I have infringed any copyright whether intentionally or otherwise, I may be subject to legal action or any other action as may be determined by UM.

Date:

Subscribed and solemnly declared before,

Witness's Signature Date: 1/8/2022

Name:

Designation:

SYNTHESIS, CHARACTERIZATION AND BIOLOGICAL ACTIVITIES OF PHOTOCORMS DERIVED FROM CYCLOPENTADIENYL IRON DIMER WITH ORGANOSULFUR AND ORGANOSELENIUM LIGANDS

ABSTRACT

Carbon monoxide releasing molecule (CORM) are well known for various biological activities but the efficacy and mode of activities are not fully understood. The objective of this research is to synthesize and evaluate the biological of diiron dimer photoCORMs. In this research, the conventional Schlenk techniques under an inert atmosphere of argon is used to synthesize and isolate the products. The reactions of $[CpFe(CO)_2]_2$ (**1**) with 2 moles equivalents of R_2E_2 (R= C_6H_{11}, C_4H_3S, $CH_2C_6H_5$; E= S, Se) have yielded dinuclear products of $[CpFe(CO)(\mu\text{-}L)]_2$ (L= $C_6H_{11}S$ (**2**), $C_4H_3S_2$ (**3**) and $CH_2C_6H_5Se$ (**4**)), respectively. An additional trinuclear compound, $C_{24}H_{22}O_2Se_2Fe_3$ (**5**) was isolated only from the reaction with dibenzyl diselenide. It was postulated that the formation of **2**, **3**, **4** and **5** proceeded via the radical pathway which involved the formation of $CpFe(CO)_2$ • radical and S-S bond or Se-Se bond cleavages of the ligands. All the products have been fully characterized by FT-IR, ^1H and ^{13}C NMR, CHN elemental analysis, GCMS and structurally elucidated by single crystal X-ray diffraction. Since **5** was a minor product, it was not involved in any further study. The stability of **2**-**4** both under dark and UV conditions were investigated by monitoring the changes in their respective UV-Vis spectra in phosphate buffered saline (PBS) solution. Their potential application as photoCORMs were also evaluated by standard myoglobin assay. **3** showed the shortest half-life and highest equivalent of CO-released. The anticancer studies of **2**-**4** were evaluated *in-vitro* on breast cancer cell lines (MCF-7, MDA-MB-231 and MDA-MB-468) and the cytotoxicity of **3** had increased approximately 4 times against MDA-MB-468 cell line upon UV irradiation, which was 11.5 ± 2.7 μM. All complexes exhibited cytotoxic

effect on specific sub-types of breast cancer cells. Antimalarial activities of **2**-**4** had also been studied and reported in this work. Unfortunately, these complexes did not display any significant effect on the *Plasmodium falciparum* 3D7 strains. The physicochemical, pharmacokinetics and drug like parameters of **2**-**4** were determined by using SwissADME tool.

Keywords: photoCORMs, cyclopentadienyliron dicarbonyl, anticancer, antimalarial

SINTESIS, CIRI-CIRI DAN AKTIVITI BIOLOGI FOTOCORMS YANG DIPEROLEH DARIPADA DIMER CYCLOPENTADIENYL IRON DENGAN ORGANOSULPHUR DAN ORGANOSELENIUM LIGANDS

ABSTRAK

Molekul pelepas karbon monoksida (CORM) terkenal dengan pelbagai aktiviti biologi tetapi keberkesanan dan cara aktiviti tidak difahami sepenuhnya. Objektif penyelidikan ini adalah untuk mensintesis dan menilai biologi fotoCORM diiron dimer. Dalam penyelidikan ini, teknik Schlenk konvensional di bawah suasana lengai argon digunakan untuk mensintesis dan mengasingkan produk. Tindak balas $[CpFe(CO)_2]_2$ (**1**) dengan 2 mol bersamaan R_2E_2 (R= $C6H_{11}$, C_4H_3S, $CH_2C_6H_5$; E= S, Se) telah menghasilkan produk dinuklear $[CpFe(CO)(\mu\text{-}L)]_2$ (L= $C_6H_{11}S$ (**2**), $C_4H_3S_2$ (**3**) dan $CH_2C_6H_5Se$ (**4**)), masing-masing. Sebatian trinuklear tambahan, $C_{24}H_{22}O_2Se_2Fe_3$ (**5**) telah diasingkan hanya daripada tindak balas dengan dibenzyl diselenide. Telah didalilkan bahawa pembentukan **2**, **3**, **4** dan **5** diteruskan melalui laluan radikal yang melibatkan pembentukan $CpFe(CO)_2\bullet$ ikatan radikal dan S-S atau belahan ikatan Se-Se ligan. Semua produk telah dicirikan sepenuhnya oleh by FT-IR, ^1H dan ^{13}C NMR, CHN, analisis unsur CHN, GCMS dan dijelaskan secara struktur oleh pembelauan sinar-X kristal tunggal. Memandangkan **5** adalah produk kecil, ia tidak terlibat dalam sebarang kajian lanjut. Kestabilan **2**-**4** kedua-duanya di bawah keadaan gelap dan UV telah disiasat dengan memantau perubahan dalam spektrum UV-Vis masing-masing dalam larutan garam terbuffer fosfat (PBS). Aplikasi berpotensi mereka sebagai photoCORM juga dinilai oleh ujian myoglobin standard. **3** menunjukkan separuh hayat terpendek dan setara tertinggi CO-dilepaskan. Kajian antikanser **2**-**4** telah dinilai secara in-vitro pada saluran sel kanser payudara (MCF-7, MDA-MB-231 dan MDA-MB-468) dan sitotoksisiti **3** telah meningkat kira-kira 4 kali ganda berbanding MDA-MB-468 garisan sel pada penyinaran UV, iaitu 11.5 ± 2.7 μM.

Semua kompleks mempamerkan kesan sitotoksik pada sub-jenis sel kanser payudara tertentu. Aktiviti antimalaria **2**-**4** juga telah dikaji dan dilaporkan dalam kerja ini. Malangnya, kompleks ini tidak menunjukkan sebarang kesan ketara pada strain Plasmodium falciparum 3D7. Parameter fizikokimia, farmakokinetik dan ubat seperti **2**-**4** ditentukan dengan menggunakan alat SwissADME.

Kata kunci: photoCORMs, cyclopentadienyliron dicarbonyl, antikanser, antimalaria

ACKOWLEDGEMENTS

First and foremost, I would like to express my sincere appreciation to my supervisor, Dr. Tan Kong Wai for his supervision and guidance throughout the course of this study, especially for the X-ray diffraction analyses. I would also like to thank my co-supervisors, Professor. Dr. Richard Wong Chee Seng and Dr. Ooi Mei Lee for their guidances and helpful suggestions, especially during the synthesis process and GCMS analyses.

Secondly, I would like to thank Dr. Jonathan Liew Wee Kent from Department of Parasitology, Faculty of Medicine for providing me useful guidance and advice in the antimalarial testing. Special thanks to Miss Norzalida Zakaria, Encik Fateh Bin Ngaliman and Ms. Nor Lela Md Ali for their technical supports (NMR and IR spectroscopy analyses).

I am also grateful to my senior Mr. Choong Zheng Lin and my colleague Mr. Lee Shiaw Xian for their encouragement and advice throughout my study. Fundamental Research Grant Scheme (FRGS) from the Malaysia Science and Technology Information Centre (MASTIC) is gratefully acknowledged.

Last but not least, I would like to dedicate this work to both my supportive parents and siblings.

TABLE OF CONTENTS

LIST OF FIGURES

LIST OF TABLES

LIST OF ABBREVIATIONS

e^-	Electron
σ	Sigma
π	Pi
δ	PPM
λ	Lambda (wavelength)
Cp	Cyclopentadienyl
h	Hour
i-C_3H_7	i-Propyl
t-C_4H_9	tert-Butyl
IR	Infrared spectroscopy
DNA	Deoxyribonucleic acid
ROS	Reactive oxygen species
CQ	Chloroquine
FQ	Ferroquine
CO	Carbon monoxide
PBS	Phosphate buffer saline
UV	Ultraviolet
TLC	Thin layer chromatography
THF	Tetrahydrofuran
DMSO	Dimethyl sulfoxide
EI	Electron ionization
DMEM	Dulbecco's Modified Eagle Medium
BMPM	blood media parasite mixture

LIST OF APPENDIX

CHAPTER 1: INTRODUCTION

Carbon monoxide (CO), an odourless and highly toxic gas with a stronger affinity to haemoglobin than oxygen (Blumenthal, 2001; Motterlini & Otterbein, 2010) about 210 times, is well-known as a "silent killer" that is responsible for many deaths each year. However, CO has been studied and explored in therapeutics in recent decades due to its cell-signalling character like nitric oxide (NO) (Verma, Hirsch, Glatt, Ronnett, & Snyder, 1993). In this context, organometallic carbonyl compounds that present with a metal centre have been proposed to serve as carbon monoxide releasing molecules (CORMs) on account of the special properties of metal centre that is rich in redox chemistry, alteration of the number of carbonyl ligand and diverse stereochemistry (Gasser & Metzler-Nolte, 2012).

Recently, CORMs have been discovered to be effective in the treatment of cancer (Carrington, Chakraborty, & Mascharak, 2013; Chakraborty, Carrington, Hauser, Oliver, & Mascharak, 2015; Loboda, Jozkowicz, & Dulak, 2015b) and malaria (Pena et al., 2012). Nevertheless, CORMs that exhibit a short half-life ($t_{1/2}$), which are relatively unstable can only release CO with a faster rate (García-Gallego & Bernardes, 2014; Johnson et al., 2007; Roberto et al., 2003). This makes the CO-delivery to become less efficiency. Therefore, to assure a more controllable way for better selectivity (Ling et al., 2018) in CO-delivery, the novel transition metal carbonyl complexes with a longer and stable half-life needed further investigation. In the recent report, it was reported that the UV-Vis light irradiation can be utilized to trigger the CO-releasing of metal carbonyl complexes. These kinds of photoactive metal carbonyl complexes were known as photoCORMs (Schatzschneider, 2010, 2011). In this regard, photoCORMs had displayed a controllable CO donor ability and better selectivity compare to the first generation solvent assisted of CORMs (Romão, Blättler, Seixas, & Bernardes, 2012).

Previous researchers have reported some iron carbonyl complexes in terms of their CO-releasing properties together with therapeutic application (Gao et al., 2018; Long, Jiang, Wang, Xiao, & Liu, 2013; Romanski et al., 2011). Iron that involved in a lot of biochemical reactions such as transportation of oxygen, electron transfer and substrate oxidation-reduction (Beard, 2001), has been chosen as a suitable metal centre in CORMs due to its rich redox chemistry characteristics. Besides, iron is also an essential nutrient in the proliferation of cancer cells (Franchini & Veneri, 2004; Kicic, Chua, & Baker, 2001; Weinberg, 1999). Iron chelators that demonstrated the potent anticancer abilities had sparked the chance to overcome the resistance to typical chemotherapy (Buss, Greene, Turner, Torti, & Torti, 2004; Kalinowski et al., 2007; Richardson, 2005). Simultaneously, iron complexes are good candidates as antimalarial agents. As a matter of fact, ferroquine that reported previously had shown a convincing impact on the CQ-resistant *P.falciparum* (Christophe, 2004).

Nevertheless, the CO releasing properties of cyclopentadienyl diiron carbonyl complexes are substantially unexplored. Besides, the previous literature that demonstrated the use of heavy atoms in ligands such as sulfur and selenium for CORMS designing is also very limited. In fact, sulfur and selenium atoms have been proven their ability to modify the CO dissociation and increase the intersystem crossing (ISC) between singlet and triplet excited states, and eventually increased the spin-orbital coupling (Salla et al., 2017).

This research reported the design of some novel cyclopentadienyl diiron carbonyl complexes that contained either sulfur or selenium atoms in their ligand framework, respectively. In this regard, **2**, **3** and **4** were synthesized by reacting the dicyclohexyl disulfide, 2-thienyl disulfide and dibenzyl diselenide with the cyclopentadienyliron dicarbonyl dimer, $[CpFe(CO)_2]_2$. These metal carbonyl complexes were characterized by various spectroscopy methods, elemental analysis, and single crystal X-ray diffraction

analysis. Their CO-releasing properties were studied under UV irradiation at 365 nm by standard approaches (Atkin et al., 2011). Their biological activities in anticancer and antimalarial are also reported in this study.

CHAPTER 2: LITERATURE REVIEW

2.1 Cyclopentadienyliron Dicarbonyl Dimer, $[CpFe(CO)_2]_2$

2.1.1 The History of Cyclopentadienyliron Dicarbonyl Dimer, $[CpFe(CO)_2]_2$

Cyclopentadienyliron dicarbonyl dimer, $[CpFe(CO)_2]_2$ was first appeared in Geoffrey Wilkinson's labs at Harvard in the early 1950s. It was first reported as an "almost black" compound with the molecular formula $C_5H_5Fe(CO)_5FeC_5H_5$ which was mischaracterized by Cotton and Wilkinson (Cotton & Wilkinson, 1954). In 1954, Cotton and Wilkinson published some transitional metals cyclopentadienyl-carbon monoxides compounds which included $(C_5H_5Fe)_2(CO)_4$. They only reported the preparation of cyclopentadienyliron dicarbonyl dimer, but with no further discussion thereof (Piper et al., 1955). Shortly afterward, a preliminary X-ray structure of $(C_5H_5Fe)_2(CO)_4$ was published by Hallam and Pauson from the University of Sheffield (Hallam, Mills, & Pauson, 1955). The distance between two iron atoms of 2.5 Å as observed from the single crystal X-ray diffraction analysis reinforce their illustration of the structure which is shown in Figure 2.1, together with the early good supporting reported IR data for both bridging and terminal COs (Piper et al., 1955). Few years later, Mills reported the full details crystal structure of $[CpFe(CO)_2]_2$. The relevant bond lengths and angles of $[CpFe(CO)_2]_2$ that reported by Mills are shown in Figure 2.2 (Mills, 1958). Cyclopentadienyliron dicarbonyl dimer, $[CpFe(CO)_2]_2$ was crystallized in monoclinic with space group $P2_1/c$. By considering the electron pairing of the Fe atoms in the Fe-Fe bond, $[CpFe(CO)_2]_2$ was deduced as a diamagnetic compounds. Three bonds that formed by each iron atoms to the carbon atoms of carbonyl groups are pointed to three corners of a distorted octahedron (Mills, 1958).

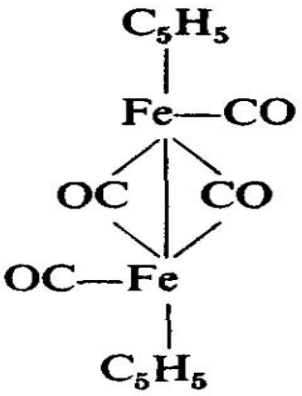

Figure 2.1: Representation of $[CpFe(CO)_2]_2$ structure in reference (Piper et al., 1955).

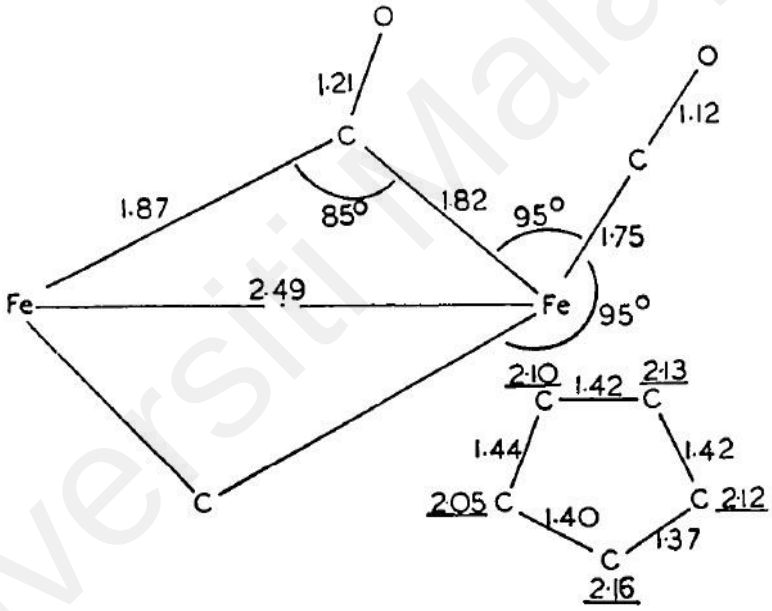

Figure 2.1: Bond Length and Bond Angles of $[CpFe(CO)_2]_2$ in reference (Mills, 1958).

Cyclopentadienyliron dicarbonyl dimer, $[CpFe(CO)_2]_2$ can be oxidized by air in the mineral acid solution to form the cyclopentadienyliron dicarbonyl halides, $CpFe(CO)_2X$ (X = Cl, Br or I) as hitherto reported (Piper et al., 1955). The red crystal, $CpFe(CO)_2Cl$, which decompose without melting above 87 °C had been successfully first extracted out and reported by Piper and Wilkinson in 1955. Few years later, the full details to synthesize

the black crystalline solid of cyclopentadienyliron dicarbonyl iodide, $CpFe(CO)_2I$, was published by King by treating the cyclopentadienyliron dicarbonyl dimer with iodide in chloroform (Eqn. 2.1) (King et al., 1963). Interestingly, cyclopentadienyliron dicarbonyl halides, $CpFe(CO)_2X$ can undergo reduction to form the cyclopentadienyliron dicarbonyl dimer by treating with phenyllithium or sodium phenylacetylide (Eqn. 2.2) (Hallam & Pauson, 1956). Nevertheless, dicyclopentadienyliron dicarbonyl is produced when cyclopentadienyliron dicarbonyl halides, $CpFe(CO)_2X$ is treated with cyclopentadienyllithium or cyclopentadienylsodium (Eqn. 2.3) (Hallam & Pauson, 1956). As a result, the oxidation of cyclopentadienyliron dicarbonyl dimer that lead to the formation of cyclopentadienyliron dicarbonyl halides had successfully gained a lot of interests of researchers to synthesize a variety of organoiron compounds in organometallic chemistry, together with their applications.

$$[CpFe(CO)_2]_2 + X_2 \longrightarrow 2\ CpFe(CO)_2X \qquad \text{... Eqn. (2.1)}$$

$$2\ CpFe(CO)_2X + PhLi \text{ or } Ph{\cdot}C{:}CNa \longrightarrow [CpFe(CO)_2]_2 \qquad \text{... Eqn. (2.2)}$$

$$CpFe(CO)_2X + CpNa \text{ or } CpLi \longrightarrow Cp_2Fe(CO)_2 \qquad \text{... Eqn. (2.3)}$$

2.1.2 Thermolysis of Cyclopentadienyliron Dicarbonyl Dimer, $[CpFe(CO)_2]_2$

It is important to study the thermolysis of cyclopentadienyliron dicarbonyl dimer, $[CpFe(CO)_2]_2$ so that the mechanism pathway of $[CpFe(CO)_2]_2$ with other ligands is predictable and foreseeable. The previous thermolysis study of $[CpFe(CO)_2]_2$ by Wilkie and Huettl in a sealed tube at 300 °C had led to the production of carbon monoxide, carbon

dioxide, cyclopentadiene, elemental carbon, elemental iron, ferrocene and biferrocene (Wilkie & Huettl, 1989). Besides, they also suggested a reaction scheme which can lead to the observed products from the thermolysis of $[CpFe(CO)_2]_2$ in a sealed tube at 300 °C concurrently (Scheme 2.1). They believed there were at least three distinct pathways for the thermolysis of the $[CpFe(CO)_2]_2$, these were (I) formation of the tetramer; (II) formation of ferrocene; and (III) formation of biferrocene. The first proposed step is the formation of $CpFe(CO)_2^{\bullet}$ radical (Step [1] in Scheme 1). $CpFe(CO)_2^{\bullet}$ radical then lost a carbon monoxide to form a $CpFe(CO)^{\bullet}$ radical. The $CpFe(CO)^{\bullet}$ radical might be able to tetramerize to form a tetramer or recombine with carbon monoxide to produce back the monomer radicals, $CpFe(CO)_2^{\bullet}$ radical. Besides, $CpFe(CO)_2^{\bullet}$ radical is also possible to lost the Cp ring to give a dicarbonyliron diradical (Step [2] in Scheme 2.1). The $CpFe^{\bullet}$ radical is produced when the $CpFe(CO)^{\bullet}$ radical lose a carbon monoxide under the severe condition. The interaction of two $CpFe^{\bullet}$ radicals give rise to the elemental iron and ferrocene (Step [3] in Scheme 2.1). The scheme (Scheme 2.1) that suggested by Wilkie and Huettl is also in agreement with the previous report (Hallam & Pauson, 1956). The ferrocenyl radicals will undergo dimerization to give the biferrocene (Step [5] in Scheme 2.1). The previous workers that produce the biferrocene suggested that the reaction is likely involved the coupling of two ferrocenyl radicals (Rausch, 1961), as proposed in Scheme 2.1.

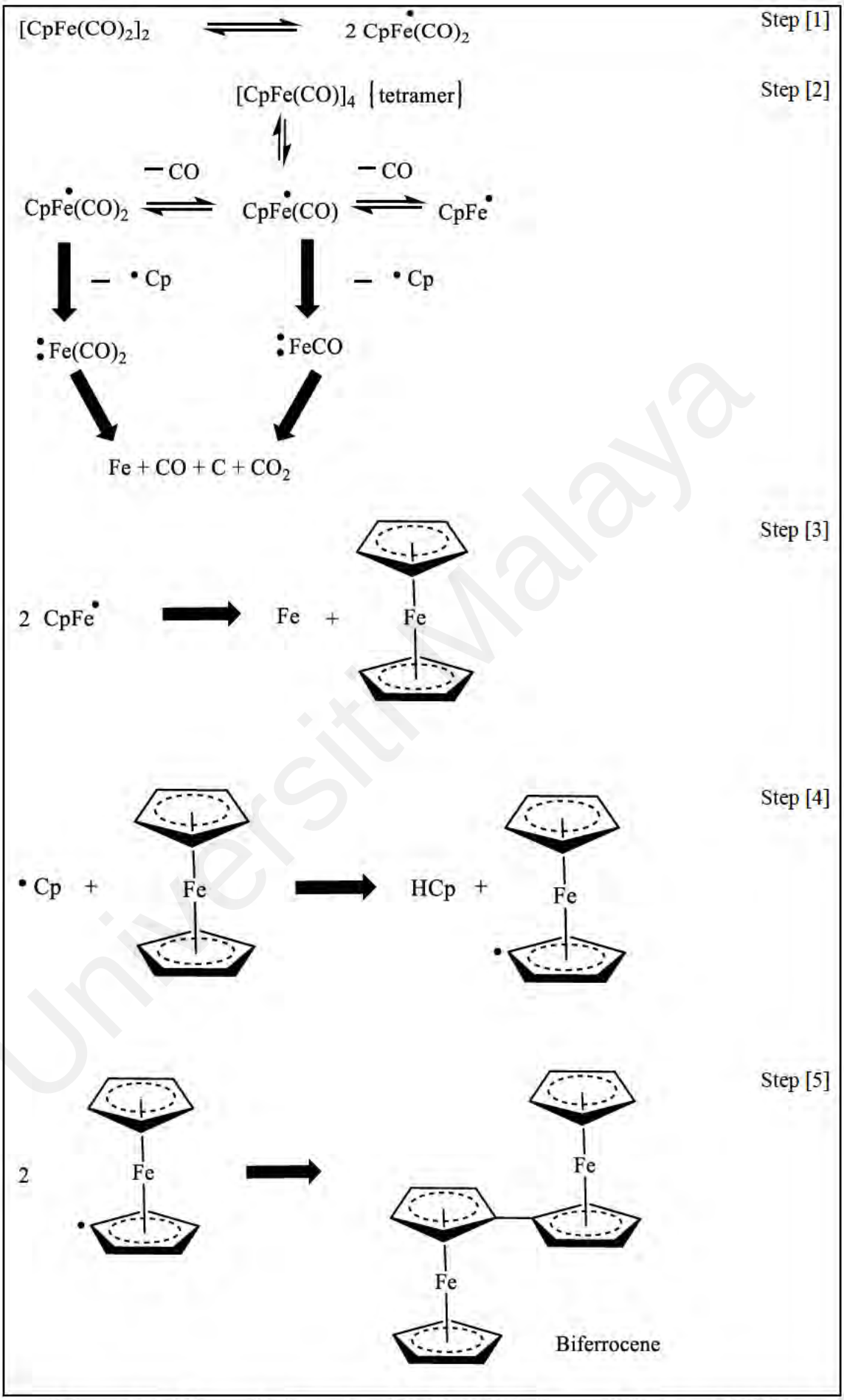

Scheme 2.1: Thermolysis study of $[CpFe(CO)_2]_2$ in a sealed tube at 300 °C.

2.2 Organochalcogenide Derivatives of Iron Complexes

2.2.1 Sulfur Derivatives of Cyclopentadienyliron Dicarbonyl Dimer

In 1961, R.B. King first reported the reaction between cyclopentadienyliron dicarbonyl dimer, $[CpFe(CO)_2]_2$ with dimethyl disulfide (Eqn. 2.4) by refluxing them in 2,2,4-trimethylpentane for 2.5 hours. He discovered that the iron-iron bond in the binuclear products was not paired up in order to achieve the diamagnetism (King, Treichel, & Stone, 1961), which indicated that no iron-iron bond was formed in the binuclear products.

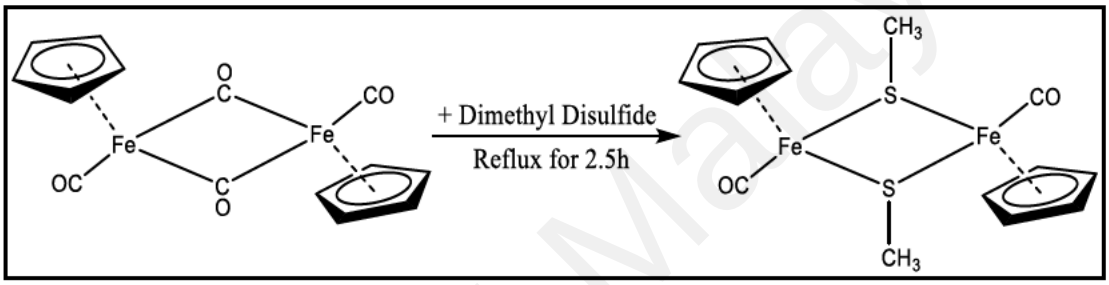

... Eqn. (2.4)

R.J. Haines then reported several reactions of cyclopentadienyliron dicarbonyl dimer with dialkyl disulfides (R= CH_3, C_2H_5, t-C_4H_9 and $CH_2C_6H_5$) in benzene under reflux condition. Besides the dinuclear compounds $[Fe(\pi\text{-}C_5H_5)(CO)SR]_2$, low yields of trinuclear compounds $[Fe_3(\pi\text{-}C_5H_5)_3(CO)_2(S)SR]$ was first observed from the reaction of cyclopentadienyliron dicarbonyl dimer with dialkyl disulfides (Haines, De Beer, & Greatrex, 1973). The structure of trinuclear compounds $[Fe_3(\pi\text{-}C_5H_5)_3(CO)_2(S)SR]$ have also been illustrated and proposed in the Figure 5. Later on, he further reported the reactions of cyclopentadienyliron dicarbonyl dimer with various types of dialkyl disulfides (R= CH_3, C_2H_5, i-C_3H_7, t-C_4H_9, $CH_2C_6H_5$ and C_6H_5) in more details (Eqn. 5) (Haines et al., 1975).

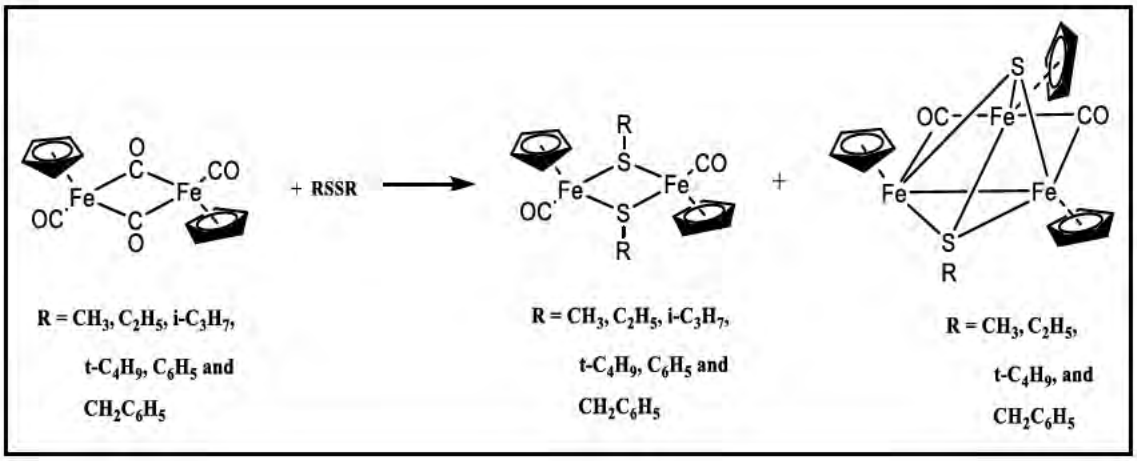

... Eqn. (2.5)

The five possible stereoisomers of the $[CpFe(CO)_2SR]_2$ was illustrated in Figure 2.3. The previous researchers had isolated two isomeric forms of $[CpFe(CO)_2SR]_2$ (R= CH_3, C_2H_5 or C_6H_5) (M. Ahmad, Bruce, & Knox, 1966). They found that one of these isomers was thermally stable with respect to the other. IR and NMR studies have been carried out to differentiate these isomers.

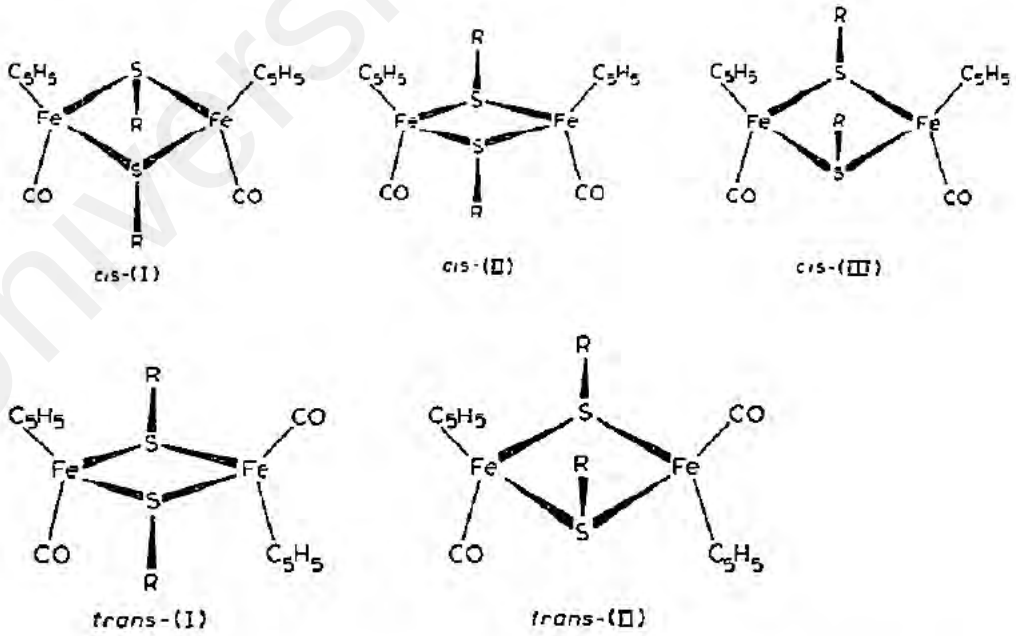

Figure 2.2: Five possible stereoisomers of $[CpFe(CO)_2SR]_2$ (Haines et al., 1975).

The IR spectrum showed the C-O stretching frequency of the thermally stable isomer is about 20-40 cm^{-1} higher than that for the thermally unstable isomer. In contrast, these isomers only showed single resonance for the cyclopentadienyl and methyl or phenyl group in NMR spectra (M. Ahmad et al., 1966). Two years later, the crystal structure of the more stable *cis*- isomer of $[CpFe(CO)_2S(C_6H_5)]_2$ as shown in Figure 2.4 had been published (Ferguson et al., 1968). The folding of the Fe-S was observed in this crystal structure.

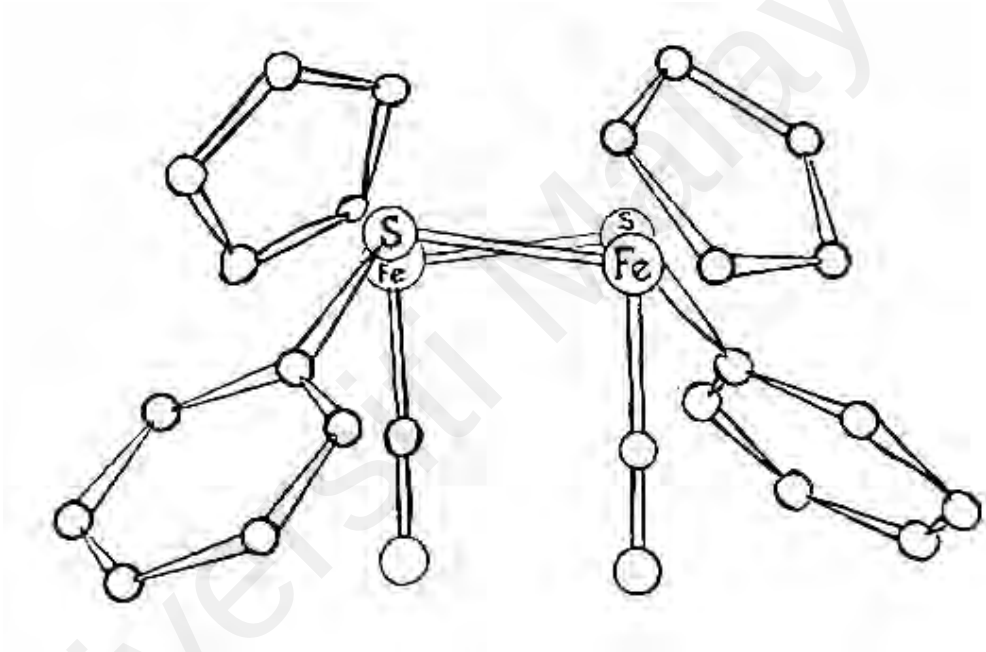

Figure 2.3: Molecular structure of $[CpFe(CO)_2S(C_6H_5)]_2$ (Ferguson et al., 1968).

Haines had successfully isolated two isomers, which is *cis*-(I) and *cis*-(III) isomers of $[CpFe(CO)_2SR]_2$ (R= CH_3, C_2H_5, i-C_3H_7) by refluxing the cyclopentadienyliron dicarbonyl dimer with the dialkyl disulfide ligands respectively in benzene, followed by chromatography. On the other hand, the yield of *cis*-(III) product obtained was very low. All attempts to obtain the *cis*-(III) isomers from the reaction of $[CpFe(CO)_2]_2$ with the dialkyl disulfide (R= t-C_4H_9 and $CH_2C_6H_5$) was unsuccessful. Only both the

$[CpFe(CO)_2S(t\text{-}C_4H_9)]_2$ and $[CpFe(CO)_2S(CH_2C_6H_5)]_2$ existed in *cis*-(I) isomerism (Haines et al., 1975).

Besides, Haines had also reported that the trinuclear products could not be separated and isolated from the reactions of cyclopentadienyliron dicarbonyl dimer with di-isopropyl and diphenyl disulfide (Eqn. 2.5). From their observations, there were no bands for the stretching of terminal carbonyl of trinuclear compounds in the I.R. spectrum, but the present of bridging carbonyl groups is espied. Moreover, there were two different chemical shifts recorded in the NMR spectrum which was corresponding to the cyclopentadienyl resonances with the relative intensity of 2/1. This result clearly revealed that one of the cyclopentadienyl groups was having the non-equivalent chemical environment from the other two (Haines et al., 1975).

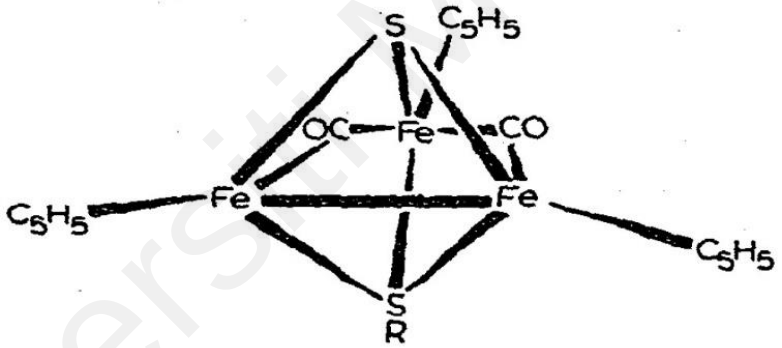

Figure 2.4: Representation of trinuclear compounds structure in reference (Haines et al., 1975).

2.2.2 Selenium and Tellurium Derivatives of Cyclopentadienyliron Dicarbonyl Dimer

E. D. Schermer and W. H. Baddley investigated the donor properties of chalcogenides towards the π- cyclopentadienyliron dicarbonyl in 1970. They had decided to use the diphenyl ligands with heavier and "softer" chalcogens of selenium and tellurium to react with cyclopentadienyliron dicarbonyl dimer, $[CpFe(CO)_2]_2$ in their study. Hence, they can compare the donor properties of these compounds with the softer sulfur derivatives

of cyclopentadienyliron dicarbonyl dimer (Schermer & Baddley, 1971). They successfully obtained 30% yield of $[\pi\text{-CpFe(CO)SePh}]_2$ and 60% yield of $[\pi\text{-CpFe(CO)TePh}]_2$ in their experiment (Eqn. 2.6). In addition, they also claimed that dinuclear selenium and tellurium compounds had a better stability than dinuclear sulfur species by observing the rate of decompositions of these compounds in unsealed sample bottles for three years. Qualitatively, they noticed that the rate of reaction of Ph_2E_2 with the cyclopentadienyliron dicarbonyl dimer was decreased in the order of E = S >Se >Te (Schermer & Baddley, 1971).

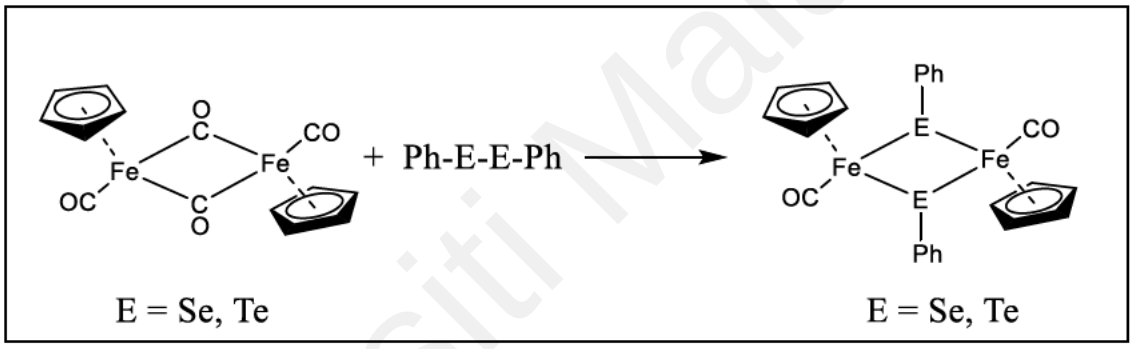

... Eqn. (2.6)

Two years later, Welcman and Rosenbuch had published two noble compounds of the type $[\pi\text{-CpFe(CO)Se(R)}]_2$ (R = C_2H_5 or $\eta\text{-}C_3H_7$) from the reaction between the cyclopentadienyliron dicarbonyl dimer with the particular dialkyl diselenide (Eqn. 2.7) (Rosenbuch & Welcman, 1972). They agreed with the previous researchers (Osborne & Stone, 1966) where the formation of binuclear carbonyl compounds involved two-step mechanism. The monomer of the iron carbonyl complexes was produced in the first stage. Next, the chalcogen atom with the lone pair of electrons acted as a Lewis base to replace the carbonyl group from another monomeric species to give the dimer (Osborne & Stone, 1966).

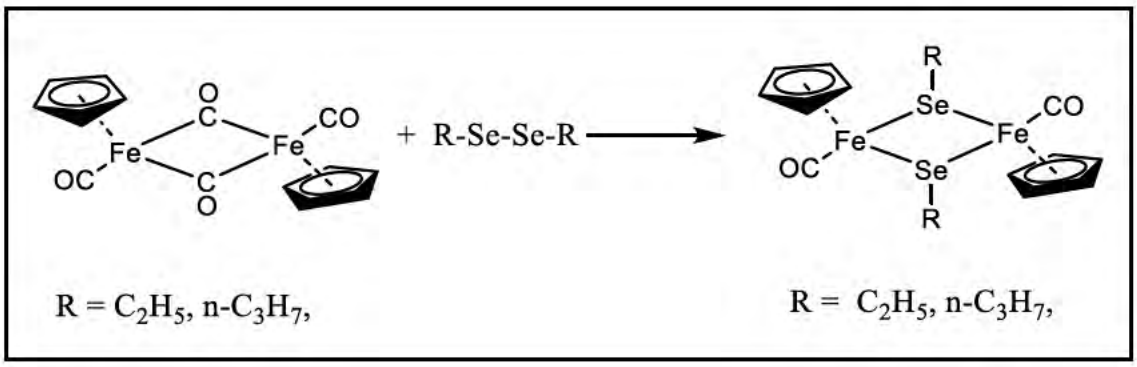

... Eqn. (2.7)

The dinuclear compounds can be synthesized also by treating the cyclopentadienyliron dicarbonyl iodide, $CpFe(CO)_2I$ with di(organyl)dichalcogenides, E_2R_2 (E = S, Se and Te). Recently, a group of researchers from India had reported the organochalcogenolato-bridged complexes, $[CpFe(CO)(\mu\text{-}L)]_2$, (L = SePh, $SeCH_2Ph$ and $S(2,6\text{-}(^tBu)_2\text{-}C_6H_2OH)$ and organotellurato-bridged complex, $[CpFe(CO)(\mu\text{-}TeC_4H_3O)]_2$ (Figure 6) from the reaction between cyclopentadienyliron dicarbonyl iodide, $CpFe(CO)_2I$ and ligands respectively with lithium borohydride (Geetharani, Bose, Basak, Suresh, & Ghosh, 2011). The possible sequences of the actions for the formation of dinuclear compounds is demonstrated in Scheme 2.2 (Geetharani et al., 2011).

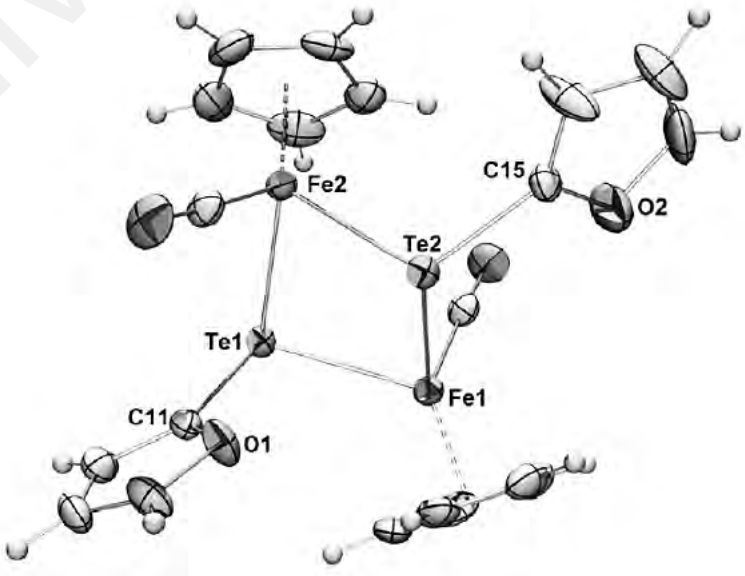

Figure 2.5: Molecular structure of $[CpFe(CO)(\mu\text{-}TeC_4H_3O)]_2$.

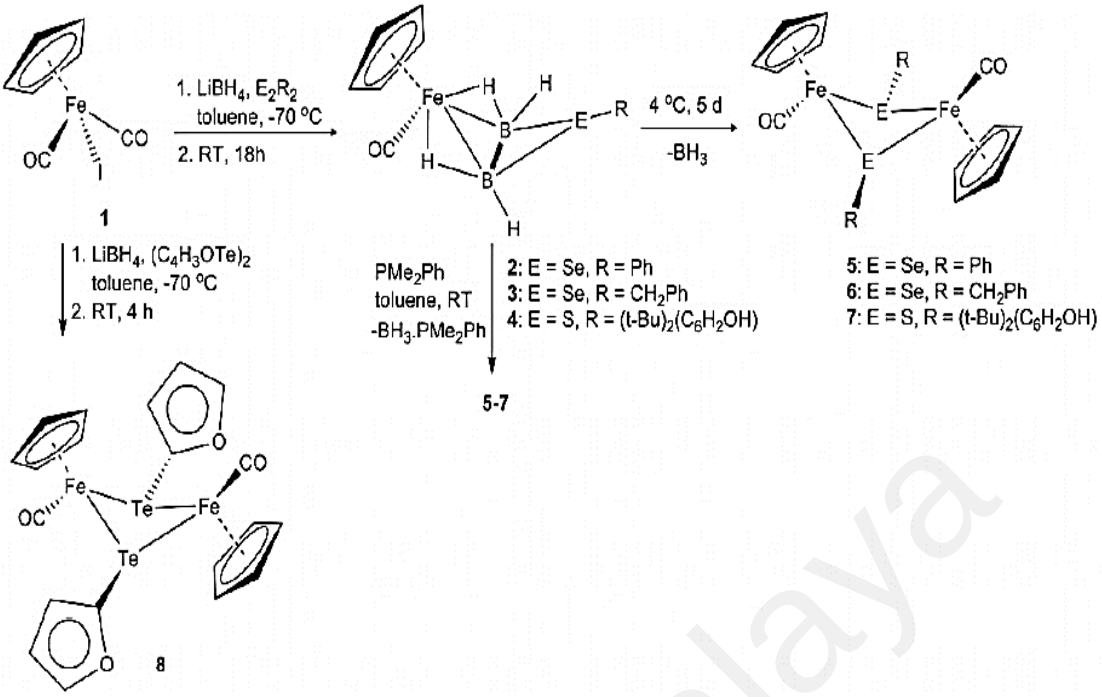

Scheme 2.2. Reaction pathways for the formation of $[CpFe(CO)(\mu\text{-}L)]_2$ from heteroferraboranes in reference (Geetharani et al., 2011).

2.3 Iron Complexes as Anticancer Agents

Cancer is a critical illness that concerns everyone all over the world. It had been consistently ranked by Americans as one of the most essential and major health problems since 20th century (Blendon et al., 2001). In 2020, it is estimated that 1.8 million new cancer cases will be diagnosed and 606,520 cancer deaths in the United States (Siegel, Miller, & Jemal, 2020). In Malaysia, cancer has also been recognized as the most common diseases that has result in high mortality rate. Based on the statistics from Global Cancer Observatory (GCO), 26395 cases of death in 2018 among all Malaysians were related to cancer. In 2003, when National Cancer Registry (NCR) was established in Malaysia, 3738 cases of breast cancer were reported. This clearly shows that 1 in 20 women in Malaysia will have the risk to suffer from the breast cancer in their lifetimes (Yip, Taib, & Mohamed, 2006).

Organometallic compounds have potential to be applied a useful platform for the development of potential anticancer drugs. Cisplatin is the most well-known metal complex that was used in chemotherapy to treat various types of cancers (Ott & Gust, 2007). The accidental discovery of cisplatin by Rosenberg and his co-workers (Barnett Rosenberg, Van Camp, & Krigas, 1965; B. Rosenberg, VanCamp, Trosko, & Mansour, 1969) had led to a remarkable enhancement in cancer chemotherapy. Cisplatin was used to treat the cancer through apoptosis. In general, Scheme 2.3 summarizes the pathways involved in cisplatin-induced cytotoxicity (Siddik, 2003). The effectiveness of cisplatin was determined by the efficiency ratio of cancerous and healthy cells.

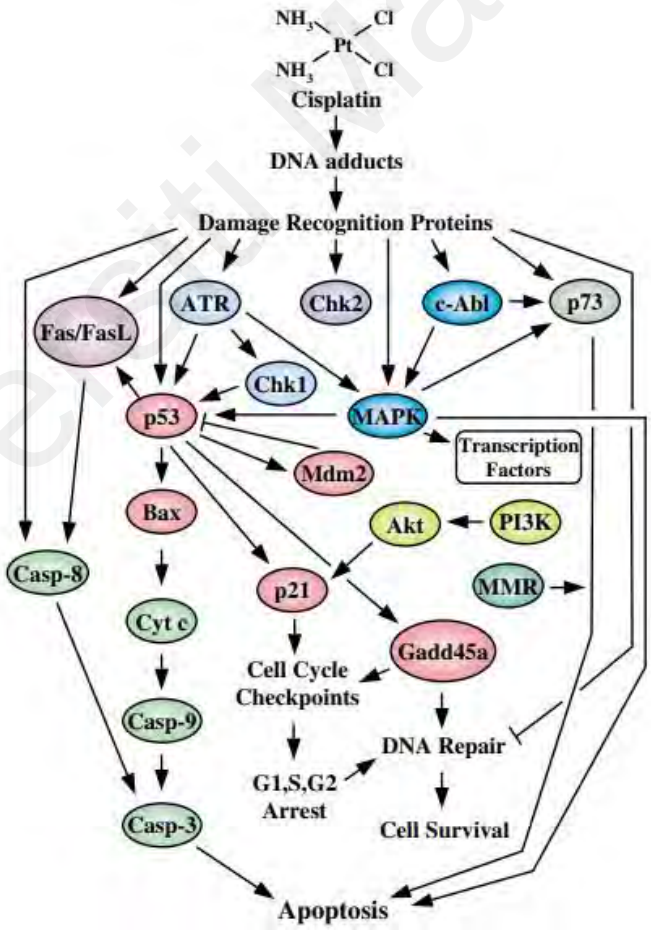

Scheme 2.3. An overview of the pathway that involved in cisplatin-induced cytotoxicity in reference (Siddik, 2003).

The other cisplatin analogues such as carboplatin, nedaplatin, lobaplatin and oxaliplatin (Figure 2.7) were then discovered and had been approved for the use of the present state of cancer chemotherapy. Nonetheless, the number of cancers that have been treated with cisplatin and its analogues had undesirable side effects. Unfortunately, common severe side effects of cisplatin and its analogues were kidney blood test abnormalities, ototoxicity, peripheral neuropathy, toxicity nausea and vomiting. The occurrence of drug-resistance cancer that further lowering the impact of these metallodrugs has made the situation worse for chemotherapy (Galanski, Jakupec, & Keppler, 2005; Ott & Gust, 2006). Consequently, there is a need to design of a more effective and safer non platinum-based metal complex to treat these types of cancers.

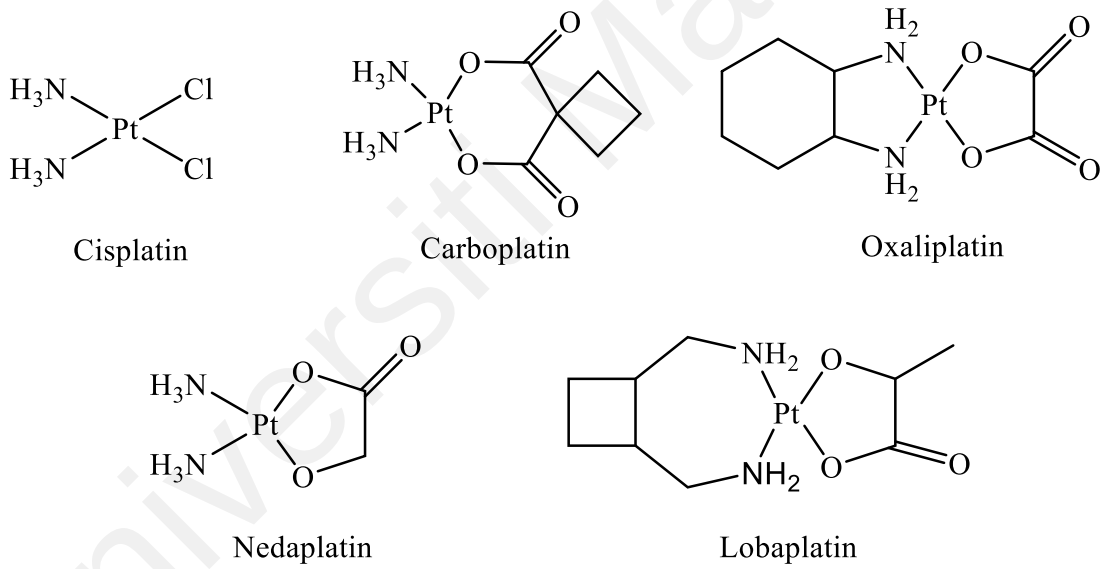

Figure 2.6: Types of platinum complexes that were used in cancer chemotherapy.

Iron is a transition metal that is well-known as an important element in the biological terms. The rich redox chemistry of iron allowed it to involve in a lot of biochemical reactions. For example, the myoglobin and haemoglobin that consist of one and four repeating unit of the iron heme group, respectively, allow the oxygen molecule coordinated to the iron metal centre. The myoglobin is used to store oxygen while

haemoglobin is used to transport oxygen in the respiratory system of mammals. Additionally, iron is also a vital nutrient in the proliferation of cancer cells (Franchini & Veneri, 2004; Kicic et al., 2001; Weinberg, 1999). Bleomycin that isolated from the *Streptomyces verticillus* (Umezawa, Maeda, Takeuchi, & Okami, 1966) is a water soluble and iron chelating glycopeptidic antibiotic that had been used in the anticancer chemotherapy up to the present (Lin, Kwock, Hefter, & Misslbeck, 1983; Mir, Tounekti, & Orlowski, 1996). Oxidative DNA damage and consequent death of cancer cells occurred due to the bleomycin in the presence of H_2O_2 and O_2 (Burger, 1998; Claussen & Long, 1999; Hoehn, Junker, Bunt, Turner, & Stubbe, 2001; Stubbe & Kozarich, 1987; Stubbe, Kozarich, Wu, & Vanderwall, 1996). Moreover, the potential of anticancer abilities that was shown by iron chelators had sparked the chance to solve the resistance to typical chemotherapy (Buss et al., 2004; Kalinowski et al., 2007; Richardson, 2005). Consequently, reactivity of iron with a wide range of ligands has gained the attentions of researchers to confront with cancer cells constructively without any severe damages to the normal body cells and tissues.

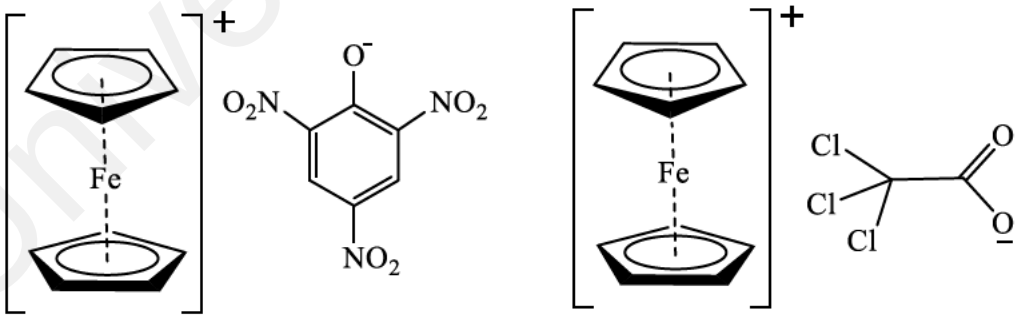

Ferrocenium picrate Ferrocenium trichloroacetate

Figure 2.7: Structures of ferrocenium picrate and ferrocenium trichloroacetate salts.

Previous researches had also shown that the iron carbonyl diene nucleoside complex can exhibits powerful apoptosis-inducing properties in cancer cells (Franke et al., 2010;

Schlawe et al., 2004). Besides, iron dithiocarbamate carbonyl complex that acted as a CO-releasing molecule (CORM) had been proven to exhibit antitumor properties (Hewison et al., 2012). There were quite a number of "FeCp" analogues (Florindo et al., 2015; Kopf-Maier, Kopf, & Neuse, 1984; Valente et al., 2014) and monoiron carbonyl derivatives (Hewison et al., 2012; Pilon et al., 2017) that had been employed in the study of anticancer property. However, investigation of anticancer property of diiron complexes was relatively unexplored. The study on cyclopentadienyliron dicarbonyl dimer, $[CpFe(CO)_2]_2$ had displayed cytotoxicity towards breast cancer cells (MDA-MB-231) and HeLa cervical cancer cells, but it was non-cytotoxic towards the normal cell lines (MCF-10A, TAMH, HL-1) (Poh, Ho, & Fan, 2016). The deduction of $[CpFe(CO)_2]_2$ as the Fenton-type catalysts was proposed which might have caused the disorder in ROS-mediated cell cycles, the later causing the death of premature cancer cell (Poh et al., 2016; Trachootham, Alexandre, & Huang, 2009).

The latest discovery of a series of $[CpFe(CO)_2]_2$ complexes with a bridging vinyliminium ligand by Dalila Rocco and co-workers (Scheme 2.4) has shown favourable properties in anticancer properties due to their well stability and solubility in aqueous medium (Rocco et al., 2019). Remarkably, these compounds remained water soluble although the IC_{50} values decreased due to the increasing of lipophilicity in general trend. Multiple effects included DNA binding and generation of reactive oxygen species (ROS) that could contribute to the cytotoxicity of the metal complexes was suggested according to their investigations. The diiron complexes that fragmentized into the monoiron species possibly could increase the production of ROS and DNA bindings (Rocco et al., 2019).

Sulfur and selenium containing compounds often displayed the biological activities with therapeutic properties (Gandin & Fernandes, 2018; Pathania, Narang, & Rawal, 2019). The anticancer behaviour that was shown by the organo-selenium complexes recently had triggered the interests of many researchers, either using them solely in the

cancer treatment or combined together with other drugs (Fernandes & Gandin, 2015; Gandin, Khalkar, Braude, & Fernandes, 2018; Spengler, Gajdács, Marć, Domínguez-Álvarez, & Sanmartín, 2019; Tan, Mo, Lau, & Xu, 2018). Moreover, being crucial to the fundamental redox process in living organisms, when incorporated within the structure of a drug, disulfide and diselenide have shown their potential behaviour in cancer treatment by inducing apoptotic and differentiation, together with antiproliferative effect on cancer cells (Álvarez-Pérez, Ali, Marć, Handzlik, & Domínguez-Álvarez, 2018; Yi & Su, 2013). Recent research that shown the anticancer and antiproliferative activity by diiron complexes with sulfur and selenium functionalized vinyliminium ligands have encouraged the further investigation and exploration in this area (Agonigi et al., 2020).

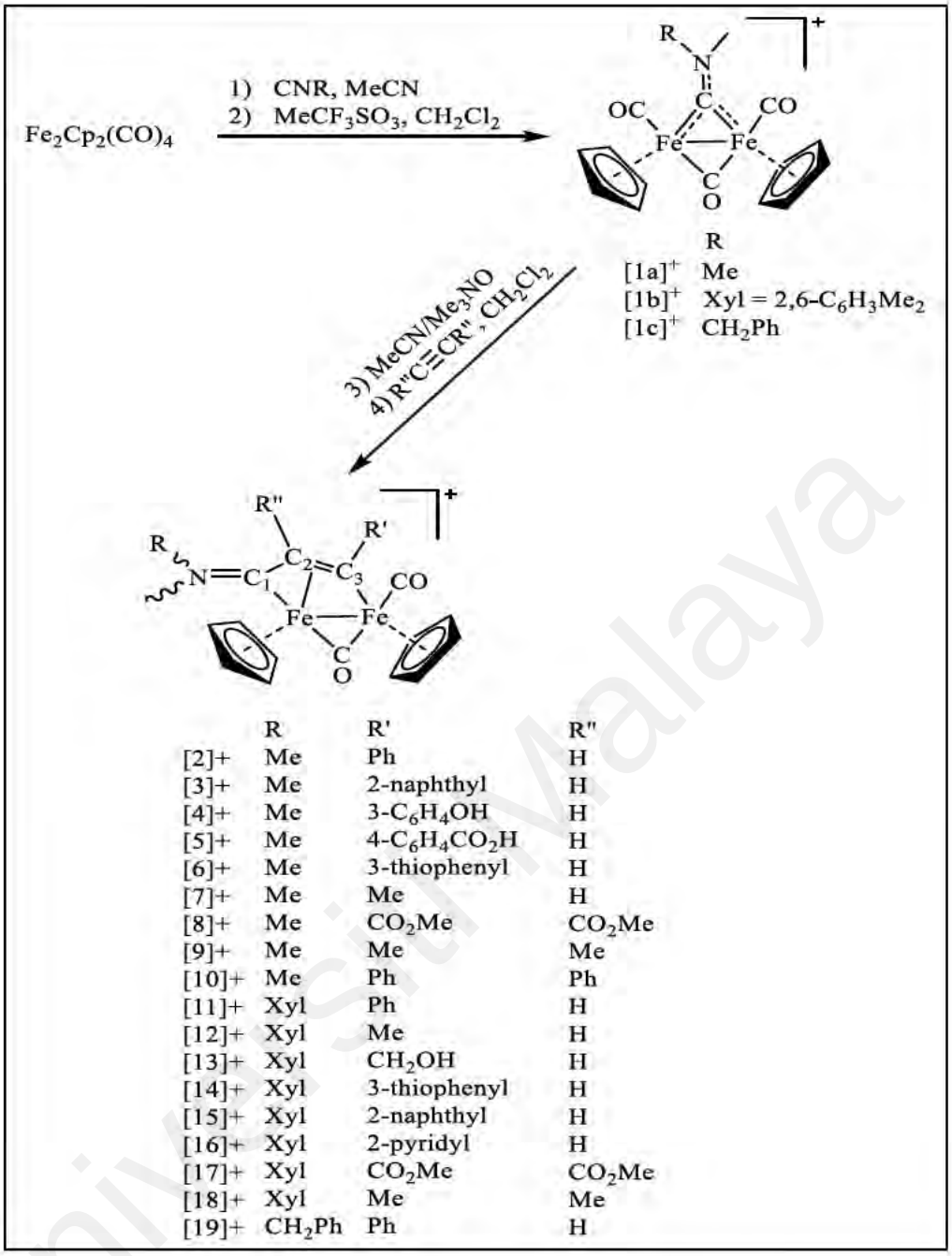

	R	R'	R"
[1a]$^+$	Me		
[1b]$^+$	Xyl = 2,6-$C_6H_3Me_2$		
[1c]$^+$	CH_2Ph		
[2]+	Me	Ph	H
[3]+	Me	2-naphthyl	H
[4]+	Me	3-C_6H_4OH	H
[5]+	Me	4-$C_6H_4CO_2H$	H
[6]+	Me	3-thiophenyl	H
[7]+	Me	Me	H
[8]+	Me	CO_2Me	CO_2Me
[9]+	Me	Me	Me
[10]+	Me	Ph	Ph
[11]+	Xyl	Ph	H
[12]+	Xyl	Me	H
[13]+	Xyl	CH_2OH	H
[14]+	Xyl	3-thiophenyl	H
[15]+	Xyl	2-naphthyl	H
[16]+	Xyl	2-pyridyl	H
[17]+	Xyl	CO_2Me	CO_2Me
[18]+	Xyl	Me	Me
[19]+	CH_2Ph	Ph	H

Scheme 2.4. Synthesis of diiron μ-vinyliminium complexes.

2.4 Relationship Between Anticancer Drugs and Antimalarial Agents

Malaria is a disease caused by *Plasmodium* parasite that spread through the bites of Anopheles mosquito vector to the people even in the 21st century. It has been reported to infected human populations for over 50,000 years (Urban, Ing, & Stevenson, 2005). The existence of *Plasmodium* was first discovered in a fossilized Culex mosquito that aged almost 30 million years old in a piece of amber (Poinar, 2005). In general, there are only 4 species of Plasmodium that frequently cause malaria in humans, which are *P.falciparum, P.malariae, P.ovale* and *P.vivax*. These four species contribute about 95% of the malaria infections globally (Vangapandu et al., 2007). *P.faciparum* is the most common and virulent that caused malaria in human. Besides, it also caused the highest mortality rate for human malaria. A fifth species that infected humans in Southeast Asia was discovered recently and had been named as *P.knowlesi*, which was found from the parasite of Old World monkeys (Yap et al., 2017). The normal symptoms of malaria disease are fever, fatigue, headaches and vomiting. In severe cases, it may cause coma, seizures, yellow skins and even death (Caraballo & King, 2014).

Quinine, which was extracted from the bark of Cinchona tree, was the first medicine to treat malaria. It was first introduced to treat malaria in Rome in 1630s. Quinine is very effective against the erythrocytic form of *Plasmodium* and this allowed it to destroy the schizogonic stages in malaria. However, it is not able to cause the malarial parasites to disappear in the other cell and its impact on the exoerythrocytic stages of gametocytes is very low (Kalotka-Kręglewska, 2011). The history of development of antimalarial drugs was then followed by the discovery of Atabrine dihydrochloride (quinacrine hydrochloride) in 1936 in Germany (Schadewaldt, 1975). Like quinine, although Atabrine was less effective against exoerythrocytic stages, it was highly active against the erythrocytic stages of all the *Plasmodium* species. The side effects such as abdominal cramps, anorexia, diarrheal, dizziness and headache, in contrast was inevitable by the

usage of Atabrine in the treatment of malaria (Wallace, 1989). The treatment of malaria was then followed by the utilization of amodiaquine, chloroquine and primaquine since World War II.

The discovery of chloroquine (CQ) (Figure 2.9) in 1934 had had shown its effectiveness against malarial parasite during its intra-erythrocytic stage (Slater & Cerami, 1992). The conversion of inert haemazoin crystals are prohibited when the binding occurs between CQ and the toxic haem metabolites that lowered down the effectiveness of the parasite to digest the haemoglobin (Sullivan, Gluzman, Russell, & Goldberg, 1996). However, the challenge of the drug resistance of CQ since the last two decades against *P.falciparum* had led to the artemisinin combination therapy (ACT) (Beeson, Boeuf, & Fowkes, 2015), and this treatment later on had become a famous treatment even until today, to treat the malaria (Eastman & Fidock, 2009). Artemisinin was rediscovered by Youyou Tu (Neill, 2011), the Nobel laureate from China from Chinese wormwood (*Artemisia annua*) or *Qing Hao* that has been used to cure the fevers and a wide range of diseases for more than 2,000 years ago. Nevertheless, the onset of artemisinin resistance towards the *P.falciparum* in Cambodia had alarmed researchers to source out new agents against malaria (Noedl et al., 2008).

The breakthrough was followed by the idea to combine the CQ together with ferrocene. Ferroquine [FQ, (SSR97193)] (Figure 2.9) that was designed by Biot and his co-workers in 1994 had displayed a remarkably impact on the CQ-resistant *P.falciparum* (Christophe, 2004) in mice (Pierrot et al., 2005). This interesting antimalarial properties of ferroquine (FQ) had significantly become the source of inspiration for the derivatives and analogues of FQ with promising antimalarial properties. Other metals such as gold, platinum rhodium and ruthenium had also been studied and developed for antimalarial purpose (Biot, Castro, Botte, & Navarro, 2012).

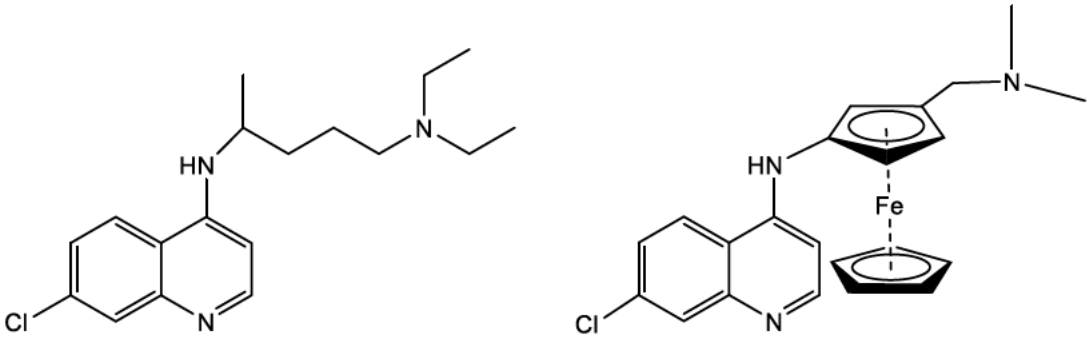

Figure 2.8: Structure of Chloroquine (CQ) and Ferroquine (FQ).

However, the activities of metal carbonyl complexes on antimalarial are substantially unexplored. Biot and his co-workers had continued their research to develop the antimalarial metal carbonyl compounds after they discovered the FQ. They had studied the antimalarial properties of some rhenium carbonyl complexes (Figure 2.10), but the outcomes were less active than FQ (Arancibia et al., 2010). This further encourage researchers worldwide to carry out more study on the antimalarial properties of metal carbonyl complexes. Recently, a chromium arene chloroquine derivative that contained the carbonyl groups had displayed a better antimalarial activity than CQ. This chromium compound, named as [η^6-N-(7-chloroquinolin-4-yl)-N′-(2-dimethylamino-methylbenzenyl)-ethane-1,2-diamine]tricarbonylchromium (Figure 2.11) had shown amazing results where it is not only active against CQ-sensitive strains, but also active against CQ-resistant strains of *P.falciparum* in *in vitro* study (Glans et al., 2011). Despite of many antimalarial activity studies of mononuclear carbonyl complexes had been reported, the studies of bimetallic carbonyl compounds have not yet been reported so far.

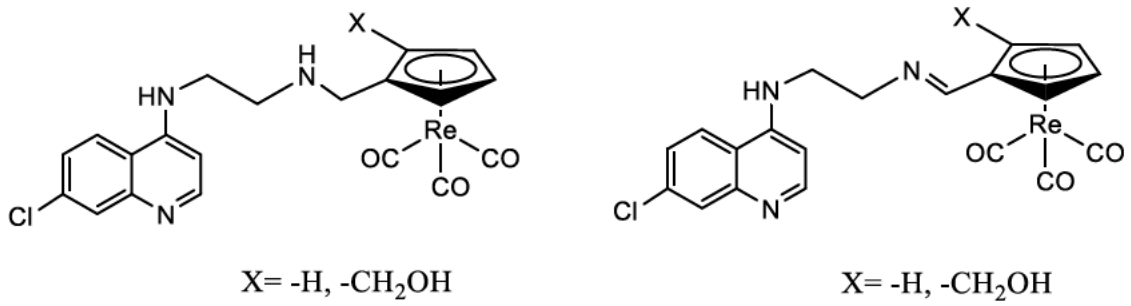

Figure 2.9: Structures of cyclopentadienyltricarbonylrhenium analogues.

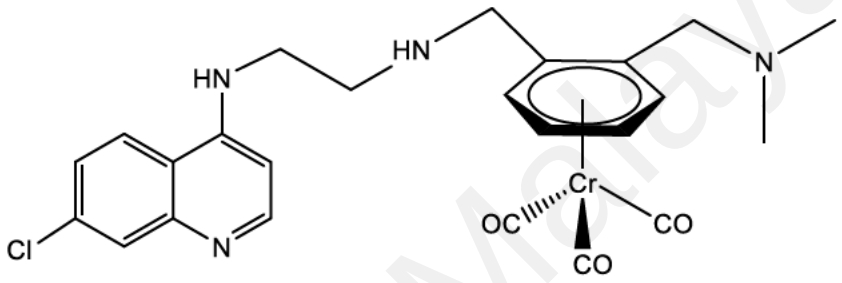

Figure 2.10: Structure of [η^6-N-(7-chloroquinolin-4-yl)-N′-(2-dimethylamino methylbenzenyl)-ethane-1,2-diamine]tricarbonylchromium.

The cytotoxicity of artemisinin was first tested against Ehrlich ascites tumor (EAT) cells, together with other artemisinin derivatives in 1993 (Woerdenbag et al., 1993). The ether dimer of dihydroartemisinin (Figure 2.12) was tested as a potentially anticancer agent compared to artemisinin and other artemisinin derivatives (Woerdenbag et al., 1993). Although artemisinin and its derivatives are designed for antimalarial purpose, this study had become the first approach to repurpose antimalarial drugs for anticancer purpose. Later, some of the researches had reinvestigated the relationship between the present anticancer drugs and antimalarial drugs (Amewu et al., 2013; Crespo-Ortiz & Wei, 2012; Nzila et al., 2010; Posner et al., 2004; Verbaanderd et al., 2017). Repurposing the existing antimalarial and anticancer drugs in both treatments is a very attractive strategy

because this could help to save a lot of time and efforts. The only challenge in this issue is it takes time to study the dosage for anticancer or antimalarial purpose, which can be done easily.

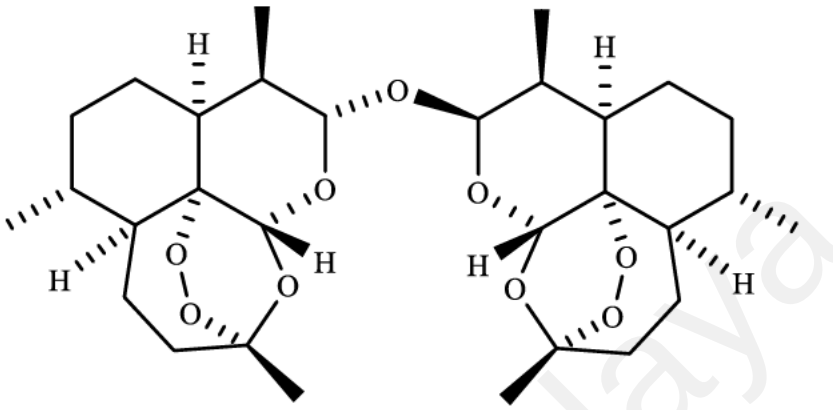

Figure 2.11: Structure of ether dimer of dihydroartemisinin.

2.5 Carbon Monoxide Releasing Molecules (CORMs)

Carbon monoxide (CO) is a colourless, odourless and highly toxic gas that is generally produced by the incomplete combustion of hydrocarbon compounds. It is well-known as a "silent killer" that responsible for many deaths each year. CO has a stronger affinity to haemoglobin than oxygen, which is roughly 220 times greater than the affinity between oxygen and haemoglobin (Motterlini & Otterbein, 2010). This characteristic causes CO to bind very strongly to haemoglobin, which leads to the formation of carboxyhaemoglobin (COHb). However, the discovery of CO as a cell-signalling molecule like nitric oxide (NO) in 1990s (Verma et al., 1993) had successfully gained the interests of scientists to explore more on the role of CO in therapeutic and medicinal area. After that, the idea of carbon monoxide releasing by metal carbonyl complexes had been proposed as a promising strategy to deliver the CO in cellular tissues, known as carbon monoxide releasing molecules (CORMs).

After studied the first generated CORMs, which is CORM-1 and CORM-2 (Figure 2.13), Motterlini et al. first suggested the application of CORMs in pharmaceutical field (Motterlini et al., 2002). These molecules had displayed a more safety and efficiency way to deliver the CO. There are many potential compounds that can be used as CORMs, such as aldehydes, silacarboxylates, unsaturated cyclic α-diketones (Bohlender et al., 2012) and organometallic compounds (Gasser & Metzler-Nolte, 2012). The special physico-chemical properties of organometallic compounds, for example metal carbonyl complexes that exhibit a transition metal centre had attained increasing popularity in medicinal chemistry to serve as anticancer, antimalarial and antimicrobial agents due to their specific advantages: structural variety and diverse stereochemistry, metal centre that rich in redox chemistry and alteration of the number of carbonyl ligand (Gasser & Metzler-Nolte, 2012).

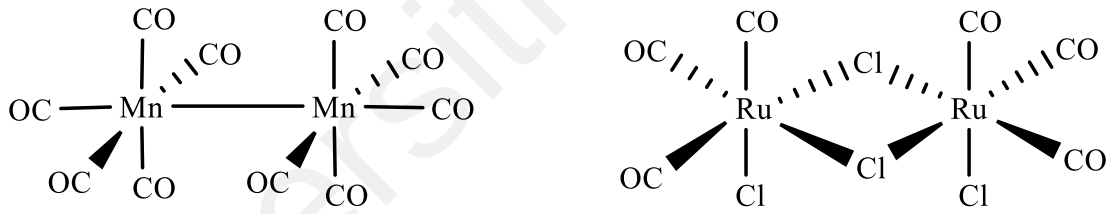

CORM-1 CORM-2

Figure 2.12: Structures of CORM-1 and CORM-2.

2.5.1 Carbonyl Chemistry

Carbonyl group, CO is a common ligand in organometallic transition metal chemistry. It is easily coordinated to the metal to form the metal carbonyl complexes with the general formula $L_xM(CO)_y$, where M is the transition metal with different oxidation states, L_x is the other coordinated ligands and $y \geq 1$. Metal carbonyl complexes are the famous classes studied compounds because of the special bonding mode of CO ligands.

There are two main bonding involved in the M-CO bonding: σ bond and π-backbonding. The lone pair of the carbon donate electrons into an empty *d*-orbital on the metal and formed the σ bond, thus caused the electron density on the metal increases. The filled metal *d*-orbital then backdonate the electrons to an empty π* orbital on carbonyl ligand, known as π-backbonding. The energy level diagram of CO (Figure 2.14) is needed to explain the bonding between the transition metal and carbonyl ligand. The molecular orbital (MO) of CO is formed from the combination of atomic orbital (AO) of carbon and oxygen.

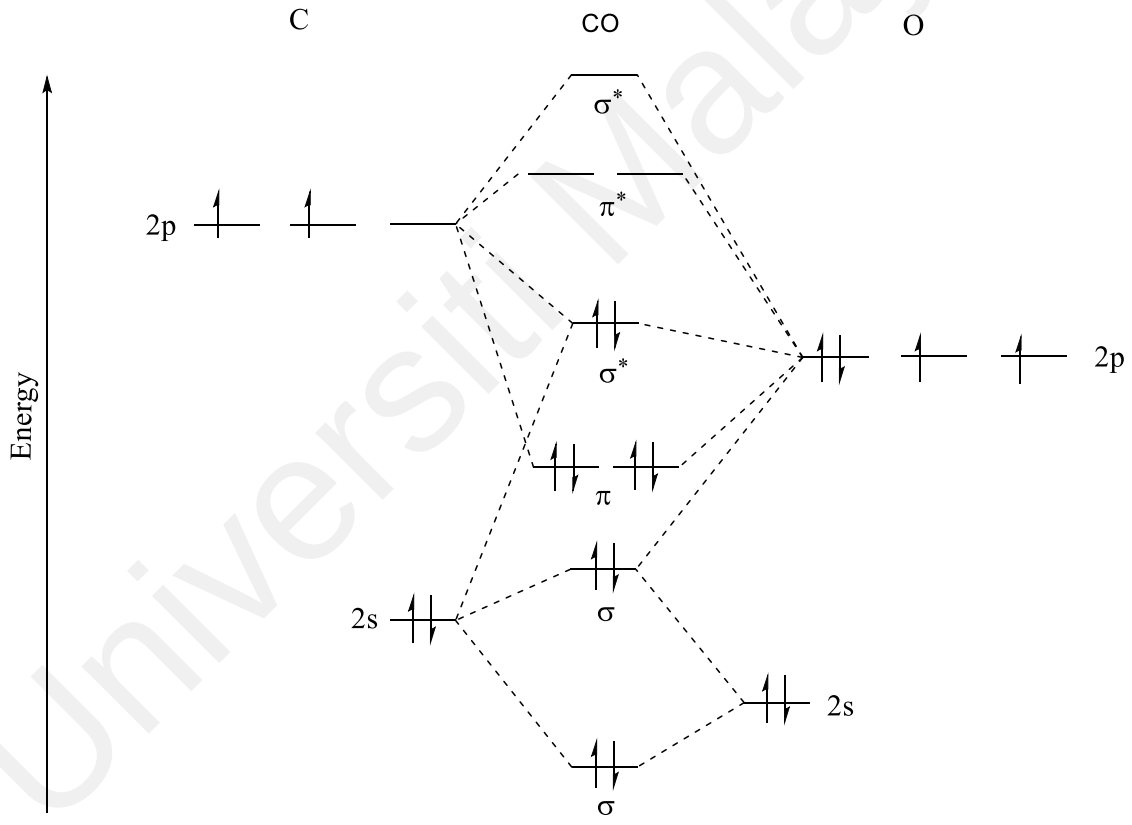

Figure 2.13: The energy level diagram of CO which made up from the molecular orbital (MO) of CO and atomic orbital (AO) of carbon and oxygen.

In general, carbonyl ligand is a good σ-donor and good π-accepter ligand (Figure 2.15). The empty *d*-orbital of metal is filled by the electrons from carbon monoxide (HOMO-

σ*). This increased the electron density on the metal and in order to balance back the electron density, the electron-rich metal *d*-orbital will back donate the electrons into the vacant LUMO- π* orbital on the carbonyl ligand. Consequently, the carbon-oxygen bond will be weaken compared with a free carbon monoxide, while the metal-carbon bond will be strengthened. The weaker the C-O bond, the stronger the M-CO bond or vice versa. In short, the length and strength of the C-O and M-CO bonds is dependent on the π-backbonding into the antibonding CO (π*) orbital.

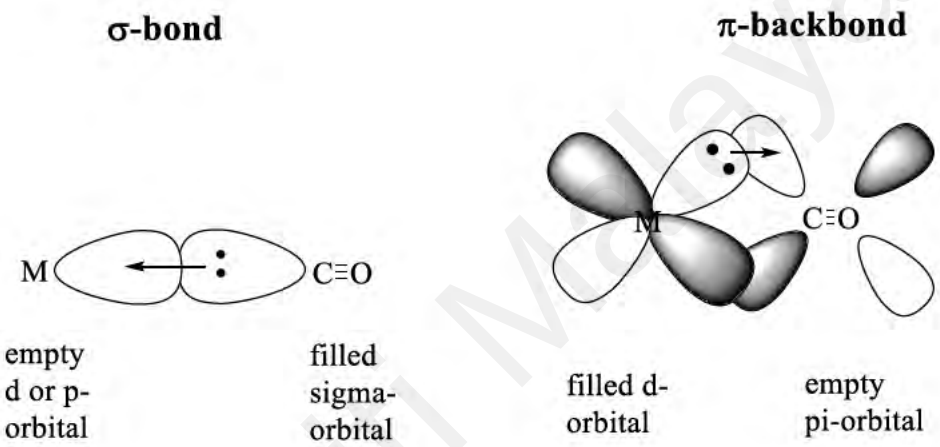

Figure 2.14: Bonding of metal carbonyl: σ-bond and π-backbond.

2.5.2 CORMs and Breast Cancer Therapy

CO and CORMs could have the ability to fight against cancer. Nonetheless, their application in cancer therapy is a still contentious subject (Loboda et al., 2015b; Romão & Vieira, 2014). The CO's molecular targets and basic signalling mechanisms are unknown, which often leads to conflicting results (S. Ahmad et al., 2015; Chatterjee, 2007; Volti et al., 2005). The most likely possibility is that CO could stimulate opposing consequences in different biological processes. The ability and effect of CORMs on apoptosis, proliferation, and the main pathway involved in cancer initiation and progression have been investigated. However, until now, the inference has been that the

effect of CORMs on these studies is variable and appears to be cell-type specific (Loboda, Jozkowicz, & Dulak, 2015a; Loboda et al., 2015b). Moreover, many CORMs could release CO faster in physiological buffer and have a brief half-life ($t_{1/2}$) (García-Gallego & Bernardes, 2014; Johnson et al., 2007; Roberto et al., 2003). In order to improve the bioavailability and functions, CORMs with a stable and longer half-life are needed. As a result, research on transition metal carbonyl complexes with good bioavailability, excellent biocompatibility and low cost that are ideal for site-specific CO release need to be explored further.

Metal carbonyl complexes are ideal candidates for CORMs (Chaves-Ferreira et al., 2015; García-Gallego & Bernardes, 2014; Johnson et al., 2007; Marques et al., 2012; Roberto et al., 2003). CORM-2 (Figure 13) and water-soluble CORM-3 (Figure 2.16) are the most commonly used CORMs for both in vitro and vivo research into the physiological role of CO release (García-Gallego & Bernardes, 2014; Johnson et al., 2007; Roberto et al., 2003). In this scope, two manganese photo-CORMs that were synthesized by previous researchers had shown the significant cytotoxicity under the unique control of visible light towards HeLa cells and MDA-MB-231 breast cancer cells via MTT assay (Carrington et al., 2013). After that, Chakraborty (Chakraborty et al., 2015) from the same group utilised a new method for drug delivery, using the AL-MCM-41 mesoporous silica nanoparticles (MSNs) loaded with a novel rhenium photo-CORM for the special delivery of photo-CORM to breast cancer cells. Owing to a "turn-off" reaction caused by a systemic decrease in luminescence intensity upon UV irradiation, the trackable of CO transmission was allowed by the endocytosis of the [Re-CO] @ AL-MCM-41 MSNs inside the MDA-MB-231 breast cancer cells. They also used the MTT assay to study the anticancer behaviour of endocytosed particles after light-induced CO release on MDA-MB-231 breast cancer cells. The results proved a much greater impact than the photo-

CORM alone, on account of the extravasation of nanoparticles occurring in a tumour-selective way (Chakraborty et al., 2015).

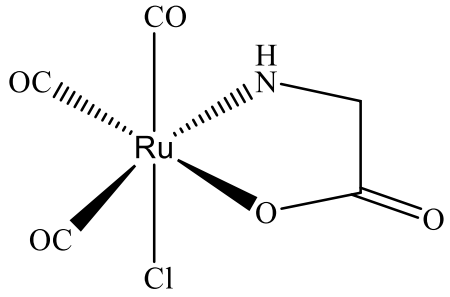

Figure 2.15: Structure of CORM-3.

The novel fac-manganese (I) tricarbonyl bipyridine complexes that synthesized by Üstün et al. (Üstün et al., 2016) were able to emit CO upon UV light irradiation. The cytotoxicity of these compounds was study against the MCF-7 breast cancer cell line. They all had shown the promising IC_{50} in the low micromolecular range. However, UV irradiation did not improve the cytotoxicity of most of these complexes when the same in vitro experiment was repeated with a 10-minute UV irradiation at 365 nm. This result revealed that the anticancer potential of CORMs may not depend on the UV irradiation as the effect of CORMs seem to be variable and cell-type specific (Loboda et al., 2015a, 2015b).

Although the research on iron CORMs is popular, the anticancer properties of diiron CORMs are substantially unexplored. In this scope, Gao et al. (Gao et al., 2018) had reported a water-soluble, nontarget reagent and a carrier-free diiron hexacarbonyl complex, named as TG-FeCORM (Figure 2.17). TG-FeCORM had also been found to be biocompatible as iron was an essential element in human life (Chen et al., 2014; Long et al., 2013).

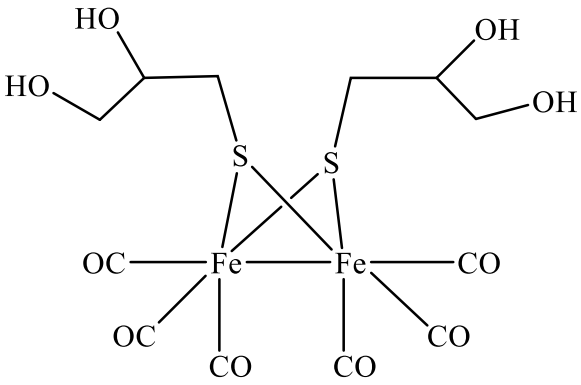

Figure 2.16: Structure of $[Fe_2\{\mu\text{-}SCH_2CH(OH)\text{-}\ CH_2(OH)\}_2(CO)_6]$ (TG-FeCORM).

TG-FeCORM could emit CO via substitution reaction by thiol groups of cysteamine (CysA) (Long et al., 2013). They observed that the TG-FeCORM could be stimulated by glutathione (GSH) that carried a thiol group to emit CO in a concentration-dependent way. Furthermore, there was a significant difference in CO-releasing rate of TG-FeCORM that triggered by GSH in normal and cancer cells. As the level of endogenous GSH in cancer cells is higher than in normal cells, the CO-releasing rate is faster in cancer cells. Thus, TG-FeCORM, a transition metal carbonyl compound, was a capable of achieving site-specific CO release in cancer cells (Scheme 2.5) (Gao et al., 2018).

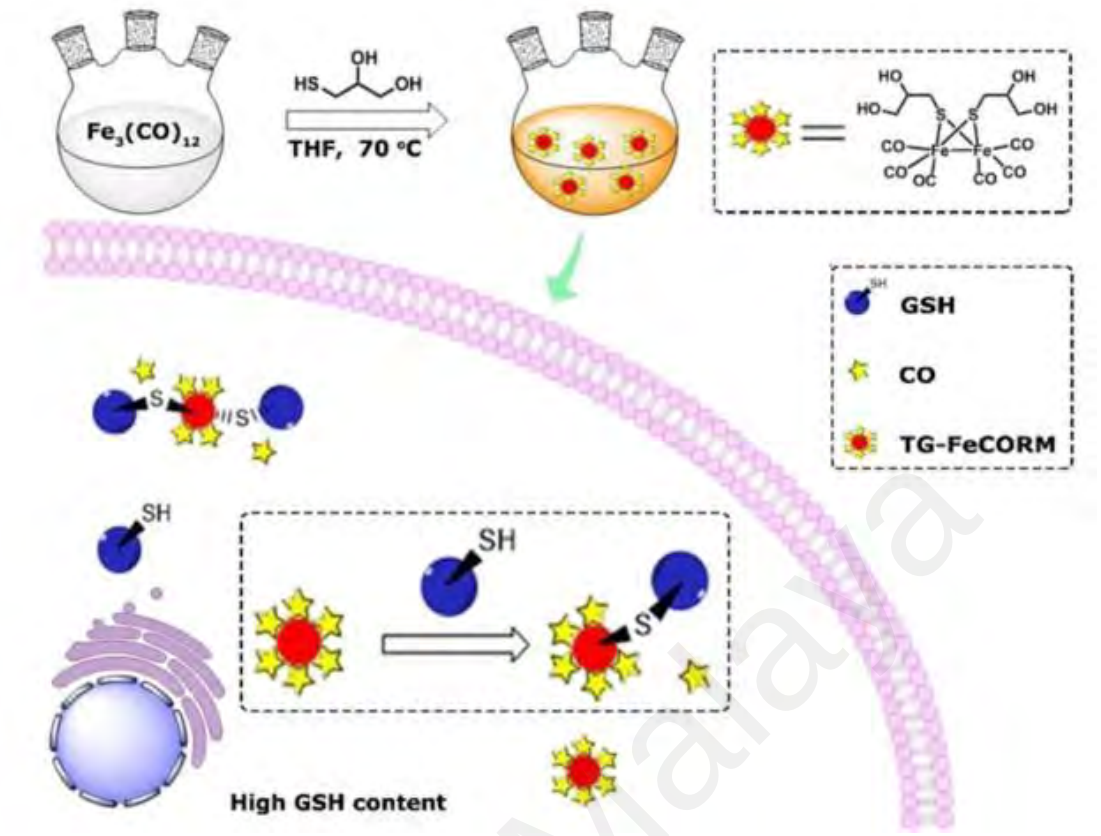

Scheme 2.5. Schematic Illustration of TG-FeCORM Synthesis and Its Proposal Site-Specific CO Release in Cancer Cells Triggered by Endogenous GSH in Reference (Gao et al., 2018).

2.6 ADME Properties

A potential compound must able to reach its target in the body to be effective as a drug in adequate concentration. Besides, it must be able to stay there in a in a bioactive state that long enough for the anticipated biologic activities to occur (Silakari & Singh, 2021). The effective compound must also display a high level of biological activity and low toxicity. In this content, drug development that includes the process of evaluating absorption, distribution, metabolism, and excretion (ADME) are very important in the preliminary study of the effective compound (Daina, Michielin, & Zoete, 2017). Early estimation of ADME in the discovery phase had significantly demonstrated a lower proportion of pharmacokinetics-related failure in the clinical phases (Hay, Thomas,

Craighead, Economides, & Rosenthal, 2014). In this perspective, computer model has played an important role as an alternative for the prediction of ADME before the trial clinical experiment (Dahlin, Inglese, & Walters, 2015).

The SwissADME, a free open-access web tool, which can be found at http://www.swissadme.ch, is established and designed for non-experts in CADD to submit and analyse their findings in a user-friendly manner (Daina et al., 2017). In comparison to the state-of-the-art of free web-based tools for ADME and pharmacokinetics (e.g. pk-CSM (Pires, Blundell, & Ascher, 2015) and admetSAR (Cheng et al., 2012)), and aside from unique access to proficient methods (e.g. iLOGP (Daina, Michielin, & Zoete, 2014)or the BOILED-Egg (Daina & Zoete, 2016)), SwissADME strong points included, but are not limited to: multiple input methods, computation for multiple molecules, and the ability to display, save, and share results per individual molecule or through globally intuitive and interactive graphs (Daina et al., 2017). Lastly, SwissADME is integrated in the SwissDrugDesign workspace. One-click interoperability provides direct access to various CADD tools developed by the Molecular Modeling Group of the SIB Swiss Institute of Bioinformatics, such as ligand-based virtual screening (SwissSimilarity) (Zoete, Daina, Bovigny, & Michielin, 2016), biotarget prediction (SwissTargetPrediction) (Gfeller et al., 2014), molecular docking (SwissDock) (Grosdidier, Zoete, & Michielin, 2011), bioisosteric design (SwissBioisostere) (Wirth, Zoete, Michielin, & Sauer, 2013), and molecular mechanics (SwissParam) (Zoete, Cuendet, Grosdidier, & Michielin, 2011). Consequently, SwissADME has been created to assist the entire community (specialists and non-experts) in their drug development process.

2.6 Objectives

The aims of this project are consisted of the followings:

I. To study the reactivity of $[CpFe(CO)_2]_2$ towards dichalcogenide ligands of dicyclohexyl disulfide, 2-thienyl disulfide and dibenzyl diselenide, respectively, which involves isolation, characterization and structural elucidation.

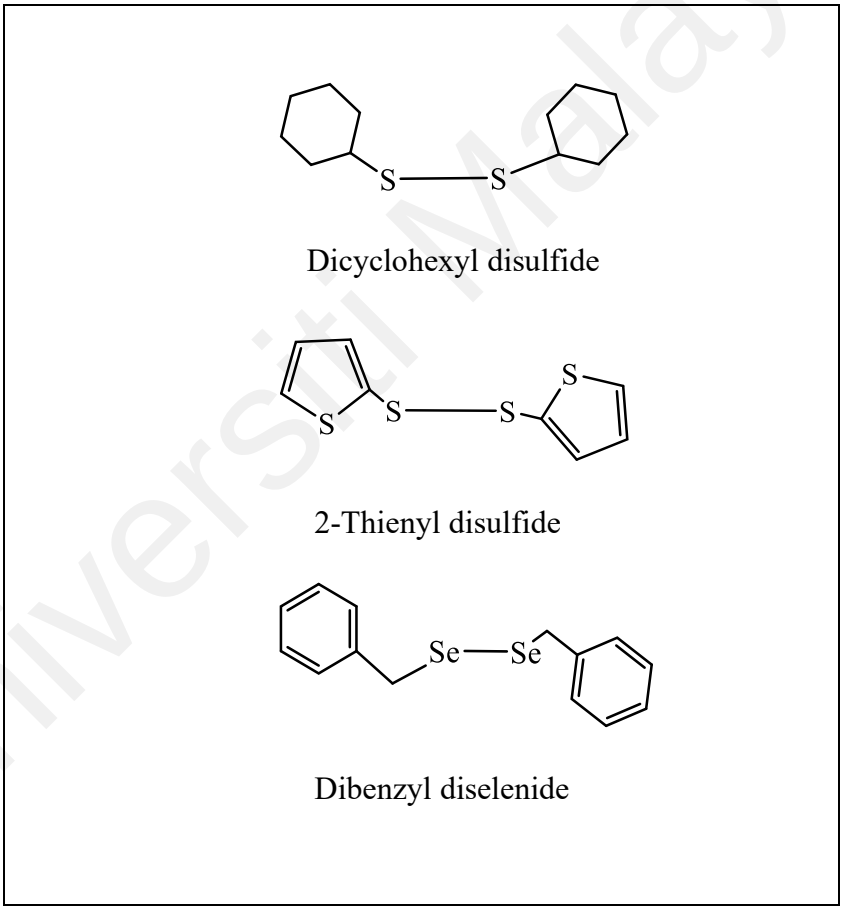

Figure 2.17: Structure of dicyclohexyl disulfide, 2-thienyl disulfideand dibenzyl diselenide.

II. To investigate the ability of the complexes **2**-**4** as potential photoCORMs. The stability of the **2**-**4** was first observed in the dark and UV. CO-releasing testing will be conducted in order to investigate the ability of these novel complexes as potential photoCORMs.

III. To investigate the potential of the complexes **2**-**4** as anticancer and antimalarial agents. These isolated novel products are to be employed for activity study as potential photoCORMs for anticancer and antimalarial properties. The results derived from this study are expected to contribute and provide informative remarks with respect to the ability of these dicyclopentadienyliron complexes to have any anticancer and antimalarial properties.

CHAPTER 3: RESULTS AND DISCUSSIONS

3.1 Studies with Dicyclohexyl Disulfide

3.1.1 Reaction of $[CpFe(CO)_2]_2$ (1) with dicyclohexyl disulfide

A magenta solution of $[CpFe(CO)_2]_2$ (**1**) underwent complete reaction with two equivalent moles of dicyclohexyl disulfide after refluxing in toluene for 21 hours. From TLC analysis, the reaction mixture showed two spots indicating the presence of two products. A yellow spot was observed at the R_f = 0.74 and a pink spot at R_f = 0.72, respectively. The reaction mixture was separated *via* column chromatography where the first fraction after dried was obtained yellowish brown crystalline solids of $[CpFe(CO)(C_6H_{11}S)]_2$ (**2**) (21.6% yield). The second fraction was isolated as a pink solution which upon evaporation gave a dark brownish pink oily precipitate. TLC analysis for this pink oily precipitate showed the presence of complex **2** together with the pink spot (R_f = 0.72). Several attempts to recrystallize the pink fraction was unsuccessful. Apparently, similar observations were reported from published works for the reaction of $[CpFe(CO)_2]_2$ (**1**) with other REER ligands (Schermer & Baddley, 1971) whereby such inseparable fractions were encountered. However, the yield of ~15% for the pink fraction was estimated from TLC analysis.

3.1.2 Synthetic and Mechanistic pathways

According to the literature (Wilkie & Huettl, 1989) when $[CpFe(CO)_2]_2$ (**1**) was subjected to ~~a~~ reflux conditions under nitrogen atmosphere, it will dissociate to form monomeric dicarbonyl radicals species of $CpFe(CO)_2\cdot$ as shown in (Eqn. 3.1). The subsequent decarbonylation will occur to give the monocarbonyl radical species of $CpFe(CO)\cdot$ and the total decarbonylated species of $CpFe\cdot$, respectively.

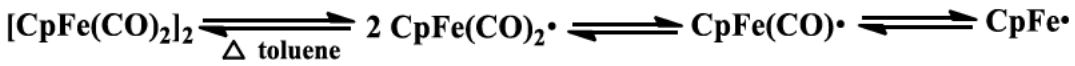

... Eqn. (3.1)

Meanwhile, under thermolytic condition, dicyclohexyl disulfide could undergoes a homolytic or heterolytic bond scission to give the C_6H_{11}-S· moiety (Mayer, 1977). Moreover, the S-S linkage in the RSSR ligand was recognized for its vulnerability towards cleavages by electrophilic, nucleophilic and radical attacks. Hence, it is plausible that there are two possible pathways could led to the formation of $[CpFe(CO)(C_6H_{11}S)]_2$ (**2**). We proposed that, the first pathway involved the nucleophilic addition where a C_6H_{11}-S· moiety was added to the $CpFe(CO)_2$· to form the $19e^-$ intermediate species of $CpFe(CO)_2(C_6H_{11}S)$ (**2a**). Later, **1a** underwent further decarbonylation to form the $17e^-$ $CpFe(CO)(C_6H_{11}S)$ (**2b**). Due to the instability nature of the $17e^-$ species, **2b** will undergo dimerization in a concerted manner to form a more stable $18e^-$ dimer $[CpFe(CO)(C_6H_{11}S)]_2$ (**2**). Similar synthetic pathway was also reported for $[CpFe(CO)(SPh)]_2$ (M. Ahmad et al., 1966).

The proposed second pathway was *via* a radical attack where the radical species of $CpFe(CO)$· attacked the S-S linkage in the dicyclohexyl disulfide ligand followed by the insertion of two $C_6H_{11}S$· in between two $CpFe(CO)$· moieties. Concomitantly, $[CpFe(CO)(C_6H_{11}S)]_2$ (**2**) with two bridging sulfide ligands was formed. The proposed synthetic and mechanistic pathways were shown in Scheme 3.1.

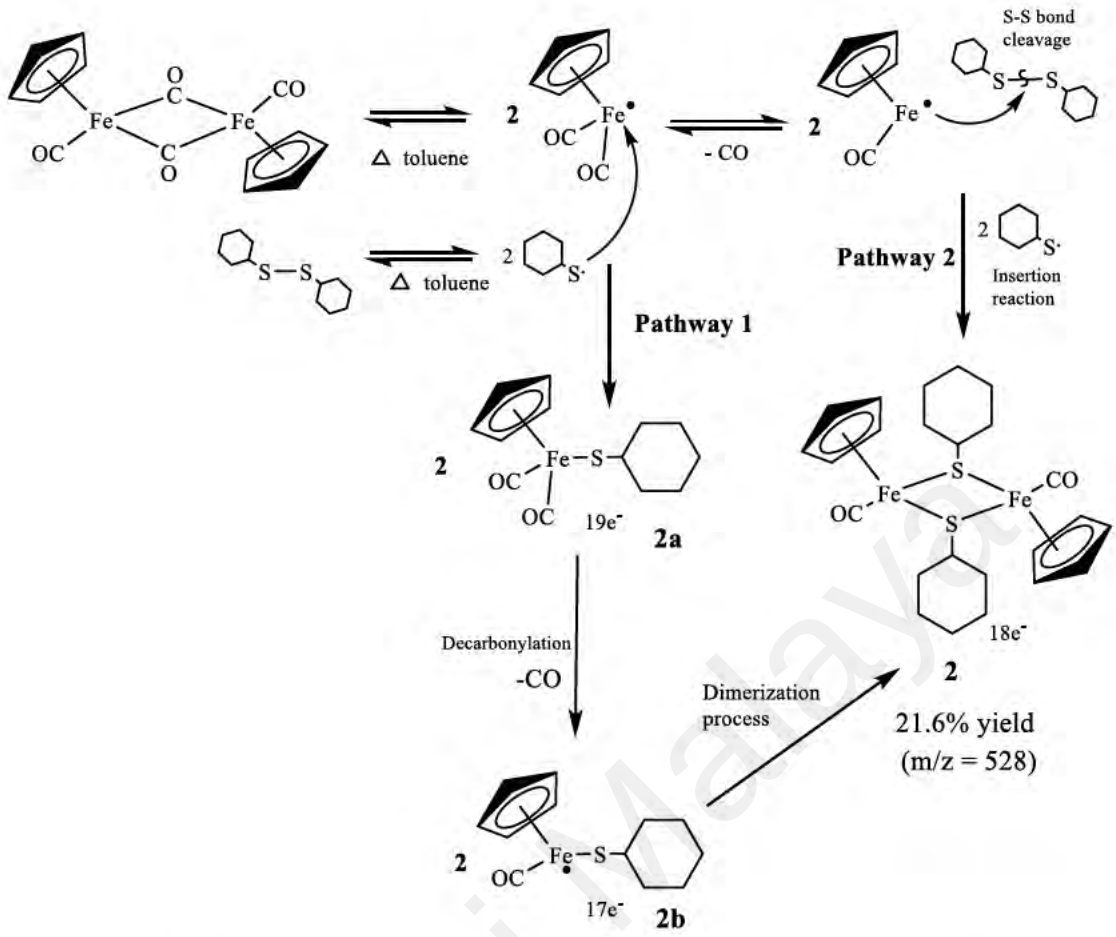

Scheme 3.1. Proposed synthetic pathways for the reaction of $[CpFe(CO)_2]_2$ with dicyclohexyl disulfide.

3.1.3 Physical Properties of $[CpFe(CO)(C_6H_{11}S)]_2$ (2)

$[CpFe(CO)(C_6H_{11}S)]_2$ (**2**) exists as a yellowish-brown crystalline solid. It is air-stable for prolonged periods at room temperature. It is soluble in toluene to give a dark brown colour solution which is stable at ambient temperature under an inert atmosphere. The melting point of **2** is 177.1˚C-178˚C.

3.1.4 Spectral Characteristics

3.1.4.1 I.R. Spectra

Complex **2** in crystalline form is used for the interpretation of I.R. study. The I.R. spectrum shows the *v*(CO) stretching frequencies at 1946s and 1905m cm^{-1}, which indicated that only terminal CO present in complex **2** and it is in the highly symmetrical order. There are no bands exist in the bridging CO stretching region. In fact, the CO stretching frequency of complex **2** in the I.R. spectrum is very similar compare to previous compounds (Haines et al., 1975). C-H stretching of the of the $C_6H_{11}S$ moieties is located at the 2923vs and 2853vs cm^{-1} (Hasanzadeh, Ghammamy, & Mohammadi, 2010). The I.R. spectrum of complex **2** also shows the C-S stretching frequencies of the $C_6H_{11}S$ moieties at 1195vw and 1171vw cm^{-1} (Hasanzadeh et al., 2010). Figure 3.1 demonstrates the I.R. spectrum of complex **2.**

3.1.4.2 NMR Spectra

Complex **2** in crystalline form is used for the NMR study. Complex **2** is diamagnetic (Hallam et al., 1955) and highly symmetrical (Haines et al., 1975) complex. The Cp rings exist as singlet in both ^1H and ^{13}C NMR spectra in benzene-d_6. The proton NMR chemical shift for Cp is δ 4.17. The ^{13}C NMR chemical shift for Cp is recorded at δ 81.99; terminal CO at δ 225.30. The proton NMR chemical shift for C_6H_{11} was recorded at δ 1.76-1.79 (*d*, $-CH_2$), δ 1.60-1.64 (*d*, $-CH_2$), δ 1.46-1.49 (*d*, -CHS), δ 1.26-1.35 (*q*, $-CH_2$), 0.98-1.08 (*q*, $-CH_2$) and 0.60-0.68 (*q*, $-CH_2$). In the ^{13}C NMR spectrum, the C_6H_{11} was assigned at δ 26.84, δ 35.29 and 47.66 (C_6H_{11}). Figure 3.2 and figure 3.3 display the ^1H and ^{13}C NMR spectra of complex **2** in benzene-d_6.

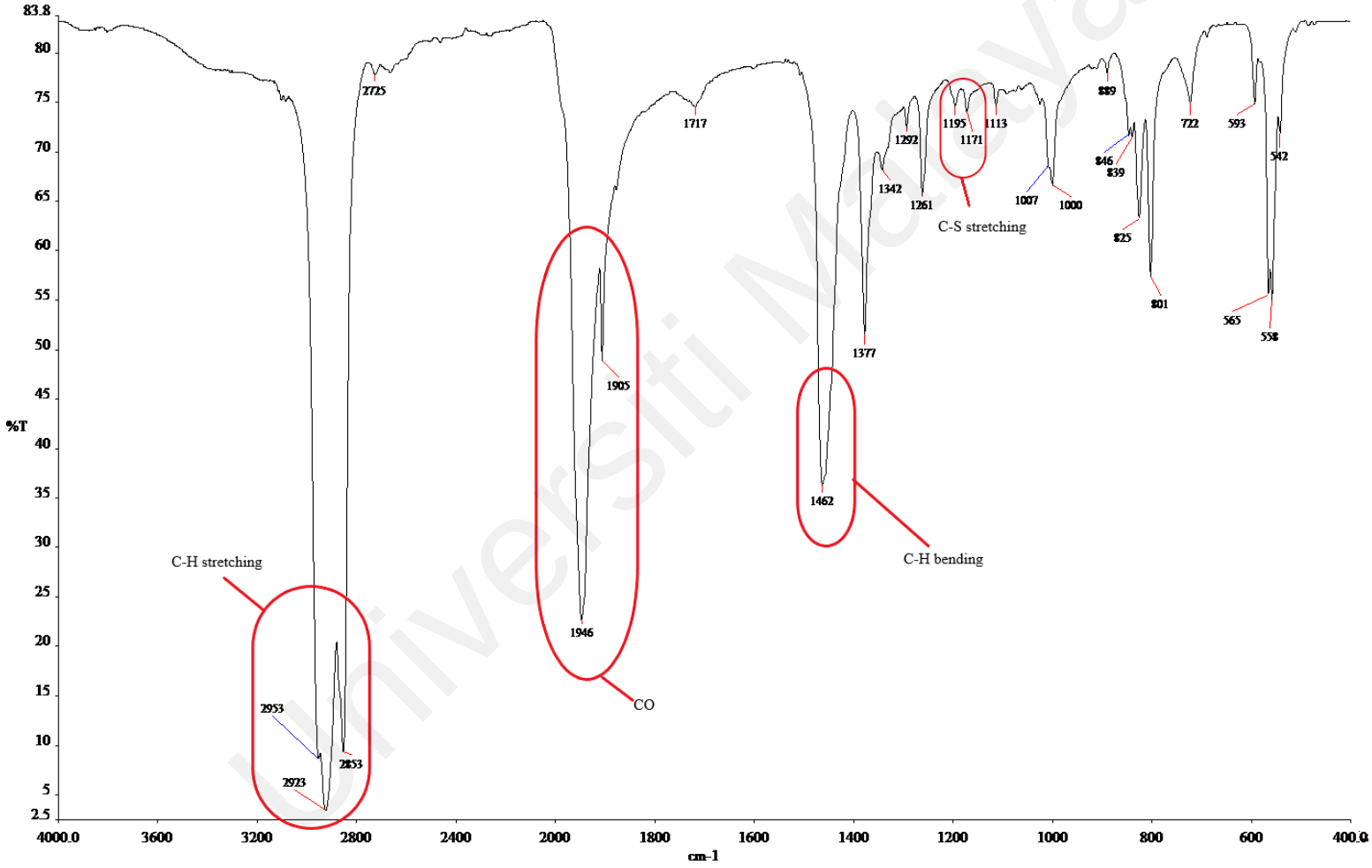

Figure 3.1: The I.R. spectrum of complex 2.

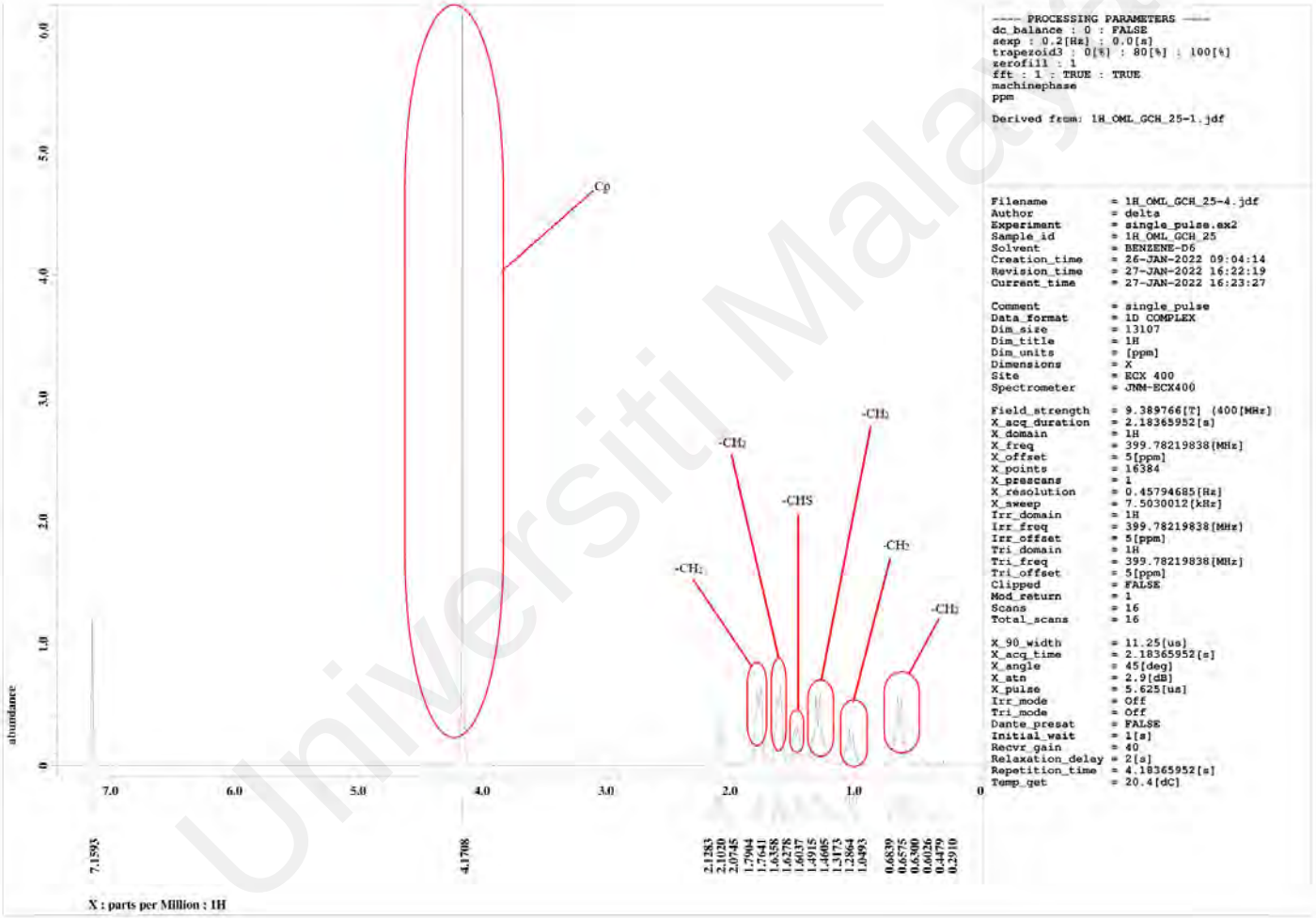

Figure 3.2: ^{1}H NMR spectra of complex 2 in benzene-d_6.

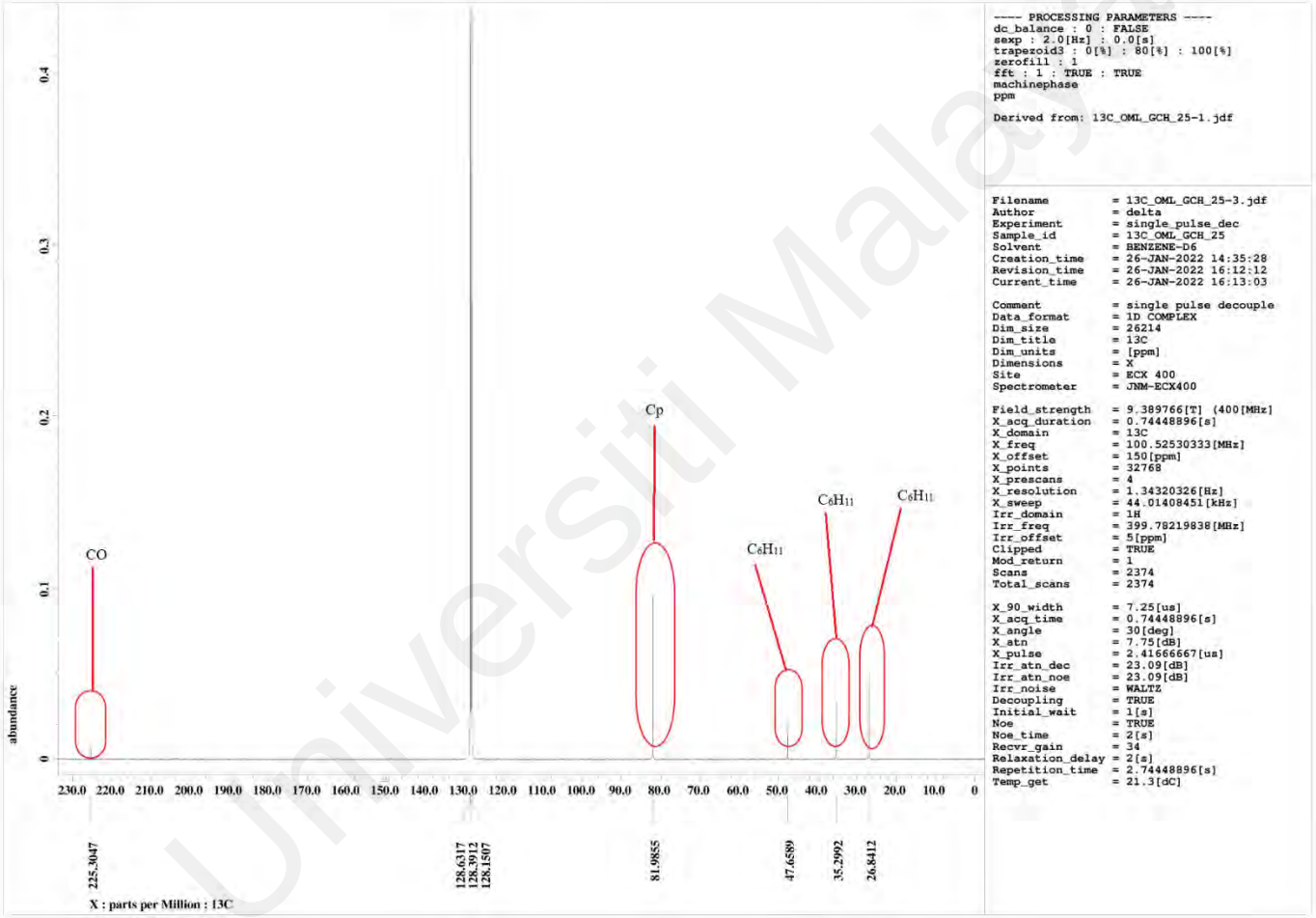

Figure 3.3: ^{13}C NMR spectra of complex 2 in benzene-d_6.

3.1.4.3 Mass Spectrum

The EI mass spectrum of complex **2** shows the parent ion *m/z* = 528 $[CpFe(CO)(C_6H_{11}S)]_2$ and its fragmentation ions are tabulated in Table 3.1.

Table 3.3. Electrospray ionization mass spectrum of $[CpFe(CO)(C_6H_{11}S)]_2$ (2)

m/z	Assignments
528	$[Cp_2Fe_2(CO)_2(C_6H_{11}S)_2]^+$
500	$[Cp_2Fe_2(CO)(C_6H_{11}S)_2]^+$
472	$[Cp_2Fe_2(C_6H_{11}S)_2]^+$
389	$[Cp_2Fe_2(C_6H_{11}S)(S)]^+$
306	$[Cp_2Fe_2S_2]^+$
241	$[CpFe_2S_2]^+$
209	$[CpFe_2S]^+$
176	$[Fe_2S_2]^+$

3.1.5 Crystal Structure $[CpFe(CO)(C_6H_{11}S)]_2$ (2)

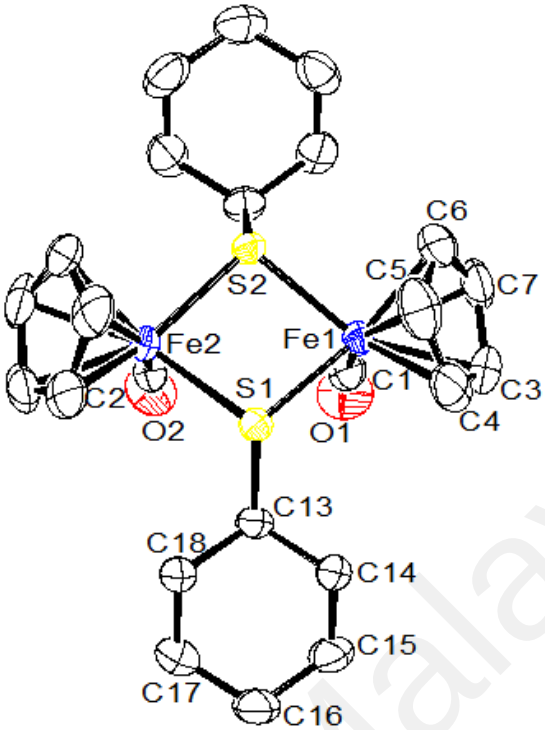

Figure 3.4: Molecular structure of $[CpFe(CO)(C_6H_{11}S)]_2$ (2).

The crystal structure of **2** is shown in figure 3.4 and its bonding parameters are tabulated in Table 3.2. **2** crystallized in monoclinic with space group $P2_1/c$. **2** was found as an isomer of *cis* arrangement of the carbonyl ligands. The Fe(1)...Fe(2) separation in **1** of 3.411 Å indicates that no bond was formed (Pauling, 1976) by comparing with other reported iron complexes which consisted of Fe—Fe single bond such as $(AsCH_3)_4Fe_2(CO)_6$ (2.68 Å) and $CHP(CH_3)_2Fe_2(CO)_5$ (2.63 Å) (Pauling, 1976). The absence of the metal-metal bonding in **2** is corresponding to the 18-electron rule where each sulfide ligand is contributing 1.5 e^- to each Fe metal centre (Ooi, Lim, Wong, & Ng, 2017; Wachter, 1989). The angle between S(1)-Fe(1)-S(2) which is 80.73˚(2) and the angle between S(1)-Fe(2)-S(2) which is 80.83˚(2) shows that the complex **2** is highly symmetrical (Haines et al., 1975; Hallam et al., 1955; Piper et al., 1955).

Table 3.4. Bond lengths [Å] and angles [°] for $[CpFe(CO)(C_6H_{11}S)]_2$ (2)

Bond lengths			
Fe(1)—S(1)	2.2640 (7)	Fe(1)—C(7)	2.103 (3)
Fe(1)—C(1)	1.730 (3)	Fe(2)—S(1)	2.2639 (7)
Fe(1)—C(3)	2.089 (3)	Fe(2)—S(2)	2.2691 (7)
Fe(1)—C(4)	2.085 (3)	S(1)—C(13)	1.832 (2)
Fe(1)—C(5)	2.082 (3)	O(1)—C(1)	1.152 (3)
Fe(1)—C(6)	2.104 (3)	Fe(1). . .Fe(2)	3.411
Bond angles			
S(1)—Fe(1)—S(2)	80.73 (2)	S(1)—Fe(2)—S(2)	80.83 (2)
C(1)—Fe(1)—S(1)	94.48 (9)	C(2)—Fe(2)—S(1)	95.57 (8)
C(1)—Fe(1)—S(2)	96.05 (8)	C(2)—Fe(2)—S(2)	94.25 (9)
C(1)—Fe(1)—C(3)	93.75 (13)	Fe(2)—S(1)—Fe(1)	97.78 (3)
C(1)—Fe(1)—C(4)	122.71 (14)	Fe(2)—S(2)—Fe(1)	97.34 (3)
C(1)—Fe(1)—C(5)	158.49 (12)	O(1)—C(1)—Fe(1)	176.3 (2)
C(1)—Fe(1)—C(6)	132.18 (13)	O(2)—C(2)—Fe(2)	177.6 (2)
C(1)—Fe(1)—C(7)	98.05 (12)	C(18)—C(13)—S(1)	109.60 (15)

3.2 Studies with 2-Thienyl Disulfide

3.2.1 Reaction of $[CpFe(CO)_2]_2$ (1) with 2-Thienyl Disulfide

The reaction of a magenta solution of $[CpFe(CO)_2]_2$ (**1**) with two moles of 2-thienyl disulfide was refluxed under stirring in toluene for 18 hours. A resultant dark orangy-brown reaction mixture was obtained. From the TLC analysis of the reaction mixture solution, a brownish orange spot at $R_f = 0.66$ and a dark brown spot at $R_f = 0.49$ were

identified as the products. Using column chromatography, two fractions were obtained. The first fraction after concentration to dryness gave $[CpFe(CO)(C_4H_3S_2)]_2$ (**3**) (26.4% yield) as orangy-brown crystalline solids. The second fraction after concentration gave an oily dark brown residue. Several attempts to purify and recrystallize this fraction failed mainly because decomposition eventually occurred. TLC of this inseparable fraction showed the presence of complex **3** and a dark brown spot at $R_f = 0.49$. The yield for the brown fraction estimated from the TLC analysis was 17.6%.

3.2.2 Synthetic and Mechanistic pathways:

From the above experimental findings, it was conceivable that the synthetic pathways of $[CpFe(CO)(C_4H_3S_2)]_2$ (**3**) is similar as for **2**. $[CpFe(CO)_2]_2$ (**1**) underwent thermolytic bond cleavage during reflux to form two radical species of $17e^-$ $CpFe(CO)_2\cdot$ and $15e^-$ $CpFe(CO)\cdot$, respectively. The S-S bond cleavage occurred for the 2-thienyl disulfide ligand due to prolonged heating has resulted in the formation of $C_4H_3S_2\cdot$ moiety. Subsequently, the $C_4H_3S_2\cdot$ moiety act as a nucleophile to attack the $CpFe(CO)_2\cdot$ and resulting in the formation of a $19e^-$ $CpFe(CO)_2(C_4H_3S_2)\cdot$ (**3a**) radical. The unstable **3a** underwent further decarbonylation to give the $17e^-$ $CpFe(CO)(C_4H_3S_2)\cdot$ (**3b**) radical under prolonged thermolysis (M. Ahmad et al., 1966). Subsequently, the monomeric species **3b** proceed to dimerize to give $[CpFe(CO)(C_4H_3S_2)]_2$ (**3**).

On the other hand, the 2-thienyl disulfide ligand which consisted of a S-S linkage is susceptible towards cleavages by electrophilic, nucleophilic and radical attack (Eqn. 3.2).

$$R\text{-}S\text{-}S\text{-}R \longrightarrow 2\ R\text{-}S\cdot \qquad \ldots \text{Eqn.}(3.2)$$

Hence, the formation of the radical species, $CpFe(CO)\cdot$ during the reflux of $[CpFe(CO)_2]_2$ with 2-thienyl disulfide had led to the radical attack of $CpFe(CO)\cdot$ towards the S-S linkage in 2-thienyl disulfide followed by a thienyl sulfide insertion in between two $CpFe(CO)\cdot$ moiety to form the sulfur bridged $[CpFe(CO)(C_4H_3S_2)]_2$ (**3**). The synthetic and mechanistic pathways proposed for the reactions above were demonstrated in Scheme 3.2.

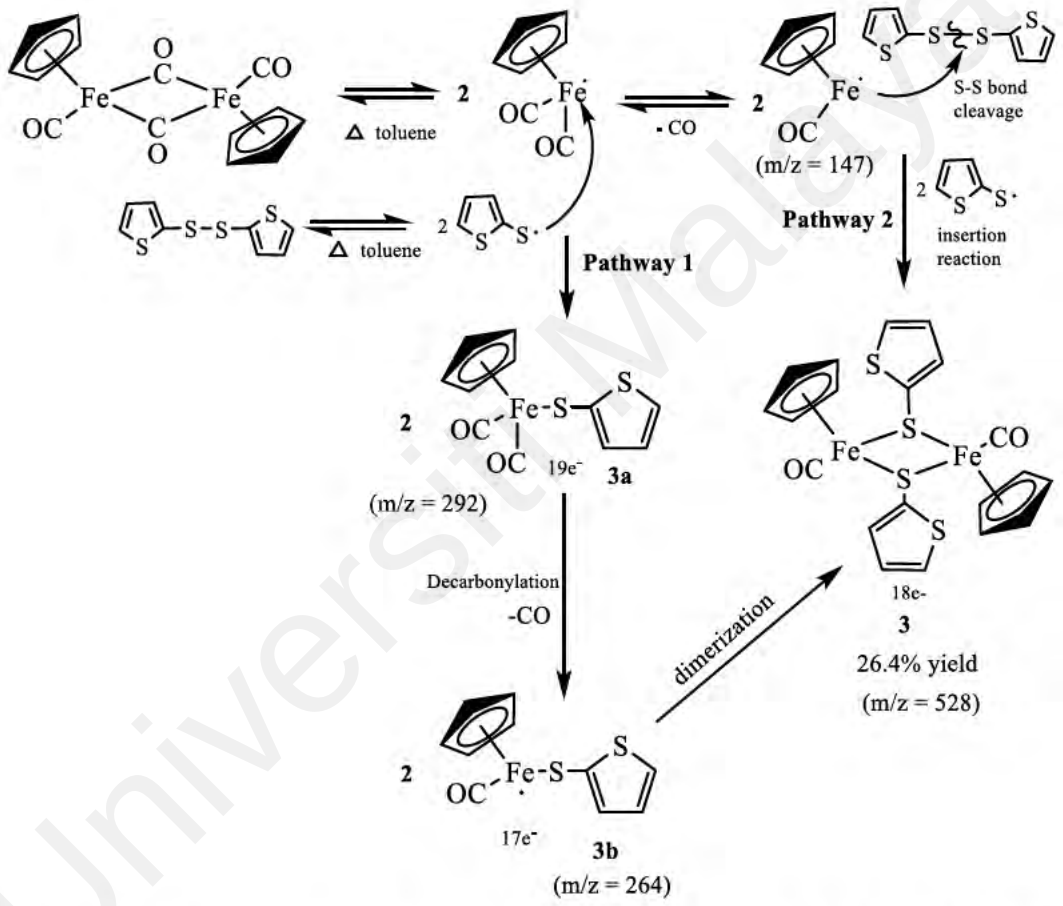

Scheme 3.2. Proposed synthetic pathways for the reaction of $[CpFe(CO)_2]_2$ (1) with 2-thienyl disulfide.

3.2.3 Physical Properties of $[CpFe(CO)(C_4H_3S_2)]_2$ (3)

$[CpFe(CO)(C_4H_3S_2)]_2$ (**3**) exists as an orangy-brown crystalline solid. It is air-stable for a prolonged period at ambient temperature. It is soluble in toluene to give an orange-brown colour solution which is stable at room temperature under an inert atmosphere. The melting point of **3** is 172.6˚C-174.4˚C.

3.2.4 Spectral Characteristics

3.2.4.1 I.R. Spectra

Complex **3** in crystalline form is used for the I.R. study. The I.R. spectrum shows the *v*(CO) stretching frequencies for terminal CO at 1966vs, 1942m and 1901sh (refer to Appendix I). The assigned terminal CO peak of complex **3** that exists in this range is supported by the previous literature (Avanzino & Jolly, 1976) and the CO stretching frequency of complex **3** in the I.R. spectrum is very similar compare to previous compounds (Haines et al., 1975). The C-H stretching of the 2-thienyl group is presented in the 3095w, 2952vs, 2924vs, 2854vs, 1403w and 1207vw cm^{-1} (refer to Appendix A). The I.R. spectrum of complex **3** also shows the =C-H bending frequencies of the 2-thienyl group at 837w, 818m, 701w, 676m, 562m, 546w cm^{-1} (refer to Appendix A). The outcomes of the C-H stretching and =C-H bending frequencies obtained from the I.R. spectrum is in agreement with the previous IR study about 2-thienyl compound (Korepanov, Popov, Senyavin, Yurovskaya, & Chernyshova, 2007).

3.2.4.2 NMR Spectra

Complex **3** in crystalline form is used for the NMR study. Complex **3** is a diamagnetic (Hallam et al., 1955) and highly symmetrical (Haines et al., 1975) complex. The Cp rings exist as singlet in both ^1H and ^{13}C NMR spectra in benzene-d_6. Compare to the previous

literature (Haines et al., 1975), the peak that Cp rings present is in the acceptable range (Aime, Cordero, Gobetto, & Szalontai, 1993) in both ^{1}H and ^{13}C NMR. The Cp signal is recorded at δ 4.17 while the ^{1}H NMR chemical shift for 2-thienyl peaks (-$C_4H_3S_2$) are assigned at δ 6.65 – 6.67 (*t*, $C_4H_3S_2$), 6.79-6.80 (*d*, $C_4H_3S_2$), 6.95 (*s*, $C_4H_3S_2$) in the ^{1}H NMR spectrum (refer to Appendix B). The ^{13}C NMR chemical shift for Cp is recorded at δ 80.83; -$C_4H_3S_2$ peaks are at δ 125.87, 127.73, 131.11 and 148.78; terminal CO at δ 222.72 (refer to Appendix C). The assignatin of 2-thienyl peaks in both ^{1}H and ^{13}C NMR are admissible compare to the previous study regarding to the previous compounds that contained 2-theinyl groups (Al-Omar, 2010; Davis, Carroll, & Quinn, 2003; Kanemoto, Sugimura, Shimizu, Yoshida, & Hosoya, 2017; Rajappa, 1984).

3.2.4.3 Mass Spectrum

The EI mass spectrum of complex **3** shows the parent ion *m/z* = 528 $[CpFe(CO)(C_4H_3S_2)]_2$ and its fragmentation ions are tabulated in Table 3.3.

Table 5.3. Electrospray ionization mass spectrum of $[CpFe(CO)(C_4H_3S_2)]_2$ (3)

m/z	Assignments
528	$[Cp_2Fe_2(CO)_2(C_4H_3S_2)_2]^+$
500	$[Cp_2Fe_2(CO)(C_4H_3S_2)_2]^+$
472	$[Cp_2Fe_2(C_4H_3S_2)_2]^+$
389	$[Cp_2Fe_2(C_4H_3S_2)S]^+$
357	$[Cp_2Fe_2(C_4H_3S_2)]^+$
292	$[CpFe(CO)_2(C_4H_3S_2)]^+$
264	$[CpFe(CO)(C_4H_3S_2)]^+$
236	$[CpFe(C_4H_3S_2)]^+$
186	$[CpFeS_2]^+$
180	$[Fe_2S_2]^+$
147	$[CpFe(CO)]^+$
121	$[CpFe]^+$

3.2.5 Crystal Structure of $[CpFe(CO)(C_4H_3S_2)]_2$ (3)

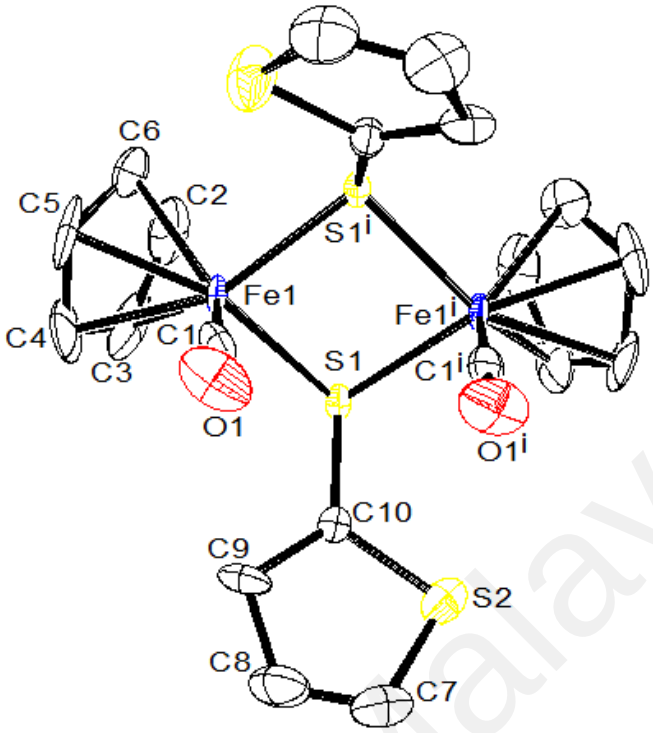

Figure 3.5: Molecular structure of $[CpFe(CO)(C_4H_3S_2)]_2$ (3).

The crystal structure of **3** is illustrated in Figure 3.5 and its bonding parameters are tabulated in Table 3.4. **3** crystallized in a monoclinic with space group C2/*c*. The two carbonyl moieties in complex **3** were *cis* to each other while the cyclopentadienyl moieties attached to the iron atoms were in the axial position. Besides, the two SR moieties that coordinated to Fe in **3** were in the *cis-syn* position. Both SR moieties were bridged across the two CpFe(CO)- fragments led to a formation of butterfly core complex (Wei, Goh, & Sinn, 1988) in **3**.The Fe(1). . .Fe(1^i) separation in **3** with 3.401 Å that calculated by Ortep indicates that Fe(1). . .Fe(1^i) is not bonded together (Pauling, 1976). The absence of the metal-metal bonding in **3** is corresponding to the 18-electron rule (Ooi et al., 2017).

Table 3.6. Bond lengths [Å] and angles [°] for $[CpFe(CO)(C_4H_3S_2)]_2$ (3)

Bond lengths			
Fe(1)—S(1^i)	2.2731 (9)	Fe(1)—C(5)	2.089 (4)
Fe(1)—S(1)	2.2689 (9)	Fe(1)—C(6)	2.101 (4)
Fe(1)—C(1)	1.753 (4)	S(1)—C(10)	1.761 (4)
Fe(1)—C(2)	2.102 (4)	S(2)—C(7)	1.694 (5)
Fe(1)—C(3)	2.097 (4)	S(2)—C(10)	1.722 (3)
Fe(1)—C(4)	2.102 (4)	O(1)—C(1)	1.148 (5)
Fe(1). . .Fe(1^i)	3.401		
Bond angles			
S(1)—Fe(1)—S(1^i)	81.97 (3)	C(4)—Fe(1)—C(2)	65.6 (2)
C(1)—Fe(1)—S(1)	95.32 (12)	C(5)—Fe(1)—S(1)	154.24 (17)
C(1)—Fe(1)—S(1^i)	94.07 (11)	C(5)—Fe(1)—S(1^i)	119.74 (19)
C(1)—Fe(1)—C(2)	161.45 (18)	C(5)—Fe(1)—C(2)	65.0 (2)
C(1)—Fe(1)—C(3)	133.1 (2)	C(5)—Fe(1)—C(3)	65.0 (2)
C(1)—Fe(1)—C(4)	99.1 (2)	C(5)—Fe(1)—C(4)	39.3 (2)
C(1)—Fe(1)—C(5)	96.59 (19)	C(5)—Fe(1)—C(6)	38.3 (2)
C(1)—Fe(1)—C(6)	126.6 (2)	C(6)—Fe(1)—S(1^i)	91.17 (14)
C(2)—Fe(1)—S(1^i)	97.20 (16)	C(6)—Fe(1)—S(1)	137.96 (16)
C(2)—Fe(1)—S(1)	100.80 (16)	C(6)—Fe(1)—C(2)	38.7 (2)
C(3)—Fe(1)—S(1^i)	132.8 (2)	C(6)—Fe(1)—C(4)	65.2 (2)
C(3)—Fe(1)—S(1)	90.30 (14)	Fe(1)—S(1)—Fe(1^i)	96.97 (3)
C(3)—Fe(1)—C(2)	38.6 (2)	C(10)—S(1)—Fe(1^i)	110.28 (12)
C(3)—Fe(1)—C(4)	39.1 (2)	C(10)—S(1)—Fe(1)	111.15 (11)
C(3)—Fe(1)—C(6)	64.5 (2)	C(7)—S(2)—C(10)	92.4 (2)

C(4)—Fe(1)—S(1)	116.07 (19)	O(1)—C(1)—Fe(1)	178.1 (4)
C(4)—Fe(1)—S(1^{i})	156.29 (17)	S(2)—C(10)—S(1)	119.8 (2)

3.3 Studies with dibenzyl diselenide

3.3.1 Reaction of $[CpFe(CO)_2]_2$ (1) with dibenzyl diselenide

Reaction of $[CpFe(CO)_2]_2$ (**1**) with two moles of dibenzyl diselenide in refluxing toluene for 21 hours had led to the isolation of $[CpFe(CO)(C_6H_5CH_2Se)]_2$ (**4**) (19.97% yield) as yellowish-brown crystalline solids and $[(CpFe)_3(\mu\text{-}CO)_2(\mu_3\text{-}Se)(C_6H_5CH_2Se)]$ (**5**) (3.0% yield) as fine crystalline greenish-black solids, respectively. Complex **3** was previously isolated through the reaction of ferraborane, arachno-$[CpFe(CO)B_3H_8]$, with dibenzyl diselenide (Geetharani et al., 2011). But the group only reported the ^{1}H and ^{13}C NMR, IR and mass spectroscopies for **4**, however, we managed to perform a single crystal X-ray diffraction measurement and collected the following data as tabulated in Table 3.7 and the molecular structure of **4** was presented in Figure 3.6, respectively.

3.3.2 Synthetic and Mechanistic pathways:

In general, the Se-Se bond cleavage was considered the crucial steps towards photolysis and thermolysis of organic diselenide ligands to produce the monoselenide radicals (Chu & Lewicki, 1977) (Eqn. 3.3)

$$R\text{-}Se\text{-}Se\text{-}R \longrightarrow 2\,R\text{-}Se\bullet \qquad \ldots Eqn.(3.3)$$

Comparably to the reaction of $[CpFe(CO)_2]_2$ (**1**) with dicyclohexyl disulfide, we proposed that the formation of $[CpFe(CO)(C_6H_5CH_2Se)]_2$ (**4**) also involved two pathways.

In this reaction of $[CpFe(CO)_2]_2$ (**1**) with dibenzyl diselenide, the first pathway was initiated by the nucleophilic addition of $C_6H_5CH_2$-Se· moiety towards the $CpFe(CO)_2$· fragment and formed the 19e$^-$ $CpFe(CO)_2(C_6H_5CH_2$-Se)· (**4a**) followed by decarbonylation and dimerization to give $[CpFe(CO)(C_6H_5CH_2Se)]_2$ (**4**). For the second pathway, it was believed that the initial radical attack involving the CpFe(CO)· radical towards the dibenzyl diselenide ligand was feasible. Consequently, this resulted in the cleavage of the diselenide ligand to take place. Subsequently, the resulting monomeric benzylselenide radical, $C_6H_5CH_2Se$·, underwent an insertion reaction between the two CpFeCO fragments which led to the formation of $[CpFe(CO)(C_6H_5CH_2Se)]_2$ (**4**). The synthetic and mechanistic pathways proposed for the above reaction was shown in Scheme 3.3. This plausible mechanism was different as compared to the previous literature (Geetharani et al., 2011), which was not completely implicit for the formation of $[CpFe(CO)(C_6H_5CH_2Se)]_2$ (**4**) probably due to the difference in starting reactants employed in the reaction. In this respect, the previous group (Geetharani et al., 2011) had successfully synthesized $[CpFe(CO)(C_6H_5CH_2Se)]_2$ (**4**) by reacting [CpFe(CO)I] with dibenzyl diselenide at -70˚C in toluene with $[LiBH_4$.thf], which had suggested a different reaction mechanism as from Scheme 3.3.

Herein, for the formation of $[(CpFe)_3(\mu\text{-}CO)_2(\mu_3\text{-}Se)(C_6H_5CH_2Se)]$(**5**), it was postulated that CpFe(CO)Se· which was substantiated by the presence of molecular ion (m/z = 228) in the mass spectrum of **5**, together with CpFe(CO)·, CpFe· and Se· which were residues derived from the thermolytic bond scission of both $[CpFe(CO)_2]_2$ and dibenzyl diselenide, respectively, has undergone nucleophilic addition toward the $CpFe(CO)(C_6H_5CH_2Se)$· moiety concomitantly to form-complex **5**. Only complex **5** was able to form in this reaction but similar trimeric complex was not isolated from the reaction of $[CpFe(CO)_2]_2$ with dicyclohexyl disulfide and 2-thienyl disulfide. This phenomenon could be due to the heavier and softer characters of Se as compared to S

which allowed the alkyl selenide ligand to form a more stable complex with the soft substrate of $[CpFe(CO)_2]_2$ (Schermer & Baddley, 1971).

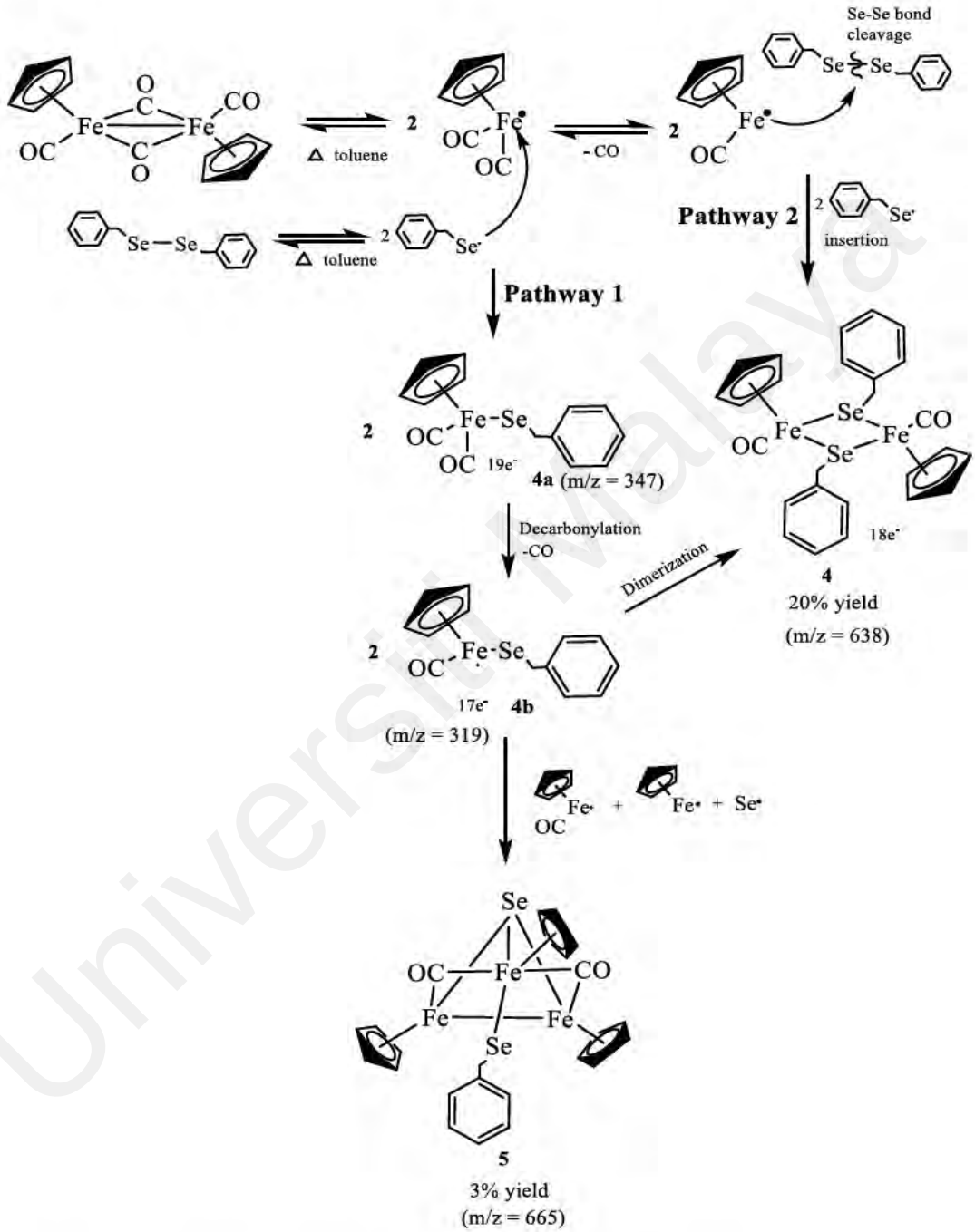

Scheme 3.3. Proposed synthetic pathways for the reaction of $[CpFe(CO)_2]_2$ (1) with dibenzyl diselenide.

3.3.3 Physical Properties

[CpFe(CO)($C_6H_5CH_2Se$)]$_2$ (4)

[CpFe(CO)($C_6H_5CH_2Se$)]$_2$ (**4**) exists as a yellowish-brown crystalline solid. It is air-stable for prolonged periods at ambient temperature. It is soluble in toluene to give a yellowish -brown colour solution which is stable at room temperature under an inert environment. The melting point of **4** is 154.7˚C-156.5˚C.

[(CpFe)$_3$(μ-CO)$_2$(μ$_3$-Se)($C_6H_5CH_2Se$)] (**5**)

[(CpFe)$_3$(μ-CO)$_2$(μ$_3$-Se)($C_6H_5CH_2Se$)] (**5**) exists as a greenish-black crystalline solid. It is air-stable for a prolonged period at ambient temperature for several weeks. It is soluble in toluene to give a dark green solution which is stable at room temperature under an inert atmosphere. The melting point of **5** is 177.8˚C-179.1˚C.

3.3.4 Spectral Characteristics

3.3.4.1 I.R. Spectra

[CpFe(CO)($C_6H_5CH_2Se$)]$_2$ (4)

Complex **4** in crystalline form is used for the I.R. study. The I.R. spectrum that shows the *ν*(CO) stretching frequencies of complex **4** at 1927vs, 1886m and 1960sh cm^{-1} is supported by the previous literature (Avanzino & Jolly, 1976; Schermer & Baddley, 1971). There is no stretching frequency of bridging CO exist in the I.R. spectrum of complex 4 (refer to Appendix A). The CO stretching frequency of complex **3** in the I.R. spectrum is very similar compare to previous selenium derivatives of cyclopentadienyliron dicarbonyl compounds (Schermer & Baddley, 1971). The C-H stretching of the aromatic benzyl group of complex **4** is displayed in the region 2923vs

and 2864vs cm^{-1} (Wong, Ooi, Chee, & Tan, 2005) while the C=C stretching of the aromatic benzyl group exist at 1598w, 1581w, 1492w cm^{-1} (Ooi et al., 2017). Other peaks such as =C-H bending at 835sh, 820m, 757m and 697m cm^{-1} (refer to Appendix A) also appear in the I.R. spectrum of complex **4.**

[$(CpFe)_3(\mu\text{-}CO)_2(\mu_3\text{-}Se)(C_6H_5CH_2Se)$] (5)

Complex **5** in crystalline form is used for the I.R. study. Different from the complex **2**,**3** and **4**, there is no bands are observed in the terminal carbonyl stretching region in the I.R. spectrum of complex **5.** This observation is in agreement with the previous reported trinuclear species (Haines et al., 1975). The I.R. spectrum only shows the stretching frequencies of bridging CO at 1762vs and 1723vs cm^{-1} (refer to Appendix A). Similar as complex **4**, The C-H stretching of the aromatic benzyl group of complex **5** is displayed in the region 2923vs and 2864vs cm^{-1} (Wong et al., 2005). Meanwhile, the C=C stretching of the aromatic benzyl group exist at 1490w, 1460s, 1416w, 1376 m cm^{-1} (Ooi et al., 2017). Other peaks such as =C-H bending at 817w, 745w, 690w, 608w cm^{-1} (refer to Appendix A) also displayed in the I.R. spectrum of complex **5.**

3.3.4.2 NMR Spectra

[CpFe(CO)($C_6H_5CH_2Se$)]$_2$ (4)

Complex **4** in crystalline form is used for the NMR study. Similar as complex **2** and **3,** complex **4** is also a diamagnetic (Hallam et al., 1955) and symmetrical molecule (Haines et al., 1975). The Cp rings exist as a singlet in both ^{1}H and ^{13}C NMR spectra in benzene-d_6. In the ^{1}H NMR, the Cp signal of complex **5** is recorded at δ 3.85. This value is different from the value that reported previously (Geetharani et al., 2011), which is δ 4.68. This difference is due to the solvent effect (Buckingham, Schaefer, & Schneider, 1960) of the different deuterated solvent. However, both Cp value reported are still exist in the acceptable range (Aime et al., 1993). The methyl peak (-CH_2) is assigned at δ 3.31 as a singlet while the chemical shift for the benzyl group (-$C_6H_5CH_2$) is obtained as a doublet and multiplet which is assigned at δ 7.39-7.40 and 6.98-7.05 (Wong et al., 2005), respectively. For the ^{13}C NMR, chemical shifts for Cp are recorded at δ 79.89; -CH_2 at δ 29.45; $C_6H_5CH_2$- at δ 126.70, 129.40, 129.68 and 142.08, respectively (refer to Appendix C). Terminal CO that assigned at δ 226.50 is supported by the previous literature that reported about the difference between terminal CO and bridging CO by using ^{13}C NMR instrument (Cronin, Wilkinson, & Todd, 1975; Harris, Rosenberg, & Roberts, 1974; Hickey, Wilkinson, & Todd, 1979).

[$(CpFe)_3(\mu\text{-}CO)_2(\mu_3\text{-}Se)(C_6H_5CH_2Se)$] (5)

Complex **5** in crystalline form is used for the NMR study. Different from the complex **2**,**3** and **4**, complex **5** is a trinuclear molecule. The symmetrical complex **2**,**3**, and **4** displayed only one Cp peak in both ^{1}H and ^{13}C NMR spectra in benzene-d_6. Nevertheless, there are two Cp peaks exist as two singlets in both the ^{1}H and ^{13}C NMR spectra of complex **5** in benzene-d_6. Two Cp resonances of relatively intensity 2:1 in the ^{1}H NMR

indicate that both the Cp groups are non-equivalent to each other. This phenomena also reported in the previous study (Haines et al., 1975). The crystal structure of complex **5** in figure 3.7 clearly supported this observation as the Fe(1) and Fe(3) are set in a four legged piano-stool configuration whereas Fe(2) is in a distorted pentagonal pyramidal environment. The different chemically bonding environment between the Fe(2) with Fe(1) and Fe(3) has caused the presence of two Cp peaks in both ^{1}H and ^{13}C NMR spectra (Haines et al., 1975). The Cp signals are recorded at δ 3.85 and δ 4.50, respectively, benzyl group ($-C_6H_5CH_2$) as a doublet and multiplet at δ 7.33-7.35 and 6.96-7.07 (Wong et al., 2005), respectively, and methyl group ($-CH_2$) δ 2.60 (refer to Appendix B).

The ^{13}C NMR chemical shifts for Cp are recorded at δ 81.18 and 85.19, respectively; $-CH_2$ at δ 24.60; $C_6H_5CH_2$ at δ 125.69, 126.38, 129.98 and 141.91, respectively (refer to Appendix C). Different from the complex **2**,**3** and **4**, there is no terminal CO peak present in the ^{13}C NMR spectra of complex **5**. In theory, the oxygen atom with the lower formal charge would be predicted to have lower biding energy (Avanzino & Jolly, 1976). The oxygen atom that presented in the bridging carbonyls have a lower 1s binding energy than terminal carbonyls, and this phenomenon is expected for given the greater back-bonding in the bridging carbonyl (Avanzino & Jolly, 1976; Harris et al., 1974). Therefore, the peak that exist at δ 275.00 is assigned as the bridging CO. The crystal structure of complex **5** that presented in the figure 3.7 clearly emphasised that the existence of bridging CO, not terminal CO.

3.3.4.3 Mass Spectrum

[CpFe(CO)($C_6H_5CH_2Se$)]$_2$ (4)

The EI mass spectrum of complex **4** shows the parent ion *m/z* = 638 [CpFe(CO)(C_7H_7Se)]$_2$ and its fragmentation ions are tabulated in Table 3.5.

Table 3.7. Electrospray ionization mass spectrum of [CpFe(CO)(C_7H_7Se)]$_2$ (4)

m/z	Assignments
638	$[Cp_2Fe_2(CO)_2(C_7H_7Se)_2]^+$
610	$[Cp_2Fe_2(CO)(C_7H_7Se)_2]^+$
584	$[Cp_2Fe_2(C_7H_7Se)_2]^+$
517	$[CpFe_2(C_7H_7Se)_2]^+$
402	$[Cp_2Fe_2Se_2]^+$
347	$[CpFe(CO)_2(C_7H_7Se)]^+$
335	$[CpFe_2Se_2]^+$
319	$[CpFe(CO)(C_7H_7Se)]^+$
293	$[Fe_2(C_2H_2Se)Se]^+$
276	$[Fe_2Se_2]^+$
236	$[CpFe(CO)Se]^+$
211	$[CpFeSe]^+$

[(CpFe)$_3$(μ-CO)$_2$(μ$_3$-Se)(C$_6$H$_5$CH$_2$Se)] (5)

The EI mass spectrum of complex **5** shows the parent ion *m/z* = 667.7 [(CpFe)$_3$(μ-CO)$_2$(μ$_3$-Se)(C$_6$H$_5$CH$_2$Se)] and its fragmentation ions are tabulated in Table 3.6.

Table 3.8. Electrospray ionization mass spectrum of [(CpFe)$_3$(μ-CO)$_2$(μ$_3$-Se)(C$_6$H$_5$CH$_2$Se)] (5)

m/z	Assignments
665	$[Cp_3Fe_3(\mu\text{-}CO)_2(Se)(C_7H_7Se)]^+$
637	$[Cp_3Fe_3(\mu\text{-}CO)(Se)(C_7H_7Se)]+$
612	$[Cp_3Fe_3(Se)(C_7H_7Se)]^+$
513	$[Cp_3Fe_3(Se)(Se)]^+$
450	$[Cp_2Fe_3(Se)(Se)]^+$
381	$[CpFe_3(Se)(Se)]^+$
347	$[CpFe(CO)_2(C_7H_7Se)]^+$
319	$[CpFe(CO)(C_7H_7Se)]^+$
314	$[Fe_3(Se)(Se)_2]^+$
231	$[Fe_3(Se)]^+$

3.3.5 Crystal Structures of $[CpFe(CO)(C_6H_5CH_2Se)]_2$ (4)

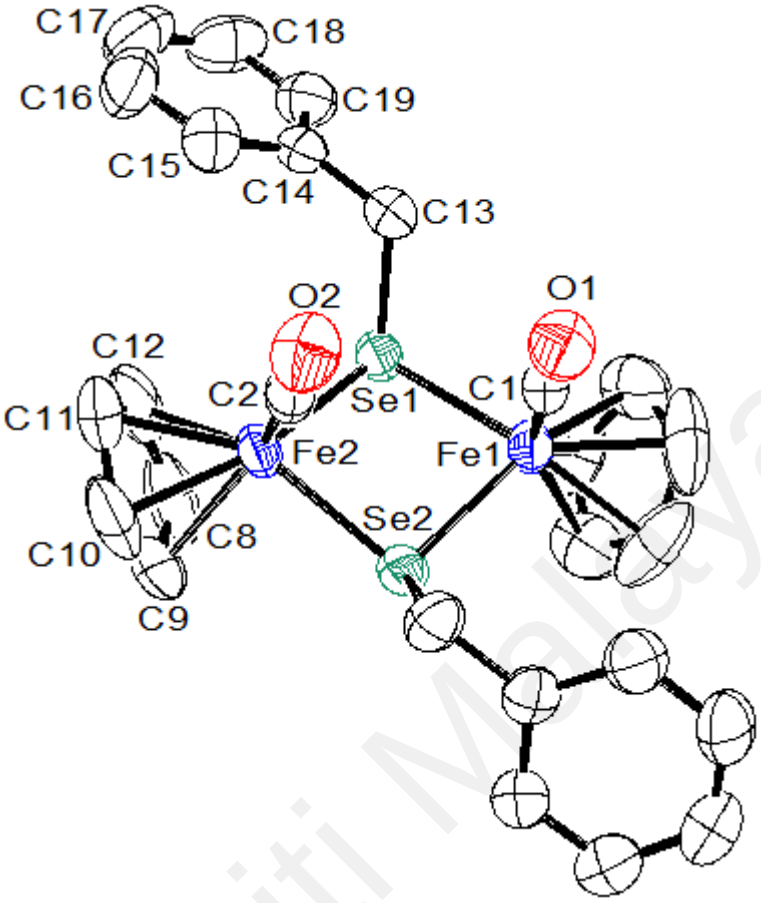

Figure 3.6: Molecular structure of $[CpFe(CO)(C_6H_5CH_2Se)]_2$ (4).

Although **4** was synthesized previously by Ghosh *et al.* (Geetharani et al., 2011), however its crystal structure **4** was not reported. Herein, we report the crystal structure of **4** as illustrated in Figure 3.6 and its bonding parameters as tabulated in Table 3.7. **4** is crystallized in a monoclinic with space group I2/a. The two carbonyl moieties in complex **4** are *cis* to each other. The iron atom is bonded tetrahedrally with two selenium atoms, together with the carbonyl group and cyclopentadienyl ligand. The Fe(1)…Fe(2) separation in **4** with 3.546 Å that calculated by ORTEP indicates that Fe(1)…Fe(2) is not bonded together (Pauling, 1976). The Fe…Fe separation in **4** is slightly longer than the Fe…Fe separation as in **1** and **2**. This implies that the larger size of the chalcogen atom could affect the distance of Fe…Fe separation (Geetharani et al., 2011; Schermer &

Baddley, 1971). However, the absence of metal-metal bonding in **4** is also in agreement according to the 18-electron rule (Ooi et al., 2017; Pauling, 1976).

Table 3.9. Bond lengths [Å] and angles [°] for $[CpFe(CO)(C_6H_5CH_2Se)]_2$ (4)

Bond lengths			
Fe(1)—Se(1)	2.3897(6)	Fe(2)—C(10)	2.068(3)
Fe(1)—Se(2)	2.3657(6)	Fe(2)—C(11)	2.068(3)
Fe(2)—Se(1)	2.3693(5)	Fe(2)—C(12)	2.074(3)
Fe(2)—Se(2)	2.3751(7)	Se(1)—C(13)	1.987(3)
Fe(1)—C(1)	1.737(3)	Se(2)—C(20)	1.997(3)
Fe(2)—C(2)	1.734(3)	O(1)—C(1)	1.152 (3)
Fe(2)—C(8)	2.079(3)	O(2)—C(2)	1.148 (3)
Fe(2)—C(9)	2.074(3)	Fe(1)…Fe(2)	3.546
Bond angles			
Fe(2)—Se(1)—Fe(1)	96.342(18)	C(8)—Fe(2)—Se(2)	104.18(15)
C(13)—Se(1)—Fe(2)	108.34(11)	C(11)—Fe(2)—Se(1)	123.66(14)
C(13)—Se(1)—Fe(1)	106.76(9)	C(11)—Fe(2)—Se(2)	153.05(13)
Fe(1)—Se(2)—Fe(2)	96.835(18)	C(11)—Fe(2)—C(9)	64.53(16)
C(20)—Se(2)—Fe(2)	108.49(9)	C(11)—Fe(2)—C(8)	64.57(17)
C(20)—Se(2)— Fe(1)	107.96(11)	C(11)—Fe(2)—C(12)	38.08(16)
Se(2)—Fe(1)—Se(1)	80.222(16)	C(12)—Fe(2)—Se(1)	93.30(12)
Se(1)—Fe(2)—Se(2)	80.448(16)	C(12)—Fe(2)—Se(2)	142.01(17)
C(10)—Fe(2)—Se(1)	157.26(13)	C(12)—Fe(2)—C(8)	38.85(16)

C(10)—Fe(2)—Se(2)	114.70(15)	C2—Fe(2)—Se(1)	96.72(9)
C(10)—Fe(2)—C(9)	38.36(16)	C2—Fe(2)—Se(2)	94.48(9)
C(10)—Fe(2)—C(8)	64.43(17)	C2—Fe(2)—C(10)	98.73(17)
C(10)—Fe(2)—C(11)	38.62(16)	C2—Fe(2)—C(9)	132.81(18)
C(10)—Fe(2)—C(12)	64.21(16)	C2—Fe(2)—C(8)	158.78(15)
C(9)—Fe(2)—Se(1)	130.38(16)	C2—Fe(2)—C(11)	94.23(16)
C(9)—Fe(2)—Se(2)	91.16(11)	C2—Fe(2)—C(12)	123.51(19)
C(9)—Fe(2)—C(8)	38.53(17)	O(1)—C(1)—Fe(1)	176.3(2)
C(9)—Fe(2)—C(12)	64.54(16)	O(2)—C(2)—Fe(2)	176.4(3)
C(8)—Fe(2)—Se(1)	96.29(13)		

[(CpFe)$_3$(μ-CO)$_2$(μ$_3$-Se)(C$_6$H$_5$CH$_2$Se)] (5)

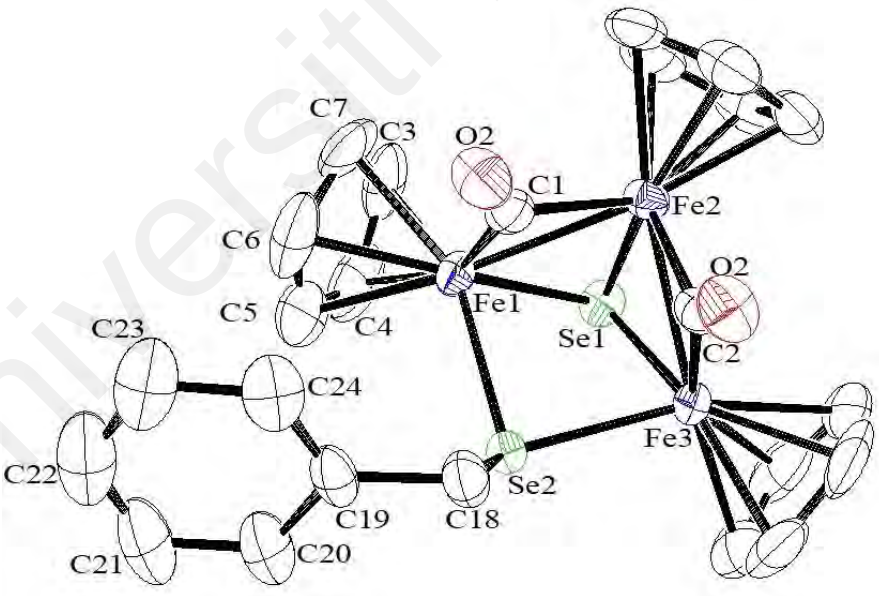

Figure 3.7: Molecular structure of [(CpFe)$_3$(μ-CO)$_2$(μ$_3$-Se)(C$_6$H$_5$CH$_2$Se)] (5).

The crystal structure of **5** is illustrated in Figure 3.7 and its bonding parameters are tabulated in Table 3.8. **5** is crystallized in a monoclinic with space group $P2_1/c$. Fe(1) and Fe(3) are set in a four legged piano-stool configuration whereas Fe(2) is in a distorted pentagonal pyramidal environment. Each Fe atom is coordinated to a cyclopentadienyl

ring in a η^5- mode. Besides, the three Fe atoms that are coordinated to the cyclopentadienyl ligands are connected by two μ_2-CO and this observation is in agreement with the recorded bridging CO absorption peak at 1755 cm^{-1} in the IR spectrum (refer to Appendix A). No terminal CO is observed from the crystal structure of complex **5**. Three Fe atoms are bonded to the same selenium atom, Se(1). The distance between Se(1)-Fe(2) was slightly shorter compared to the distance of Se(1)-Fe(1) and Se(1)-Fe(3) (refer to Table 3.8). The addition of a $C_6H_5CH_2Se$- fragment bridging Se(2) between Fe(1) and Fe(3) gives rise to a different bonding environment for Fe(2) as compared to Fe(1) and Fe(3). This observation can be substantiated from NMR analysis whereby two different Cp signals with intensities of 2:1 ratio are recorded for **5**. This observation also supported by the previous report (Haines et al., 1975). The distance of Fe(1)…Fe(3) measured by Ortep is 3.373 Å which indicates that they are not bonded while there are two single bonds detected (Pauling, 1976) between Fe(1)-Fe(2) (2.5888 Å) and Fe(2)-Fe(3) (2.5945 Å), respectively. We proposed that both Se(1) and $C_6H_5CH_2Se$- have donated three electrons which are being shared by the overall three Fe atoms in order for each of the three Fe atoms to achieve an 18 electrons configuration.

Table 3.10. Bond lengths [Å] and angles [°] for $[(CpFe)_3(\mu\text{-}CO)_2(\mu_3\text{-}Se)(C_6H_5CH_2Se)]$ (5)

Bond lengths			
Se(1)—Fe(1)	2.3061(9)	Fe(2)—C(8)	2.084(5)
Se(1)—Fe(2)	2.2734(9)	Fe(2)—C(9)	2.087(5)
Se(1)—Fe(3)	2.3134(8)	Fe(2)—C(10)	2.085(5)
Se(2)—Fe(1)	2.4028(8)	Fe(2)—C(11)	2.107(5)
Se(2)—Fe(3)	2.3996(8)	Fe(2)—C(12)	2.099(5)

Se(2)—C(18)	1.990(5)	Fe(3)—Fe(2)	2.5945(9)
Fe(1)—C(1)	1.877(5)	Fe(3)—C(2)	1.868(5)
Fe(1)—C(3)	2.078(6)	Fe(3)—C(13)	2.076(6)
Fe(1)—C(4)	2.101(6)	Fe(3)—C(14)	2.072(5)
Fe(1)—C(5)	2.076(6)	Fe(3)—C(15)	2.081(5)
Fe(1)—C(6)	2.089(6)	Fe(3)—C(16)	2.097(6)
Fe(1)—C(7)	2.080(5)	Fe(3)—C(17)	2.089(6)
Fe(2)—Fe(1)	2.5888(9)	O(2)—C(2)	1.189(5)
Fe(2)—C(1)	1.995(5)	O(1)—C(1)	1.168(6)
Fe(2)—C(2)	1.964(5)	Fe(1)—C(3)	3.373

Bond angles

Fe(2)—Se(1)—Fe(1)	96.342(18)	C(8)—Fe(2)—Se(2)	104.18(15)
C(13)—Se(1)—Fe(2)	108.34(11)	C(11)—Fe(2)—Se(1)	123.66(14)
C(13)—Se(1)—Fe(1)	106.76(9)	C(11)—Fe(2)—Se(2)	153.05(13)
Fe(1)—Se(2)—Fe(2)	96.835(18)	C(11)—Fe(2)—C(9)	64.53(16)
C(20)—Se(2)—Fe(2)	108.49(9)	C(11)—Fe(2)—C(8)	64.57(17)
C(20)—Se(2)— Fe(1)	107.96(11)	C(11)—Fe(2)—C(12)	38.08(16)
Se(2)—Fe(1)—Se(1)	80.222(16)	C(12)—Fe(2)—Se(1)	93.30(12)
Se(1)—Fe(2)—Se(2)	80.448(16)	C(12)—Fe(2)—Se(2)	142.01(17)
C(10)—Fe(2)—Se(1)	157.26(13)	C(12)—Fe(2)—C(8)	38.85(16)
C(10)—Fe(2)—Se(2)	114.70(15)	C2—Fe(2)—Se(1)	96.72(9)
C(10)—Fe(2)—C(9)	38.36(16)	C2—Fe(2)—Se(2)	94.48(9)
C(10)—Fe(2)—C(8)	64.43(17)	C2—Fe(2)—C(10)	98.73(17)
C(10)—Fe(2)—C(11)	38.62(16)	C2—Fe(2)—C(9)	132.81(18)
C(10)—Fe(2)—C(12)	64.21(16)	C2—Fe(2)—C(8)	158.78(15)

C(9)—Fe(2)—Se(1)	130.38(16)	C2—Fe(2)—C(11)	94.23(16)
C(9)—Fe(2)—Se(2)	91.16(11)	C2—Fe(2)—C(12)	123.51(19)
C(9)—Fe(2)—C(8)	38.53(17)	O(1)—C(1)—Fe(1)	176.3(2)
C(9)—Fe(2)—C(12)	64.54(16)	O(2)—C(2)—Fe(2)	176.4(3)
C(8)—Fe(2)—Se(1)	96.29(13)		

3.4 CO-Release Tests

3.4.1 Stability of the complexes

UV-Vis spectroscopy was utilized to determine the stability of the compound **2-4** as the previous literature reported (Liu et al., 2015). Compound **2-4** were first dissolved in THF (60 μM), then transferred into phosphate buffer saline (PBS). No decomposition of solid materials was observed in the dark and UV (with 365 nm light). The stability tests of compound **2-4** in the dark were carried out in three hours and no significant changes were observed from the UV-Vis spectra. All three compounds were very stable in the dark as shown in Figure 3.8-Figure 3.10.

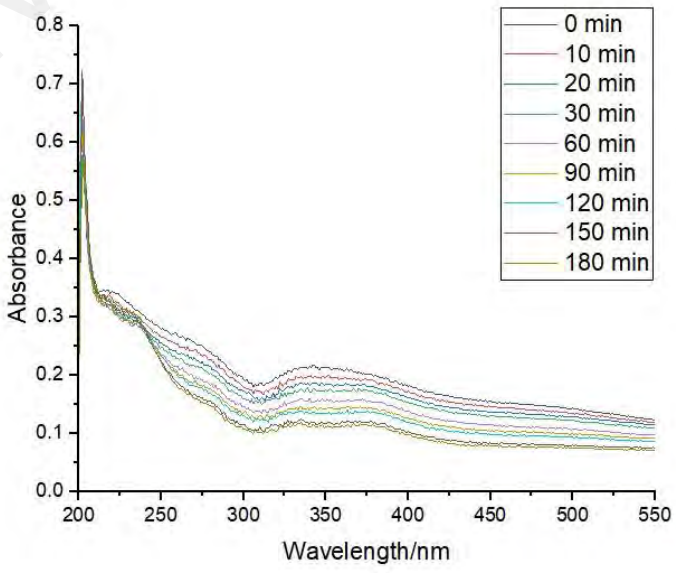

Figure 3.8: UV-Vis spectra of compound 2 in the dark.

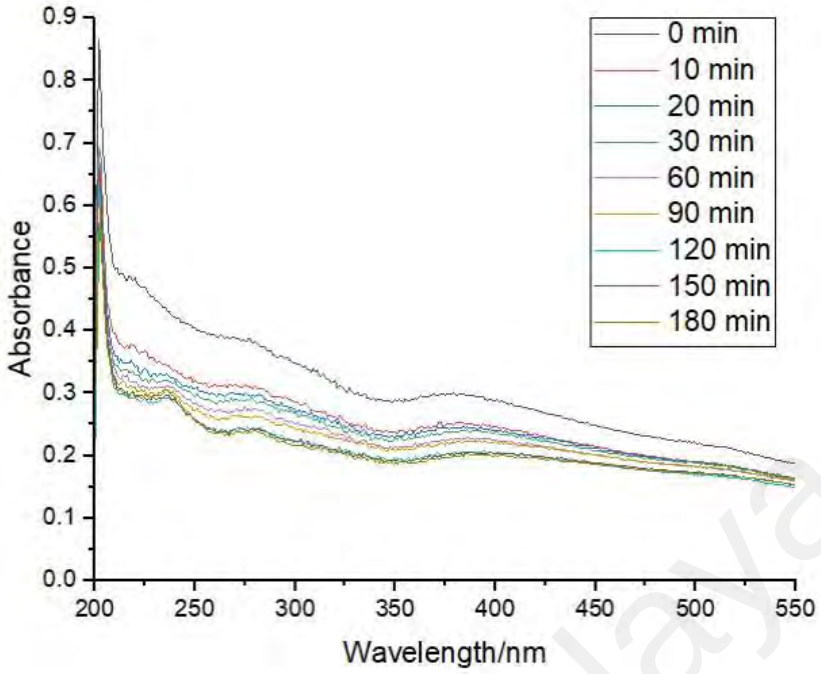

Figure 3.9: UV-Vis spectra of compound 3 in the dark.

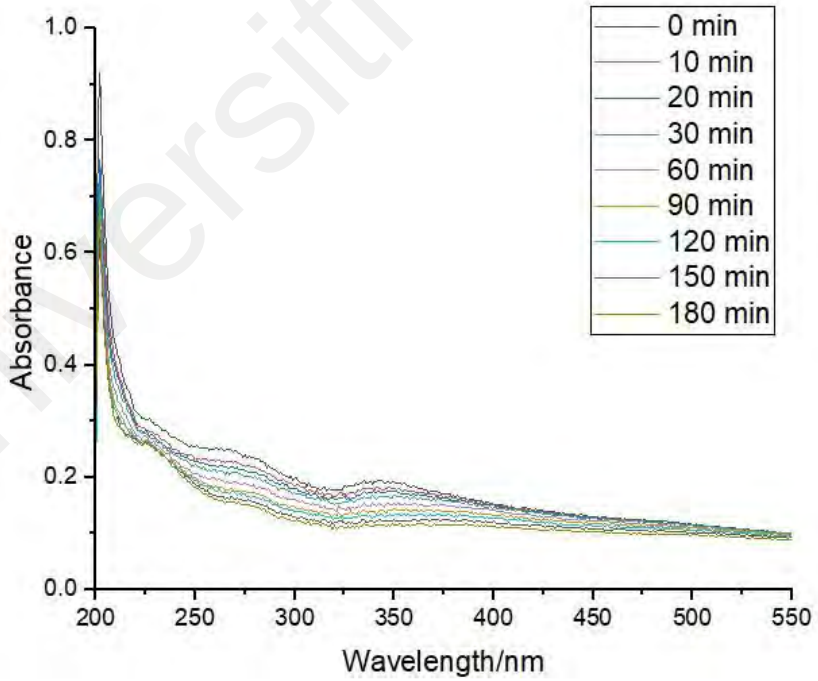

Figure 3.10: UV-Vis spectra of compound 4 in the dark.

The stability tests of compound **2-4** in UV were carried out within two hours with the irradiation of 365 nm UV light. The significant changes were observed from the UV-Vis

spectra after the compound **2**-**4** were irradiated with 365 nm UV light. Apparently, the changes in the absorbance were detected after 10 minutes irradiation with 365 nm UV light was applied to compound **2**-**4**. No further changes were observed from the UV-Vis spectra for the subsequent irradiations as demonstrated in Figure 3.11-Figure 3.13. This result revealed that compound **2**-**4** were sensitive to the UV light. Therefore, UV light utilization was needed in conducting the CO-release tests for compound **2**-**4**.

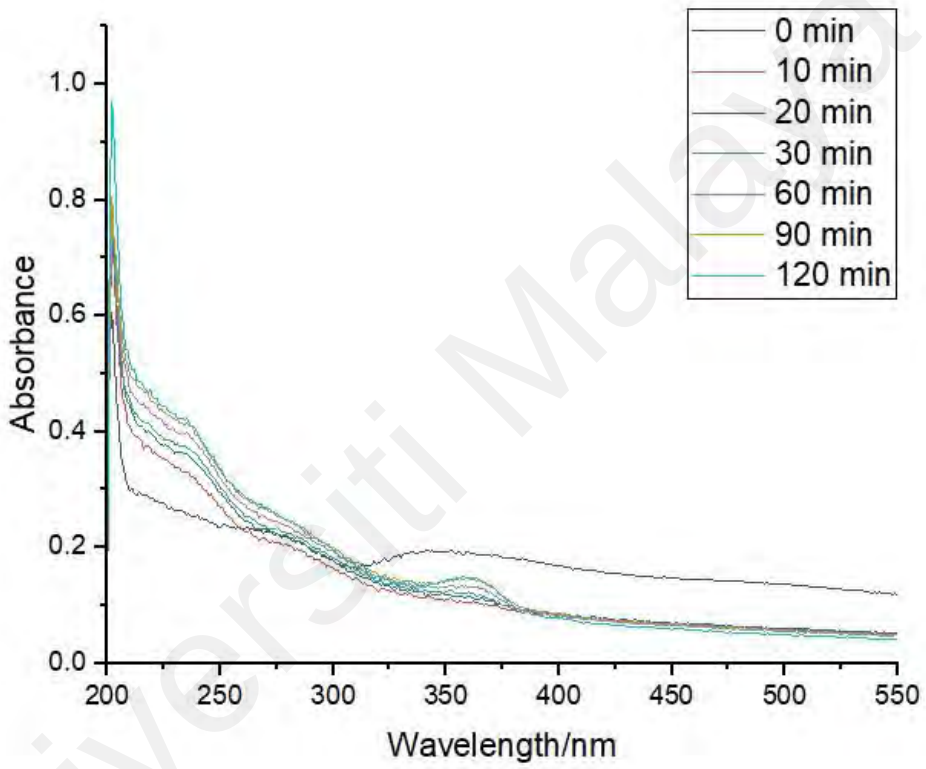

Figure 3.11: Change of the absorption spectra of 2 with 365 nm UV light.

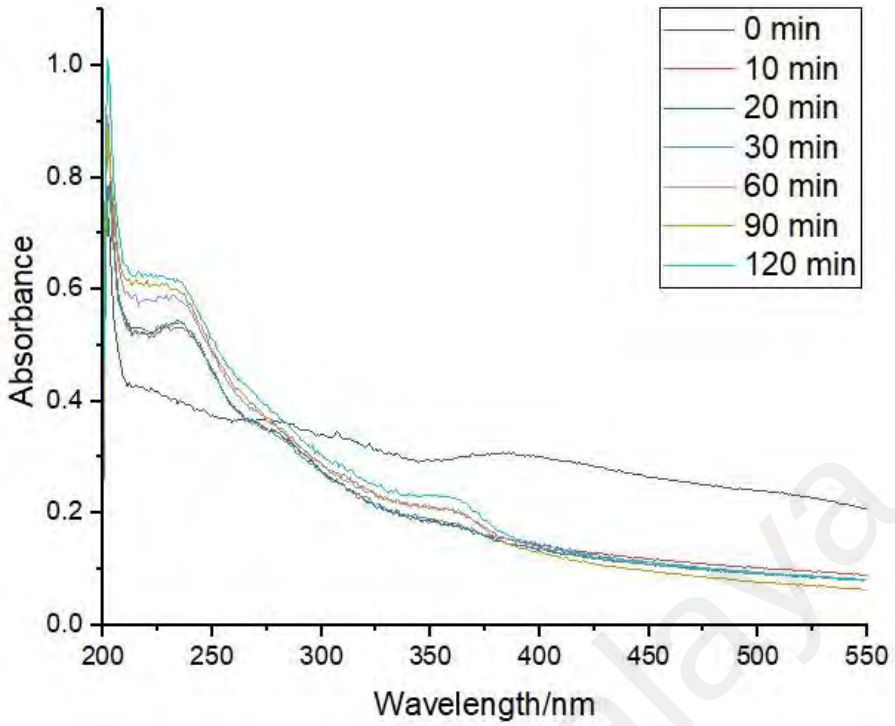

Figure 3.12: Change of the absorption spectra of 3 with 365 nm UV light.

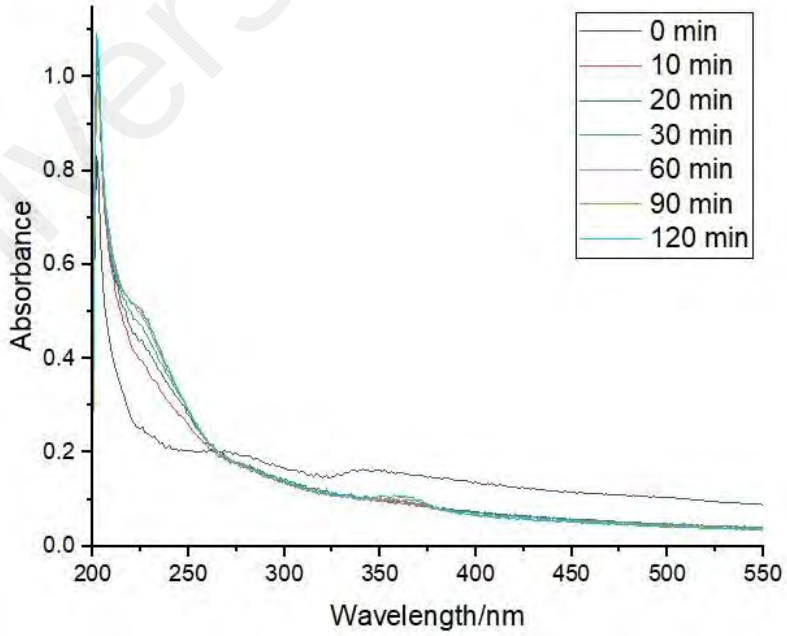

Figure 3.13: Change of the absorption spectra of 4 with 365 nm UV light.

3.4.2 Myoglobin Assay

Metal carbonyl complexes could release CO in several ways (Crook et al., 2011; Dördelmann, Pfeiffer, Birkner, & Schatzschneider, 2011; Klein et al., 2014; McLean, Mann, & Poole, 2012; Motterlini et al., 2002; Motterlini et al., 2005). The releasing of CO could be caused by a substitution reaction or decomposition. Most of the metal carbonyl compounds are UV-visible light sensitive. Light could be used to initiate and trigger the cytotoxic activity of inert prodrugs with fine spatial and temporal control. Therefore, utilization of UV-Vis light is an appropriate method for CO-releasing and these kinds of light-sensitive CORMs are called photoCORMs (Schatzschneider, 2010, 2011). The CO-releasing properties of the carbonyl complexes prepared in this study was determined by the myoglobin assay (Rimmer, Richter, & Ford, 2010). In principle, UV-vis spectrophotometer is used to monitor the CO-released by the CORMs, which resulted in the transformation of deoxymyoglobin (deoxyMb) to carbonmonoxymyoglobin (MbCO). Two maxima at 540 nm and 577 nm were given by MbCO while deoxyMb only provided one maximum at 557 nm in the UV-Vis spectra. As a result of this, the CO-releasing tests by CORMs became measurable and detectable.

Figure 3.14, 3.15 and 3.16 demonstrated the CO-release profile for compound **2**,**3** and **4**. With the irradiation of 365 nm UV light, the changes of absorption of deoxyMb for a 60 μM solution of **2**,**3** and **4** were observed in 0.01 M PBS (pH=7.4). The correction of the CORM absorbance and the data treatment were referred to the previous report (Atkin et al., 2011).

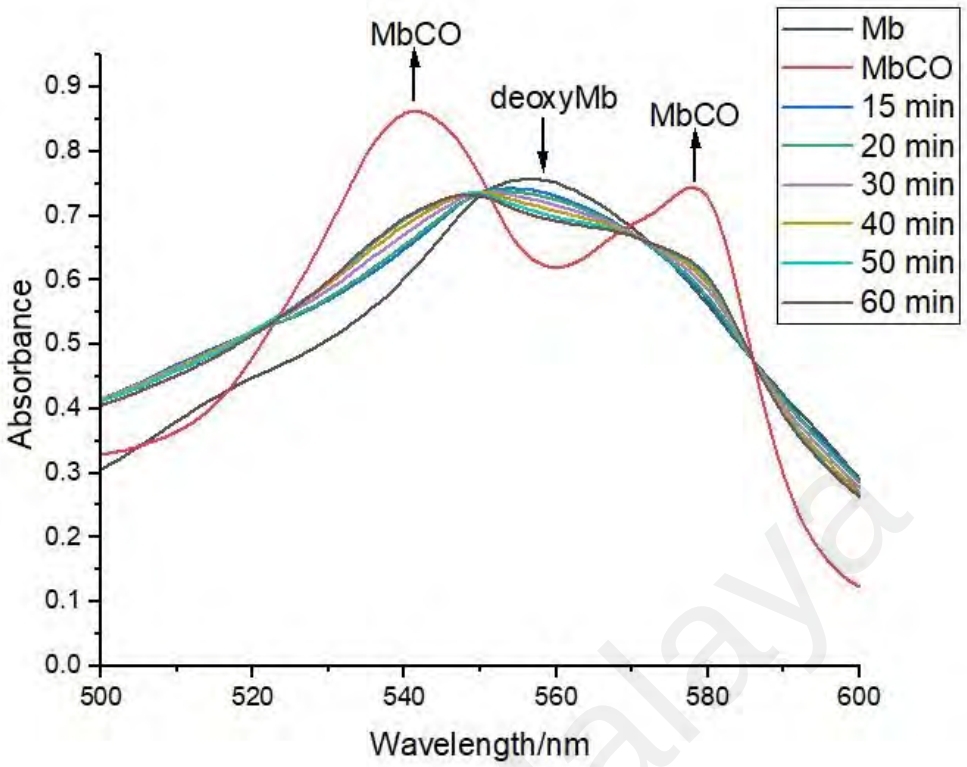

Figure 3.14: CO-release profile for a 60 µM solution of 2.

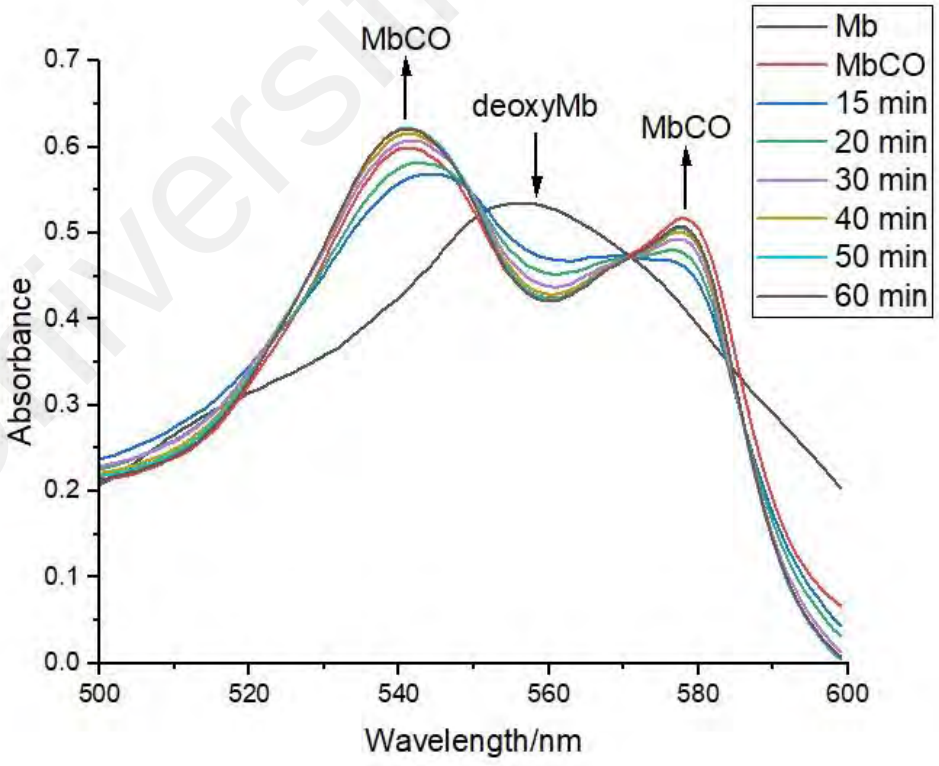

Figure 3.15: CO-release profile for a 60 µM solution of 3.

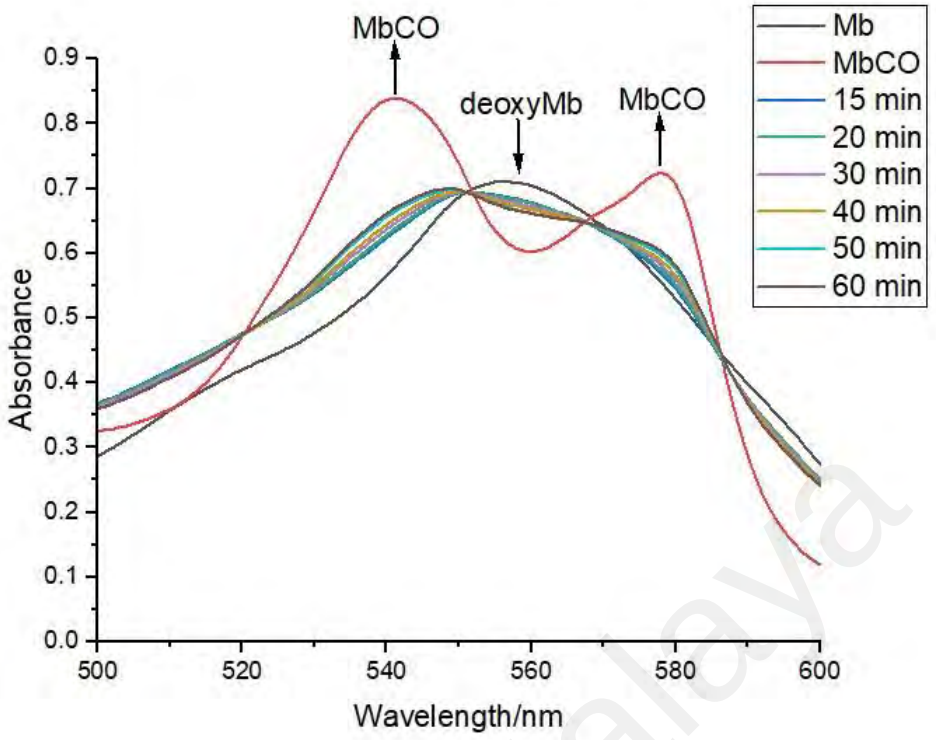

Figure 3.1618: CO-release profile for a 60 µM solution of 4.

The entire myoglobin assay measurement was carried out for 60 min in this study in 1 min intervals with a 365-nm UV lamp. CO-releasing properties of compound **2-4** were tabulated in Table 3.9. The half-life ($t_{1/2}$) of compound **2-4** and their equivalent of CO-released were calculated based on the standard myoglobin assay data treatment procedure (Atkin et al., 2011). In this study, half-life ($t_{1/2}$) of carbonyl complexes was defined as the time taken for 60 µM solution of the metal carbonyl complexes to produce a 30 µM of Mb-CO concentration.

Table 3.11. CO-release data for compounds 2-4

Compound	Half-life $t_{½}$ [min]	Equivalent of CO-released
2	56.5[a]	0.5
3	26.9	0.6
4	55[a]	0.4

[a] Time taken to achieve a Mb-CO concentration of 15μM.

The CO-releasing properties of **2-4** in the presence of UV were supported by the previous literature (Bitterwolf, Scallorn, & Li, 2000) that had already demonstrated the loss of CO of the isomers of the methylthiol derivative of $(\eta^5\text{-}C_5H_5)_2Fe_2(CO)_2(\mu\text{-}SR)_2$ due to the low energy photolysis into the πd → LUMO transition. From the result, **3** had a shorter half-life of 26.9 min among three metal carbonyl complexes. The 0.6 equivalents of total carbon monoxide that released by **3** was also the highest among all the three metal carbonyl complexes. In short, **3** released the CO more faster and efficient than **2** and **4**. However, compared to the standard CORM, which is CORM-2 (Tricarbonyldichlororuthenium (II) dimer) and CORM-3 (Tricarbonylchloro(glycinato)ruthenium (II)) (Motterlini & Otterbein, 2010), these three CORMs have present a longer half-life. This difference could be due to the presence of the electron-withdrawing Cl in CORM-2 and CORM-3 that tends to weaken the Ru-CO bonding, resulting in a faster CO-release rate. In contrast to **2-4**, the donor ability of both sulfur and selenium increases the electron density on the metal centre, strengthening the metal-CO π-backbonding and stabilized the metal carbonyl complexes. Consequently, this will hinder their CO-releasing ability. The longer half-life of complexes **2-4** also indicated that complexes **2-4** are able to emit CO in a slower and controllable way with the utilization of UV at 365nm, as the CORM with a longer half-life is more functional and stable (Gao et al., 2018; Long et al., 2013).

3.5 Biological Assays

3.5.1 MTT Cytotoxicity Assay

The interest of this study was to determine the cytotoxic activity of compound **2-4** against human breast cancer cell line (MCF-7, MDA-MB-231 and MDA-MB-468) upon UV irradiation at 365 nm. Anticancer activities of these three iron-containing carbonyl complexes were determined *in vitro* via MTT assay. The MTT assay was carried out in

the dark and in the present of UV at 365nm. Before treating the cultivated cells, all the compounds were dissolved in THF and diluted in DMEM. The results were given in Table 3.10.

Table 3.12. IC_{50} Value (μM) of 2-4 against the human breast cancer cell lines.

Compound	IC_{50} in μM					
	MCF-7		MDA-MB-231		MDA-MB-468	
	Dark	UV	Dark	UV	Dark	UV
2	9.6 ± 0.2	17.5 ± 2.9	18.5 ± 3.9	10.8±1.0	>100	6.1 ± 0.3
3	>100	>100	>100	>100	49.8 ± 11.3	11.5 ± 2.7
4	37.8 ± 1.9	>100	23.5 ± 2.0	>100	25.9 ± 0.4	27.9 ± 1.9
Cisplatin[a]	24.7 ± 2.1	-	21.1 ± 3.9	-	5.3 ± 0.4	-

[a] Positive control, cisplatin was served as a reference standard.

All three compounds were cytotoxic towards the breast cancer cell lines in the dark as well as in the presence of UV light. The main purpose of this study was to investigate the effect of CO-release of the compounds on cytotoxicity upon UV irradiation against the human breast cancer cell lines. The potency of metal carbonyl complexes as anticancer agent had been reported by previous researcher through a unique light-controlled CO delivery (Carrington et al., 2013; Chakraborty et al., 2015). **3** with the shortest half-life in CO-releasing only showed mild cytotoxic effect towards MDA-MB-468 cell line in the dark. Its cytotoxic effect was increased about four times against MDA-MB-468 cell line upon UV irradiation. However, UV light irradiation did not improve its cytotoxicity against MCF-7 and MDA-MB-231 cell lines. Potent growth inhibitory effect at 9.6±0.2 and 18.5±3.9 μM was observed for **2** when tested with MCF-7 and MDA-MB-231 cell lines in the dark. Apart from the slight improvement in cytotoxicity of **2** against the MDA-

MB-231 cell, the growth-inhibitory effect of **2** increased significantly against the MDA-MB-468 cell line upon UV light irradiation. This further exemplified the importance of CO released in enhancing the cytotoxicity of **2** towards the triple-negative breast cancer cell lines (MDA-MB-231 and MDA-MB-468), that are more aggressive and harder to treat. The only anomaly, is the slight decrease in cytotoxicity of **2** under UV towards MCF-7. It is noteworthy that **2** is the most active photoCORMs tested for all cell lines under UV irradiation. On the other hand, **4** displayed moderate growth-inhibitory effect when tested with MCF-7, MDA-MB-231 and MDA-MB-468 cell lines in the dark. Surprisingly, there was a dramatical decrease in the cytotoxicity of **4** against MCF-7 and MDA-MB-231 cell lines under UV. Meanwhile, the growth-inhibitory effect of **4** towards MDA-MB-468 cell line was also slightly decreased in the presence of UV. This indicated that UV light irradiation actually decreased the cytotoxicity of **4** in all three breast cancer cell lines in contrast to compound **2** and **3**. Taken together, **2** is the most promising compound for having lower IC_{50} than cisplatin for most of the tested cell lines in the dark and under UV irradiation.

3.5.2 Determination of *in vitro* Antiplasmodial activity

The experiment on antiplasmodial activities of **2**-**4** were performed in duplicates. The IC_{50} values of **2**-**4** against *P. falciparum* 3D7 strains were determined by using the GraphPad Prism 7 software (Graphpad software Inc., CA, USA). Table 3.11 presented the activities of **2**-**4** against *P. falciparum* 3D7 strains. It was concluded that **2**-**4** were not active against the parasite.

Table 3.13. IC_{50} for *P. falciparum* 3D7 strains.

Complexes	IC_{50} (μM)
2	>25
3	>25
4	>25
Chloroquine[a]	4.69 ± 0.26

[a] Positive control.

3.5.3 ADME Properties

The physicochemical, pharmacokinetics and drug like parameters of **2**-**4** were determined by using SwissADME tool (Daina et al., 2017). **2**-**4** exhibited a topological polar surface area (TPSA) value lower than 140 $Å^2$, which suggested that they all had the certain cell membrane permeability. The number of rotatable bonds displayed by **2**-**4** was related to the intestinal adsorption. In this case, **4** exhibited a better absorption than **2** and **3** as it had more rotatable bond than **2** and **3**. Besides, all the complexes were suggested to have a high skin permeation ability according to their Log K_p parameters. The more negative the value of log K_p, the less skin permeation is the compound. Lipophilicity, the essential physicochemical parameter for pharmacokinetics drug discovery (Arnott & Planey, 2012) was described by the partition coefficient between *n*-octanol and water (log $P_{o/w}$) (Daina et al., 2017). Literature reported that the log *P value of* optimum range for lipophilicity to achieve a good availability should fall between ~1 and 3 (Arnott & Planey, 2012). By using SwissADME tool, **2**, **3** and **4** were predicted to exhibit the similar lipid water partition coefficients of 4.51, 4.41 and 4.01. This showed that all three complexes were more lipophilic. The results were tabulated in Table 3.12.

Table 3.14. Prediction of ADME properties of 2-4.

Compound	M.W.	Consensus log $P_{o/w}$	No. H-Bond Acceptors	No. H-Bond donors	TPSA (≤140 Å^2)	Log K_p (skin permeation/cm/s)	Rotatable bond	Blood-brain barrier (BBB) permeant
2	528.33	4.51	2	0	50.60	-0.99	2	No
3	528.29	4.41	2	0	107.08	-1.33	2	No
4	638.08	4.01	2	0	0.00	-2.51	4	No

CHAPTER 4: EXPERIMENTAL

4.1 General Procedures

All reactions were carried out by using the conventional Schlenk techniques under an inert atmosphere of argon. The work-up procedure and the isolation of the products were carried out in a Vacuum Atmosphere Dribox which was equipped with a HE-493 dri-train.

4.1.1 Physical Measurements

I.R. spectra were obtained by using Perkin-Elmer RX1 FTIR spectrophotometer. ^{1}H and ^{13}C NMR spectra were measured on deuterated benzene on a Jeol EDX 400 MHz FT-NMR spectrometer. ^{1}H and ^{13}C chemical shifts were referenced to residual C_6H_6 in C_6D_6. Elemental C, H and S analyses were performed by a Thermo Scientific Flash 2000 elemental analyser. Mass spectrometry measurements were performed by direct probe on Shimadzu GCMS-QP2010 Plus in Universiti Tunku Abdul Rahman Kampar Campus. Single crystal X-ray diffractometry services were analysed by using a Rigaku Oxford (formerly Agilent Technologies) Super Nova Dual diffractometer with Cu Kα (λ = 1.54184 Å) radiation at 160 – 170K in the X-ray Crystallography Laboratory of the Chemistry Department in University of Malaya.

4.1.2 Solvents and Reagents

Cyclopentadienylirondicarbonyl dimer, $[CpFe(CO)_2]_2$ (**1**) was purchased from Fluka company while dicyclohexyl disulfide, 2-thienyl disulfide, myoglobin (lyophilized horse skeletal muscle, 95%-100%), sodium dithionite and phosphate buffered saline tablet with highest purity were purchased from Sigma Aldrich Chemical Company and dibenzyl diselenide was purchased from Acros Organics. Silica gel (Merck Kieselgel 60) and TLC

plates (Merck Kieselgel $^{60}F_{254}$) were dried overnight at 140 °C before use. All the AR grade solvents were dried with sodium and benzophenone under the argon prior to use.

4.2 Reaction of $[CpFe(CO)_2]_2$ (1) with dicyclohexyl disulfide

A magenta solution of $[CpFe(CO)_2]_2$ (**1**) (500 mg, 1.413 mmol) and dicyclohexyl disulfide (0.62 mL, 2.825 mmol) in toluene (20 mL) were allowed to refluxed at 110 ˚C under stirring overnight. The final colour of the reaction mixture was dark brown after 21 h of reaction. A sample of the mixture was spotted on a TLC plate and developed using a mixture of hexane, toluene and ether (2:1:1/3 v/v). From TLC analysis, the reaction mixture showed two spots indicating the presence of two products, a yellow and a pink spot were observed at R_f = 0.74 and 0.72, respectively. The reaction mixture was then filtered through a sintered filter funnel layered with 1cm of celite. The mixture was then concentrated under vacuum to *ca.* 1.5 mL and loaded onto a silica gel packed column (1.5 x 11 cm) prepared in *n*-hexane. From column chromatography, two fractions were obtained:

(i) A yellowish-brown fraction was eluted by using *n*-hexane/toluene (35 mL, 4:2 v/v) as eluent. The collected fraction was concentrated to dryness under vacuum and recrystallized from toluene layered with ether to give fine crystalline yellowish-brown solids of $[CpFe(CO)(C_6H_{11}S)]_2$ (**2**) (161 mg, 21.6% yield). ^{1}H NMR (benzene-d_6): δ 4.17 (*s*, Cp), δ 1.76-1.79 (*d*, -CH_2), δ 1.60-1.64 (*d*, -CH_2), δ 1.46-1.49 (*d*, -CHS), δ 1.26-1.35 (*q*, -CH_2), 0.98-1.08 (*q*, -CH_2), 0.60-0.68 (*q*, -CH_2). ^{13} C NMR (benzene-d_6): δ 26.84 (C_6H_{11}), δ 35.29 (C_6H_{11}), δ 47.66 (C_6H_{11}), δ 81.99 (Cp), δ 225.30 (CO). I.R.: ν(CO) at 1946 (s), 1905 (m); ν(C-H stretching) at 2923 (vs), 2853 (vs); ν(C-S stretching) at 1195 (vw), 1171 (vw); ν(C-H bending) at 1462 (m), 1377 (w), 1342 (vw), 1261 (m) (Nujul mull, cm^{-1}). Anal. Calcd. for $[CpFe(CO)(C_6H_{11}S)]_2$ (**2**): C, 54.59; H, 6.11; S, 12.24%. Found: C, 54.93; H, 5.99; S, 12.28%.

(ii) A pink fraction was eluted by using *n*-hexane/toluene (25 mL, 1:1 v/v) as eluents. The fraction was concentrated under vacuum to give a dark brownish pink oily residue. Attempts to purify and recrystallize this fraction was futile mainly because it decomposed eventually.

4.3 Reaction of $[CpFe(CO)_2]_2$ (1) with 2-thienyl disulfide

A magenta solution of $[CpFe(CO)_2]_2$ (**1**) (500 mg, 1.413 mmol) and 2-thienyl disulfide (651 mg, 2.825 mmol) in toluene (20 mL) were refluxed at 110 ˚C under stirring overnight. The resultant reaction mixture has changed to a dark orangy-brown colour after 18 hours. A sample of the mixture was spotted on a TLC plate and developed using a mixture of hexane, toluene and ether (2:1:1/3 v/v). From TLC analysis, the reaction mixture showed two spots indicating the presence of two products, a brownish orange and a dark brown spot were observed at R_f = 0.66 and 0.49, respectively. The reaction mixture was then filtered through a sintered filter funnel layered with *ca.*1 cm of celite. The mixture was then concentrated under vacuum to *ca.* 1.5 mL and loaded onto a silica gel packed column (1.5 x 11 cm) prepared in *n*-hexane. Column chromatography gave two fractions:

(i) An orangy brown solution was eluted using *n*-hexane/toluene (40 mL, 1:1 v/v) as eluent. The fraction was concentrated to dryness under vacuum and recrystallized from toluene layered with ether to yield fine orangy-brown crystalline solids of $[CpFe(CO)(C_4H_3S_2)]_2$ (**3**) (197 mg, 26.41% yield). ^{1}H NMR (benzene-d_6): δ 4.17 (*s*, Cp), δ 6.65 – 6.67 (*t*, $C_4H_3S_2$), 6.79-6.80 (*d*, $C_4H_3S_2$), 6.95 (*s*, $C_4H_3S_2$). ^{13}C NMR (benzene-d_6): δ 80.83 (Cp), δ 125.87, 127.73, 131.11, 148.78 ($C_4H_3S_2$) and δ 223.43 (CO). I.R.: ν(CO) at 1966 (vs), 1942 (m), 1901 (sh); ν(C-H stretching) at 1403 (w); 1207 (vw); ν(=C-H bending) at 837 (w), 818 (m), 701 (w), 676 (m), 562 (m), 546 (w) (Nujul mull, cm^{-1}).

Anal. Calc. for $[CpFe(CO)(C_4H_3S_2)]_2$ (**3**): C, 45.47; H, 3.05; S, 24.28%. Found: C, 45.99; H, 3.11; S, 24.45%.

(ii) A dark brown solution was eluted using toluene (25 mL) as eluent. The collected fraction was concentrated under vacuum, but an oily residue was obtained. Attempts to purify and recrystallize this fraction was futile mainly because it decomposed eventually.

4.4 Reaction of $[CpFe(CO)_2]_2$ (1) With Dibenzyl Diselenide

A magenta solution of $[CpFe(CO)_2]_2$ (**1**) (500 mg, 1.413 mmol) and dibenzyl diselenide (961 mg, 2.825 mmol) in toluene (20 mL) were refluxed at 110 ˚C under stirring overnight. The colour of the reaction mixture changed to a dark brown colour after 20 hours. A sample of the mixture was spotted on a TLC plate and developed using a mixture of hexane, toluene and ether (2:1:1/3 v/v). From TLC analysis, the reaction mixture showed two spots indicating the presence of two products, a yellowish-brown and greenish-black spot were observed at R_f = 0.73 and 0.3, respectively. The reaction mixture was then filtered through a sintered filter funnel layered with *ca.* 1cm of celite. The mixture was then chromatographed onto a silica gel packed column (1.5 x 11 cm) prepared in *n*-hexane. Two fractions were separated during chromatography:

i) A yellowish-brown fraction was eluted by using *n*-hexane/toluene (4:2 v/v) as eluents. The fraction was concentrated and recrystallized from toluene layered with ether to give fine crystalline yellowish-brown solids of $[CpFe(CO)(C_6H_5CH_2Se)]_2$ (**4**) (180 mg, 19.97% yield). ^{1}H NMR (benzene-d_6): δ 3.31 (*s*, CH_2), δ 3.85 (*s*, Cp), δ 6.98-7.05 (*m*, C_6H_5-), δ 7.39-7.40 (*d*, C_6H_5-). ^{13} C NMR (benzene-d_6): δ 29.45 (CH_2), δ 79.89 (Cp), δ 126.70, 129.40, 129.68, 142.08 (C_6H_5-), δ 226.50 (CO). I.R.: ν(CO) at 1960 (sh), 1927 (vs), 1886 (m); ν(Ar C-H stretching) at 2923 (vs), 2864 (vs); ν(Ar C=C stretching) at 1598 (w), 1581 (w), 1492 (w); ν(=C-H bending) at 835 (sh), 820 (m), 757 (m), 697 (m) (Nujul mull, cm$^-$

[1]). Anal. Calc. for $[CpFe(CO)(C_6H_5CH_2Se)]_2$ (**4**): C, 48.94; H, 3.79%. Found: C,49.31; H, 4.20%.

ii) A dark green fraction was eluted by using toluene as eluent. The collected fraction was recrystallized from toluene layered with ether to give fine crystalline greenish-black solids of $C_{24}H_{22}O_2Se_2Fe_3$ (**5**) (29mg, 3% yield). ^{1}H NMR (benzene-d_6): δ 2.60 (*s*, -CH_2-S), δ 4.50, 3.85 (*s*, Cp), δ 6.96-7.07 (*m*, C_6H_5-), δ 7.33-7.35 (*d*, C_6H_5-). ^{13} C NMR (benzene-d_6): δ 24.60 (CH_2), δ 81.18, 85.19 (Cp), δ 125.69, 126.38, 129.98, 141.91 (C_6H_5-), δ 275.00 (μ_2-CO). I.R: ν(μ_2-CO) at 1762 (vs), 1723 (s); ν(Ar C-H stretching) at 2924 (vs), 2864 (vs); ν(Ar C=C stretching) at 1490 (w), 1460 (s), 1416 (w), 1376 (m); ν(=C-H bending) at 817 (w), 745 (w), 690 (w), 608 (w) (Nujul mull, cm^{-1}). Anal. Calc. for $C_{24}H_{22}O_2Se_2Fe_3$ (**5**): C, 43.16; H, 3.32%. Found: C, 43.27; H, 3.40%.

4.5 Crystal Structures Determination

4.5.1 Structure determination of $[CpFe(CO)(C_6H_{11}S)]_2$ (2)

Diffraction quality single crystals of **2** were acquired as yellowish-brown crystalline plates which were grown in toluene layered with ether after 2 days at -28˚C. The features and details of crystal data collection, parameters and refinement of structure were given in Table 4.1. The structure was solved and refined by using OLEX2 (Dolomanov, Bourhis, Gildea, Howard, & Puschmann, 2009). Atoms of crystal structure were labelled using ORTEP-3 (Farrugia, 2012), whereas the details of crystallographic information were collected, edited and formatted by using pubCIF (Westrip, 2010).

4.5.2 Structure determination of $[CpFe(CO)(C_4H_3S_2)]_2$ (3)

Diffraction quality single crystals of **3** were acquired as fine orangy-brown crystalline solids which were grown in toluene layered with ether after 2 days at -28˚C. The features

and details of crystal data collection, parameters and refinement of structure were tabulated in Table 4.2. The structure was solved and refined by using OLEX2 (Dolomanov et al., 2009). Atoms of crystal structure were labelled using ORTEP-3 (Farrugia, 2012), whereas the details of crystallographic information were collected, edited and formatted by using pubCIF (Westrip, 2010).

4.5.3 Structure determination of $[CpFe(CO)(C_6H_5CH_2Se)]_2$. (4)

Diffraction quality single crystals of **4** was obtained as fine yellowish-brown crystalline solids which were grown in toluene layered with ether after 2 days at -28˚C. The features and details of crystal data collection, parameters and refinement of structure were given in Table 4.3. The structure was solved and refined by using OLEX2 (Dolomanov et al., 2009). Atoms of crystal structure were labelled using ORTEP-3 (Farrugia, 2012), whereas the details of crystallographic information were collected, edited and formatted by using pubCIF (Westrip, 2010).

4.5.4 Structure determination of $C_{24}H_{22}O_2Se_2Fe_3$ (5)

Diffraction quality single crystals of **5** was obtained as greenish-black needles which were grown in toluene layered with ether after 3 days at -28˚C. The features and details of crystal data collection, parameters and refinement of structure were given in Table 4.4. The structure was solved and refined by using OLEX2 (Dolomanov et al., 2009). Atoms of crystal structure were labelled using ORTEP-3 (Farrugia, 2012), whereas the details of crystallographic information were collected, edited and formatted by using pubCIF (Westrip, 2010).

Table 4.15. Crystal data and structure refinement for $[CpFe(CO)(C_6H_{11}S)]_2$ (2)

Complex	$[CpFe(CO)(C_6H_{11}S)]_2$ (**2**)
Empirical formula	$C_{24}H_{32}Fe_2O_2S_2$
Formula weight	528.31
Temperature (K)	293
Crystal system	Monoclinic
Space group	$P2_1/c$
Unit cell dimensions	
a (Å)	10.0162 (7)
b (Å)	22.6512 (13)
c (Å)	11.1713 (8)
β (°)	111.623 (8)
V (Å^3)	2356.2 (3)
Z	4
Density (mg m^{-3})	1.489
Absorption coefficient, μ (mm^{-1})	1.43
F(000)	1104
Crystal size	0. 4 × 0.4 × 0.2
Reflection collected	5341
Independent reflections (R_{int})	5341 (0.025)
Data/restraints/parameters	5341/0/271
$R[F^2 > 2\sigma(F^2)]$	0.038
$wR(F^2)$	0.089
S	1.06
Largest difference peak and hole (eÅ^{-3})	0.36 and −0.40

Table 16. Crystal data and structure refinement for $[CpFe(CO)(C_4H_3S_2)]_2$ (3)

Complex	$[CpFe(CO)(C_4H_3S_2)]_2$ (**2**)
Empirical formula	$C_{20}H_{18}Fe_2O_2S_4$
Formula weight	530.28
Temperature (K)	293
Crystal system	Monoclinic
Space group	*C*2/*c*
Unit cell dimensions	
a (Å)	15.0522 (2)
b (Å)	10.78435 (16)
c (Å)	12.75162 (19)
β (°)	97.5476 (14)
V (Å^3)	2052.01 (5)
Z	4
Density (mg m^{-3})	1.716
Absorption coefficient, μ (mm^{-1})	15.26
F(000)	1080
Crystal size	0. 2 × 0.2 × 0.2
Reflection collected	2050
Independent reflections (R_{int})	2050 (0.032)
Data/restraints/parameters	2050/0/128
$R[F^2 > 2\sigma(F^2)]$	0.050
$wR(F^2)$	0.140
S	1.07
Largest difference peak and hole (eÅ^{-3})	0.77 and −0.81

Table 17. Crystal data and structure refinement for $[CpFe(CO)(C_6H_5CH_2Se)]_2$ (4)

Complex	$[CpFe(CO)(C_6H_5CH_2Se)]_2$ (**4**)
Empirical formula	$C_{26}H_{24}Fe_2O_2Se_2$
Formula weight	626.02
Temperature (K)	293
Crystal system	Monoclinic
Space group	*I*2/*a*
Unit cell dimensions	
a (Å)	18.554 (3)
b (Å)	12.209 (3)
c (Å)	24.418 (5)
β (°)	95.104 (14)
V (Å^3)	5509.4 (19)
Z	8
Density (mg m^{-3})	1.509
Absorption coefficient, μ (mm^{-1})	3.71
F(000)	2385
Crystal size	0. 2 × 0.2 × 0.1
Reflection collected	5564
Independent reflections (R_{int})	5564 (0.018)
Data/restraints/parameters	5564/654/345
$R[F^2 > 2\sigma(F^2)]$	0.027
$wR(F^2)$	0.064
S	1.03
Largest difference peak and hole (eÅ^{-3})	0.32 and −0.27

Table 18. Crystal data and structure refinement for $C_{24}H_{22}O_2Se_2Fe_3$ (5)

Complex	$C_{24}H_{22}O_2Se_2Fe_3$ (**5**)
Empirical formula	$C_{24}H_{22}Fe_3O_2Se_2$
Formula weight	667.88
Temperature (K)	295
Crystal system	Monoclinic
Space group	$P2_1/c$
Unit cell dimensions	
a (Å)	19.7379 (15)
b (Å)	9.1871 (7)
c (Å)	12.6814 (9)
β (°)	98.545 (7)
V (Å^3)	2274.0 (3)
Z	4
Density (mg m^{-3})	1.951
Absorption coefficient, μ (mm^{-1})	5.11
F(000)	1312
Crystal size	0.2 × 0.1 × 0.05
Reflection collected	5222
Independent reflections (R_{int})	5222 (NA)
Data/restraints/parameters	5222/474/281
$R[F^2 > 2\sigma(F^2)]$	0.032
$wR(F^2)$	0.065
S	0.90
Largest difference peak and hole (eÅ^{-3})	0.75 and −0.38

4.6 CO releasing tests with a myoglobin assay

The CO-releasing tests of metal carbonyl complexes were investigated spectrophotometrically by measuring the conversion of deoxy-myoglobin to carbonmonoxy myoglobin (Mb-CO). The absorbance at 540 nm was observed and measured to quantify the amount of Mb-CO formed. A stock solution of myoglobin was freshly prepared by dissolving the protein in phosphate buffer saline (PBS) (0.01 M, pH 7.4). The myoglobin stock was degassed by bubbling with argon and reduced to deoxy-Mb by addition of sodium dithionite (0.1%). A deoxy-Mb spectrum was obtained by measuring a 2 mL quantity of deoxy-Mb solution, then bubbled with CO gas to get a Mb-CO curve. Metal carbonyl complexes were dissolved in relevant solvent (THF) in the dark and transferred into deoxy-Mb in the cuvette to achieve a final complex concentration of 20,40 and 60 μM, mixed using a pipette and the top of the mixed solution was layered with light mineral oil to prevent CO from escaping or the myoglobin being oxygenated. Illuminations were carried out by using a UV/Vis hand lamp at 365 nm. The maximal absorption peak of deoxy-Mb at 560 nm was converted to two maximal absorption peaks of Mb-CO at 540 and 578nm. This is the standard procedure; other experiments have been modified by using the different concentrations of myoglobin and different concentrations of the relevant solvent. The half-lives of CO release of the metal carbonyl complexes were determined according to the previous literature technique (Atkin et al., 2011) and the absorbance peak at 540nm was used. All CO release tests were repeated in triplicate.

4.7 Biological assays

4.7.1 Study of antimalarial activities on Plasmodium falciparum culture

P. falciparum 3D7 strains were used in this experiment. The positive control (fifty µL of seven 5-fold serial dilutions of chloroquine) and the compounds in RPMI 1640 complete culture medium, together with a maximum test concentration of 1 µM for chloroquine and 25 µM for the rest of the metal carbonyl complexes were dispensed into 96-well plates. After that, 150 mL of blood media parasite mixture (BMPM) was added into the well plates to give a final volume of 200 µL with final hematocrit of 0.5% and 2% ring stage parasite (Fatih et al., 2013). Drug plates containing the BMPM were then incubated by using a gas chamber containing 5% of CO_2, 5% of O_2 and 90% of N_2 at 37.5-38.0˚C. Incubation of drug plates for 36-42 hours was done to assure at least 50% of the ring stage parasites had matured to schizonts. Each drug concentrations and drug free control was done in duplicate. When the incubation was completed, the plates were adjusted to stand at an approximate angle of 45˚ for about 30 minutes to enable the supernatant to separate from the erythrocytes mixture. Thick blood smears resulting from each concentration from the erythrocytes in the remaining fluid were then dried thoroughly. They were then stained with 10% Giemsa stain at room temperature (Kosaisavee et al., 2006). Microscopic evaluations were done by observing and counting the number of schizonts with five or more nuclei out of a total 200 asexual parasites in each thick film. Only schizonts with at least five regular chromatin dots were included in the count. Degenerated schizonts, free merozoites and gametocytes were not counted to ensure optimal maturity (Russell et al., 2008). The schizont count is well-demonstrated as a proportion relative to the drug free control. Mean (±SD) from two different experiments performed in duplicates each were calculated and the IC_{50} values were obtained with the help of GraphPad Prism 7 software (Graphpad software Inc., CA, USA).

4.7.2 Study of cytotoxicity by MTT assay

All the breast adenocarcinoma cell lines (MDA-MB-231, MDA-MB-468 and MCF-7) were purchased from the American Type Culture Collection (ATCC, USA). MDA-MB-231, MDA-MB-468 and MCF-7 cells were grown in DMEM supplemented with 10% (v/v) fetal bovine serum (Gibco). They were seeded in 96 well plates at a density of 1 x 10^4 cells per well for MDA-MB-231 and MCF-7 cells, 1 x 10^5 cells per well for MDA-MB-468 cells. After 24 hours of incubation, the medium in the 96 well plates were removed.

Cisplatin was used as the positive control. Each cell lines were treated with drugs at various concentrations and incubated for 48 hours at 37℃ and 5% CO_2. This assay was terminated after 48 hours by adding 20 µl of MTT solution to each of the wells. The plates were incubated for another 4 hours before the removing of supernatant which was followed by the addition of 80 µl of DMSO to dissolve the formazan crystal. The absorbance of each well was measured at 570 nm (reference at 630 nm) by using SpectraMax M3. GraphPad Prism 7 software (Graphpad software Inc., CA, USA) was used to identify the IC_{50} values by plotting the percentage of cell viability against the concentration of treatment on a logarithmic scale.

4.8 ADME Properties

The prediction of ADME properties of all the synthesized complexes were done by using the free Swiss ADME website (http://www.swissadme.ch/). The predicted data and results be obtained by drawing and inputting the structures of the complexes.

CHAPTER 5: CONCLUSION

The reactivity study of $[CpFe(CO)_2]_2$ (**1**) towards dichalcogenide ligands of dicyclohexyl disulfide, 2-thienyl disulfide and dibenzyl diselenide had been successfully studied in this research. Metal carbonyl complex $[CpFe(CO)(C_6H_{11}S)]_2$ (**2**), $[CpFe(CO)(C_4H_3S_2)]_2$ (**3**), $[CpFe(CO)(C_6H_5CH_2Se)]_2$ (**4**) and $[(CpFe)_3(\mu\text{-}CO)_2(\mu_3\text{-}Se)(C_6H_5CH_2Se)]$ (**5**) had been successfully isolated out and characterized.

Since **2**-**4** could only emit CO under the UV irradiation, they were classified as photoCORMs. In terms of the CO-releasing, **3** presented a shorter half-life as compared to **2** and **4**. All the photoCORMs in this research were able to emit CO in a slower and controllable way with the utilization of UV at 365nm. For the anticancer study, the performance of **3** that exhibited the shortest half-life only showed its improvement of cytotoxicity towards the MDA-MB-468 cell line was in the presence of UV irradiation. The cytotoxicity of **2** towards the MDA-MB-231 and MDA-MB-468 cell lines were also increased with UV-irradiation but has a lower value of IC_{50} as compared to cisplatin. Notwithstanding the fact that, **2**-**4** did not work as a potent antimalarial agent, however, this has inspired and motivated us to further investigate their analogues in other pharmacological activities.

This work can be further proceeded in mice to investigate the safety and efficiency of the **2**-**4** in the future. Besides, **2**-**4** can be further react with the other more water-soluble ligand such as 1,3,5-triaza-7-phosphoadamantane to increase their water solubility in the future.

REFERENCES

Agonigi, G., Batchelor, L. K., Ferretti, E., Schoch, S., Bortoluzzi, M., Braccini, S., . . . Marchetti, F. (2020). Mono-, di- and tetra-iron complexes with selenium or sulphur functionalized vinyliminium ligands: Synthesis, structural characterization and antiproliferative activity. *Molecules, 25*(7).

Ahmad, M., Bruce, R., & Knox, G. R. (1966). Hydrocarbon metal sulphide complexes: I. Cyclopentadienylcarbonyliron mercaptides. *Journal of Organometallic Chemistry, 6*(1), 1-10.

Ahmad, S., Hewett, P. W., Fujisawa, T., Sissaoui, S., Cai, M., Gueron, G., . . . Ahmed, A. (2015). Carbon monoxide inhibits sprouting angiogenesis and vascular endothelial growth factor receptor-2 phosphorylation. *Thromb Haemost, 114*(02), 329-337.

Aime, S., Cordero, L., Gobetto, R., & Szalontai, G. (1993). 1H and 13C NMR study of cyclopentadienyl metal carbonyls in the solid state. *Spectrochimica Acta Part A: Molecular Spectroscopy, 49*(9), 1307-1314.

Al-Omar, M. A. (2010). Synthesis and antimicrobial activity of new 5-(2-thienyl)-1,2,4-triazoles and 5-(2-thienyl)-1,3,4-oxadiazoles and related derivatives. *Molecules, 15*(1).

Álvarez-Pérez, M., Ali, W., Marć, M. A., Handzlik, J., & Domínguez-Álvarez, E. (2018). Selenides and diselenides: A review of their anticancer and chemopreventive activity. *Molecules, 23*(3).

Amewu, R. K., Chadwick, J., Hussain, A., Panda, S., Rinki, R., Janneh, O., . . . O'Neill, P. M. (2013). Synthesis and evaluation of the antimalarial, anticancer, and caspase 3 activities of tetraoxane dimers. *Bioorganic & Medicinal Chemistry, 21*(23), 7392-7397.

Arancibia, R., Dubar, F., Pradines, B., Forfar, I., Dive, D., Klahn, A. H., & Biot, C. (2010). Synthesis and antimalarial activities of rhenium bioorganometallics based on the

4-aminoquinoline structure. *Bioorganic & Medicinal Chemistry, 18*(22), 8085-8091.

Arnott, J. A., & Planey, S. L. (2012). The influence of lipophilicity in drug discovery and design. *Expert Opinion on Drug Discovery, 7*(10), 863-875.

Atkin, A. J., Lynam, J. M., Moulton, B. E., Sawle, P., Motterlini, R., Boyle, N. M., . . . Fairlamb, I. J. S. (2011). Modification of the deoxy-myoglobin/carbonmonoxy-myoglobin UV-vis assay for reliable determination of CO-release rates from organometallic carbonyl complexes. *Dalton Transactions, 40*(21), 5755-5761.

Avanzino, S. C., & Jolly, W. L. (1976). A study of bridging and terminal carbonyl groups in transition metal complexes by x-ray photoelectron spectroscopy. *Journal of the American Chemical Society, 98*(21), 6505-6507.

Beard, J. L. (2001). Iron biology in immune function, muscle metabolism and neuronal functioning. *The Journal of Nutrition, 131*(2), 568S-580S.

Beeson, J. G., Boeuf, P., & Fowkes, F. J. (2015). Maximizing antimalarial efficacy and the importance of dosing strategies. *BMC Medicine, 13*, Article#110.

Biot, C., Castro, W., Botte, C. Y., & Navarro, M. (2012). The therapeutic potential of metal-based antimalarial agents: Implications for the mechanism of action. *Dalton Trans, 41*(21), 6335-6349.

Bitterwolf, T. E., Scallorn, W. B., & Li, B. (2000). Mechanisms of cis/trans isomerization of (η5-C5H5)2Fe2(CO)2(μ-SR)2, Where R = methyl or tert-butyl, under photochemical and thermal conditions. *Organometallics, 19*(17), 3280-3287.

Blendon, R. J., Scoles, K., DesRoches, C., Young, J. T., Herrmann, M. J., Schmidt, J. L., & Kim, M. (2001). Americans' health priorities: Curing cancer and controlling costs. *Health Affairs, 20*(6), 222-232.

Blumenthal, I. (2001). Carbon monoxide poisoning. *Journal of the Royal Society of Medicine, 94*(6), 270-272.

Bohlender, C., Wolfram, M., Goerls, H., Imhof, W., Menzel, R., Baumgaertel, A., . . . Schiller, A. (2012). Light-triggered NO release from a nanofibrous non-woven. *Journal of Materials Chemistry, 22*(18), 8785-8792.

Buckingham, A. D., Schaefer, T., & Schneider, W. G. (1960). Solvent effects in nuclear magnetic resonance spectra. *The Journal of Chemical Physics, 32*(4), 1227-1233.

Burger, R. M. (1998). Cleavage of nucleic acids by bleomycin. *Chemical Reviews, 98*(3), 1153-1170.

Buss, J. L., Greene, B. T., Turner, J., Torti, F. M., & Torti, S. V. (2004). Iron chelators in cancer chemotherapy. *Current Topics in Medicinal Chemistry, 4*(15), 1623-1635.

Caraballo, H., & King, K. (2014). Emergency department management of mosquito-borne illness: Malaria, dengue, and West Nile virus. *Emergency Medicine Practice, 16*(5), 1-23; quiz 23-24.

Carrington, S. J., Chakraborty, I., & Mascharak, P. K. (2013). Rapid CO release from a Mn(i) carbonyl complex derived from azopyridine upon exposure to visible light and its phototoxicity toward malignant cells. *Chemical Communications, 49*(96), 11254-11256.

Chakraborty, I., Carrington, S. J., Hauser, J., Oliver, S. R. J., & Mascharak, P. K. (2015). Rapid eradication of human breast cancer cells through trackable light-triggered CO delivery by mesoporous silica nanoparticles packed with a designed photoCORM. *Chemistry of Materials, 27*(24), 8387-8397.

Chatterjee, P. K. (2007). Physiological activities of carbon monoxide-releasing molecules: Ca ira. *British journal of pharmacology, 150*(8), 961-962.

Chaves-Ferreira, M., Albuquerque, I. S., Matak-Vinkovic, D., Coelho, A. C., Carvalho, S. M., Saraiva, L. M., . . . Bernardes, G. J. L. (2015). Spontaneous CO release from Ru(II)(CO)2-protein complexes in aqueous solution, cells, and mice. *Angewandte Chemie International Edition, 54*(4), 1172-1175.

Chen, L., Jiang, X., Wang, X., Long, L., Zhang, J., & Liu, X. (2014). A kinetic analysis of CO release from a diiron hexacarbonyl complex promoted by amino acids. *New Journal of Chemistry, 38*(12), 5957-5963.

Cheng, F., Li, W., Zhou, Y., Shen, J., Wu, Z., Liu, G., . . . Tang, Y. (2012). admetSAR: A comprehensive source and free tool for assessment of chemical ADMET properties. *Journal of Chemical Information and Modeling, 52*(11), 3099-3105.

Christophe, B. (2004). Ferroquine: A new weapon in the fight against malaria. *Current Medicinal Chemistry - Anti-Infective Agents, 3*(2), 135-147.

Chu, J. Y. C., & Lewicki, J. W. (1977). Thermal decomposition of bis(diphenylmethyl) diselenide. *The Journal of Organic Chemistry, 42*(14), 2491-2493.

Claussen, C. A., & Long, E. C. (1999). Nucleic acid recognition by metal complexes of bleomycin. *Chemical Reviews, 99*(9), 2797-2816.

Cotton, F. A., & Wilkinson, G. (1954). On the question of octahedral binding in bis-cyclopentadienyl compounds. *Zeitschrift für Naturforschung B, 9*(7), 453-456.

Crespo-Ortiz, M. P., & Wei, M. Q. (2012). Antitumor activity of artemisinin and its derivatives: From a well-known antimalarial agent to a potential anticancer drug. *Journal of Biomedicine and Biotechnology, 2012*, Article#247597.

Cronin, D. L., Wilkinson, J. R., & Todd, L. J. (1975). A 13C NMR study of isonitrile transition metal complexes. *Journal of Magnetic Resonance (1969), 17*(3), 353-361.

Crook, S. H., Mann, B. E., Meijer, A. J. H. M., Adams, H., Sawle, P., Scapens, D., & Motterlini, R. (2011). [Mn(CO)4{S2CNMe(CH2CO2H)}], a new water-soluble CO-releasing molecule. *Dalton Transactions, 40*(16), 4230-4235.

Dahlin, J. L., Inglese, J., & Walters, M. A. (2015). Mitigating risk in academic preclinical drug discovery. *Nature Reviews Drug Discovery, 14*(4), 279-294.

Daina, A., Michielin, O., & Zoete, V. (2014). iLOGP: A simple, robust, and efficient description of n-octanol/water partition coefficient for drug design using the GB/SA approach. *Journal of Chemical Information and Modeling, 54*(12), 3284-3301.

Daina, A., Michielin, O., & Zoete, V. (2017). SwissADME: A free web tool to evaluate pharmacokinetics, drug-likeness and medicinal chemistry friendliness of small molecules. *Scientific Reports, 7*(1), Article#42717.

Daina, A., & Zoete, V. (2016). A BOILED-Egg to predict gastrointestinal absorption and brain penetration of small molecules. *ChemMedChem, 11*(11), 1117-1121.

Davis, R. A., Carroll, A. R., & Quinn, R. J. (2003). The synthesis of two combinatorial libraries using a 4-(2-thienyl)-pyrrole template. *Australian Journal of Chemistry, 55*(12), 789-794.

Dolomanov, O. V., Bourhis, L. J., Gildea, R. J., Howard, J. A. K., & Puschmann, H. (2009). OLEX2: A complete structure solution, refinement and analysis program. *Journal of Applied Crystallography, 42*(2), 339-341.

Dördelmann, G., Pfeiffer, H., Birkner, A., & Schatzschneider, U. (2011). Silicium dioxide nanoparticles as carriers for photoactivatable CO-releasing molecules (PhotoCORMs). *Inorganic chemistry, 50*(10), 4362-4367.

Eastman, R. T., & Fidock, D. A. (2009). Artemisinin-based combination therapies: a vital tool in efforts to eliminate malaria. *Nature Reviews Microbiology, 7*(12), 864-874.

Farrugia, L. (2012). WinGX and ORTEP for Windows: An update. *Journal of Applied Crystallography, 45*(4), 849-854.

Fatih, F. A., Staines, H. M., Siner, A., Ahmed, M. A., Woon, L. C., Pasini, E. M., . . . Krishna, S. (2013). Susceptibility of human Plasmodium knowlesi infections to anti-malarials. *Malaria Journal, 12*(1), Article#425.

Ferguson, G., Hannaway, C., & Islam, K. M. S. (1968). The crystal structure of di-μ-phenylthio-bis(cyclopentadienyl-carbonyliron) at –160°. *Chemical Communications (London)*(19), 1165-1166.

Fernandes, A. P., & Gandin, V. (2015). Selenium compounds as therapeutic agents in cancer. *Biochimica et Biophysica Acta (BBA) - General Subjects, 1850*(8), 1642-1660.

Florindo, P. R., Pereira, D. M., Borralho, P. M., Rodrigues, C. M. P., Piedade, M. F. M., & Fernandes, A. C. (2015). Cyclopentadienyl–Ruthenium(II) and iron(II) organometallic compounds with carbohydrate derivative ligands as good colorectal anticancer agents. *Journal of Medicinal Chemistry, 58*(10), 4339-4347.

Franchini, M., & Veneri, D. (2004). Iron overload and hematologic malignancies. *Journal of Hematology, 5*(5), 381-383.

Franke, J. C., Plötz, M., Prokop, A., Geilen, C. C., Schmalz, H.-G., & Eberle, J. (2010). New caspase-independent but ROS-dependent apoptosis pathways are targeted in melanoma cells by an iron-containing cytosine analogue. *Biochemical Pharmacology, 79*(4), 575-586.

Galanski, M., Jakupec, M. A., & Keppler, B. K. (2005). Update of the preclinical situation of anticancer platinum complexes: Novel design strategies and innovative analytical approaches. *Current Medicinal Chemistry, 12*(18), 2075-2094.

Gandin, V., & Fernandes, A. P. (2018). Chapter 15 organoselenium compounds as cancer therapeutic agents. In *organoselenium compounds in biology and medicine:*

Synthesis, biological and therapeutic treatments (pp. 401-435): The Royal Society of Chemistry.

Gandin, V., Khalkar, P., Braude, J., & Fernandes, A. P. (2018). Organic selenium compounds as potential chemotherapeutic agents for improved cancer treatment. *Free Radical Biology and Medicine, 127*, 80-97.

Gao, C., Liang, X., Guo, Z., Jiang, B.-P., Liu, X., & Shen, X.-C. (2018). Diiron hexacarbonyl complex induces site-specific release of carbon monoxide in cancer cells triggered by endogenous glutathione. *ACS Omega, 3*(3), 2683-2689.

García-Gallego, S., & Bernardes, G. J. L. (2014). Carbon-Monoxide-Releasing molecules for the delivery of therapeutic CO in vivo. *Angewandte Chemie International Edition, 53*(37), 9712-9721.

Gasser, G., & Metzler-Nolte, N. (2012). The potential of organometallic complexes in medicinal chemistry. *Current Opinion in Chemical Biology, 16*(1), 84-91.

Geetharani, K., Bose, S. K., Basak, D., Suresh, V. M., & Ghosh, S. (2011). A new entry into ferraborane chemistry: Synthesis and characterization of heteroferraborane complexes. *Inorganica Chimica Acta, 372*(1), 42-46.

Gfeller, D., Grosdidier, A., Wirth, M., Daina, A., Michielin, O., & Zoete, V. (2014). Swiss Target Prediction: A web server for target prediction of bioactive small molecules. *Nucleic Acids Research, 42*(W1), W32-W38.

Glans, L., Taylor, D., de Kock, C., Smith, P. J., Haukka, M., Moss, J. R., & Nordlander, E. (2011). Synthesis, characterization and antimalarial activity of new chromium arene–quinoline half sandwich complexes. *Journal of Inorganic Biochemistry, 105*(7), 985-990.

Grosdidier, A., Zoete, V., & Michielin, O. (2011). SwissDock, a protein-small molecule docking web service based on EADock DSS. *Nucleic Acids Research, 39*(suppl_2), W270-W277.

Haines, R. J., De Beer, J. A., & Greatrex, R. (1973). Trinuclear π-cyclopentadienyl bridging sulphido derivatives of iron. *Journal of Organometallic Chemistry, 55*(1), C30-C32.

Haines, R. J., De Beer, J. A., & Greatrex, R. (1975). Reactions of metal carbonyl derivatives: XVII. Tri- as well as di-nuclear products from the reactions of bis(dicarbonyl-η-cyclopentadienyliron) with various dialkyl disulphides11A preliminary communication of some of this work has appeared [2]. *Journal of Organometallic Chemistry, 85*(1), 89-99.

Hallam, B. F., Mills, O. S., & Pauson, P. L. (1955). Dicyclopentadienyldiirontetracarbonyl. *Journal of Inorganic and Nuclear Chemistry, 1*(4), 313-316.

Hallam, B. F., & Pauson, P. L. (1956). 588. Ferrocene derivatives. Part III. Cyclopentadienyliron carbonyls. *Journal of the Chemical Society (Resumed)*(0), 3030-3037.

Harris, D. C., Rosenberg, E., & Roberts, J. D. (1974). Carbon-13 nuclear magnetic resonance spectra and mechanism of bridge–terminal carbonyl exchange in di-μ-carbonyl-bis[carbonyl(η-cyclopentadienyl)iron](Fe–Fe)[{(η-C5H5)Fe(CO)2}2]; cd-di-μ-carbonyl-f-carbonyl-ae-di(η-cyclopentadienyl)-b-(triethyl -phosphite)di-iron(Fe–Fe)[(η-C5H5)2Fe2(CO)3P(OEt)3], and some related complexes. *Journal of the Chemical Society, Dalton Transactions*(22), 2398-2403.

Hasanzadeh, N., Ghammamy, S., & Mohammadi, M. K. (2010). Microwave assisted oxidative coupling of thiols to symmetrical disulfides with tripropylammonium fluorochromate(VI) (TPAFC). *Journal of the Iranian Chemical Research, 3*(3), 155-160.

Hay, M., Thomas, D. W., Craighead, J. L., Economides, C., & Rosenthal, J. (2014). Clinical development success rates for investigational drugs. *Nature Biotechnology, 32*(1), 40-51.

Hewison, L., Crook, S. H., Mann, B. E., Meijer, A. J. H. M., Adams, H., Sawle, P., & Motterlini, R. A. (2012). New types of CO-Releasing molecules (CO-RMs), based

on iron dithiocarbamate complexes and [Fe(CO)3I(S2COEt)]. *Organometallics, 31*(16), 5823-5834.

Hickey, J. P., Wilkinson, J. R., & Todd, L. J. (1979). Oxygen-17 nuclear magnetic resonancé spectra of transition metal carbonyl compounds. *Journal of Organometallic Chemistry, 179*(2), 159-168.

Hoehn, S. T., Junker, H.-D., Bunt, R. C., Turner, C. J., & Stubbe, J. (2001). Solution structure of Co(III)-Bleomycin-OOH bound to a phosphoglycolate lesion containing oligonucleotide: Implications for bleomycin-induced double-strand DNA cleavage. *Biochemistry, 40*(20), 5894-5905.

Johnson, T. R., Mann, B. E., Teasdale, I. P., Adams, H., Foresti, R., Green, C. J., & Motterlini, R. (2007). Metal carbonyls as pharmaceuticals? [Ru(CO)3Cl(glycinate)], a CO-releasing molecule with an extensive aqueous solution chemistry. *Dalton Transactions*(15), 1500-1508.

Kalinowski, D. S., Yu, Sharpe, P. C., Islam, M., Liao, Y.-T., Lovejoy, D. B., . . . Richardson, D. R. (2007). Design, synthesis, and characterization of novel iron chelators: Structure−Activity relationships of the 2-benzoylpyridine thiosemicarbazone series and their 3-nitrobenzoyl analogues as potent antitumor agents. *Journal of Medicinal Chemistry, 50*(15), 3716-3729.

Kalotka-Kręglewska, H. (2011). Review paper antimalarial medications from native remedy. *Central European Journal of Immunology, 36*(2), 100-103.

Kanemoto, K., Sugimura, Y., Shimizu, S., Yoshida, S., & Hosoya, T. (2017). Rhodium-catalyzed odorless synthesis of diaryl sulfides from borylarenes and S-aryl thiosulfonates. *Chemical Communications, 53*(77), 10640-10643.

Kicic, A., Chua, A. C., & Baker, E. (2001). The desferrithiocin (DFT) class of iron chelators: Potential as antineoplastic agents. *Anticancer Drug Des, 16*(4-5), 195-207.

King, R. B., Stone, F. G. A., Jolly, W. L., Austin, G., Covey, W., Rabinovich, D., . . . Tsugawa, R. (1963). *Cyclopentadienyl metal carbonyls and some derivatives* (Vol. 7): Inorganic Syntheses Organization, John Wiley & Sons.

King, R. B., Treichel, P. M., & Stone, F. G. A. (1961). Chemistry of the metal carbonyls. XIV. New organosulfur derivatives of iron and cobalt1,2. *Journal of the American Chemical Society, 83*(17), 3600-3604.

Klein, M., Neugebauer, U., Gheisari, A., Malassa, A., Jazzazi, T. M. A., Froehlich, F., . . . Popp, J. (2014). IR spectroscopic methods for the investigation of the CO release from CORMs. *The Journal of Physical Chemistry A, 118*(29), 5381-5390.

Kopf-Maier, P., Kopf, H., & Neuse, E. W. (1984). Ferricenium complexes: A new type of water-soluble antitumor agent. *Journal of Cancer Research and Clinical Oncology, 108*(3), 336-340.

Korepanov, V. I., Popov, A. A., Senyavin, V. M., Yurovskaya, M. A., & Chernyshova, E. S. (2007). Infrared spectrum and structure of 2-thienyl-N-methylfulleropyrrolidine. *Moscow University Chemistry Bulletin, 62*(2), 72-78.

Kosaisavee, V., Suwanarusk, R., Nosten, F., Kyle, D. E., Barrends, M., Jones, J., . . . Lek-Uthai, U. (2006). Plasmodium vivax: Isotopic, PicoGreen, and microscopic assays for measuring chloroquine sensitivity in fresh and cryopreserved isolates. *Experimental Parasitology, 114*(1), 34-39.

Lin, P. S., Kwock, L., Hefter, K., & Misslbeck, G. (1983). Effects of iron, copper, cobalt, and their chelators on the cytotoxicity of bleomycin. *Cancer Research, 43*(3), 1049-1053.

Ling, K., Men, F., Wang, W.-C., Zhou, Y.-Q., Zhang, H.-W., & Ye, D.-W. (2018). Carbon monoxide and its controlled release: Therapeutic application, detection, and development of carbon monoxide releasing molecules (CORMs). *Journal of Medicinal Chemistry, 61*(7), 2611-2635.

Liu, H., Gong, Y., Zhang, T., Li, N., Zhao, Q., Chen, Y., . . . Zheng, Y. (2015). Syntheses, cytotoxicity and properties of CO releasing molecules containing acetyl salicylamide-3-pyridine. *Chinese Journal of Chemistry, 33*(7), 739-748.

Loboda, A., Jozkowicz, A., & Dulak, J. (2015a). Carbon monoxide: Pro- or anti-angiogenic agent? Comment on Ahmad et al. (Thromb Haemost 2015; 113: 329–337). *Thromb Haemost, 114*(08), 432-433.

Loboda, A., Jozkowicz, A., & Dulak, J. (2015b). HO-1/CO system in tumor growth, angiogenesis and metabolism — Targeting HO-1 as an anti-tumor therapy. *Vascular Pharmacology, 74*, 11-22.

Long, L., Jiang, X., Wang, X., Xiao, Z., & Liu, X. (2013). Water-soluble diiron hexacarbonyl complex as a CO-RM: Controllable CO-releasing, releasing mechanism and biocompatibility. *Dalton Transactions, 42*(44), 15663-15669.

Marques, A. R., Kromer, L., Gallo, D. J., Penacho, N., Rodrigues, S. S., Seixas, J. D., . . . Romão, C. C. (2012). Generation of carbon monoxide releasing molecules (CO-RMs) as drug candidates for the treatment of acute liver injury: Targeting of CO-RMs to the liver. *Organometallics, 31*(16), 5810-5822.

Mayer, R. (1977). Elemental sulfur and its reactions. In S. Oae (Ed.), *Organic Chemistry of Sulfur* (pp. 33-69). Boston, MA: Springer US.

McLean, S., Mann, B. E., & Poole, R. K. (2012). Sulfite species enhance carbon monoxide release from CO-releasing molecules: Implications for the deoxymyoglobin assay of activity. *Analytical Biochemistry, 427*(1), 36-40.

Mills, O. S. (1958). Studies of some carbon compounds of the transition metals. I. The crystal structure of dicyclopentadienyldiiron tetracarbonyl. *Acta Crystallographica, 11*(9), 620-623.

Mir, L. M., Tounekti, O., & Orlowski, S. (1996). Bleomycin: Revival of an old drug. *Gen Pharmacol, 27*(5), 745-748.

Motterlini, R., Clark James, E., Foresti, R., Sarathchandra, P., Mann Brian, E., & Green Colin, J. (2002). Carbon monoxide releasing molecules. *Circulation Research, 90*(2), e17-e24.

Motterlini, R., & Otterbein, L. E. (2010). The therapeutic potential of carbon monoxide. *Nature Reviews Drug Discovery, 9*(9), 728-743.

Motterlini, R., Sawle, P., Bains, S., Hammad, J., Alberto, R., Foresti, R., & Green, C. J. (2005). CORM-A1: A new pharmacologically active carbon monoxide-releasing molecule. *The FASEB Journal, 19*(2), 1-24.

Neill, U. S. (2011). From branch to bedside: Youyou Tu is awarded the 2011 Lasker~DeBakey Clinical Medical Research Award for discovering artemisinin as a treatment for malaria. *Journal of Clinical Investigation, 121*(10), 3768-3773.

Noedl, H., Se, Y., Schaecher, K., Smith, B. L., Socheat, D., & Fukuda, M. M. (2008). Evidence of artemisinin-resistant malaria in western Cambodia. *The New England Journal of Medicine, 359*(24), 2619-2620.

Nzila, A., Okombo, J., Becker, R. P., Chilengi, R., Lang, T., & Niehues, T. (2010). Anticancer agents against malaria: Time to revisit? *Trends in parasitology, 26*(3), 125-129.

Ooi, M. L., Lim, C. E., Wong, R. C. S., & Ng, S. W. (2017). Isolation and characterization of thiolato complexes of [CpCr(SBz)]2S, isomeric trans [CpMo(CO)(SBz)]2 and [CpMo(SBz)2]2 (Cp=(η5-C5H5), Bz=PhCH2) from the reactivity of bibenzyl disulfide towards [CpM(CO)3]2 (M=Cr, Mo). *Inorganica Chimica Acta, 467*, 364-371.

Osborne, A. G., & Stone, F. G. A. (1966). Chemistry of the metal carbonyls. Part XXXVI. Carbonyl(organothio)-manganese and -rhenium complexes. *Journal of the Chemical Society A: Inorganic, Physical, Theoretical*(0), 1143-1146.

Ott, I., & Gust, R. (2006). Medizinische Chemie der platinkomplexe: Besonderheiten anorganischer zytostatika. *Pharmazie in unserer Zeit, 35*(2), 124-133.

Ott, I., & Gust, R. (2007). Non platinum metal complexes as anti-cancer drugs. *Archiv der Pharmazie, 340*(3), 117-126.

Pathania, S., Narang, R. K., & Rawal, R. K. (2019). Role of sulphur-heterocycles in medicinal chemistry: An update. *European Journal of Medicinal Chemistry, 180*, 486-508.

Pauling, L. (1976). Metal-Metal bond lengths in complexes of transition metals. *Proceedings of the National Academy of Sciences, 73*(12), 4290-4293.

Pena, A. C., Penacho, N., Mancio-Silva, L., Neres, R., Seixas, J. D., Fernandes, A. C., . . . Pamplona, A. (2012). A novel carbon monoxide-releasing molecule fully protects mice from severe malaria. *Antimicrob Agents Chemother, 56*(3), 1281-1290.

Pierrot, C., Lafitte, S., Dive, D., Fraisse, L., Brocard, J., & Khalife, J. (2005). Analysis of immune response patterns in naïve and plasmodium berghei-infected young rats following a ferroquine treatment. *International Journal for Parasitology, 35*(14), 1601-1610.

Pilon, A., Gírio, P., Nogueira, G., Avecilla, F., Adams, H., Lorenzo, J., . . . Valente, A. (2017). New iron cyclopentadienyl complexes bearing different phosphane co-ligands: Structural factors vs. cytotoxicity. *Journal of Organometallic Chemistry, 852*, 34-42.

Piper, T. S., Cotton, F. A., & Wilkinson, G. (1955). Cyclopentadienyl-carbon monoxide and related compounds of some transitional metals. *Journal of Inorganic and Nuclear Chemistry, 1*(3), 165-174.

Pires, D. E. V., Blundell, T. L., & Ascher, D. B. (2015). pkCSM: Predicting small-molecule pharmacokinetic and toxicity properties using graph-based signatures. *Journal of Medicinal Chemistry, 58*(9), 4066-4072.

Poh, H. T., Ho, P. C., & Fan, W. Y. (2016). Cyclopentadienyl iron dicarbonyl (CpFe(CO)2) derivatives as apoptosis-inducing agents. *RSC Advances, 6*(23), 18814-18823.

Poinar, G. (2005). Plasmodium dominicana n. sp. (Plasmodiidae: Haemospororida) from tertiary dominican amber. *Systematic Parasitology, 61*(1), 47-52.

Posner, G. H., McRiner, A. J., Paik, I.-H., Sur, S., Borstnik, K., Xie, S., . . . Foster, B. (2004). Anticancer and antimalarial efficacy and safety of artemisinin derived trioxane dimers in rodents. *Journal of Medicinal Chemistry, 47*(5), 1299-1301.

Rajappa, S. (1984). 3.14 - Thiophenes and their benzo derivatives: (ii) Reactivity. In A. R. Katritzky & C. W. Rees (Eds.), *Comprehensive heterocyclic chemistry* (pp. 741-861). Oxford: Pergamon.

Rausch, M. D. (1961). Ferrocene and related organometallic π-complexes. IV. Some ullmann reactions of haloferrocenes1. *The Journal of Organic Chemistry, 26*(6), 1802-1805.

Richardson, D. R. (2005). Molecular mechanisms of iron uptake by cells and the use of iron chelators for the treatment of cancer. *Current Medicinal Chemistry, 12*(23), 2711-2729.

Rimmer, R. D., Richter, H., & Ford, P. C. (2010). A photochemical precursor for carbon monoxide release in aerated aqueous media. *Inorganic chemistry, 49*(3), 1180-1185.

Roberto, M., Brian, E. M., Tony, R. J., James, E. C., Roberta, F., & Colin, J. G. (2003). Bioactivity and pharmacological actions of carbon monoxide-releasing molecules. *Current Pharmaceutical Design, 9*(30), 2525-2539.

Rocco, D., Batchelor, L. K., Agonigi, G., Braccini, S., Chiellini, F., Schoch, S., . . . Marchetti, F. (2019). Anticancer potential of diiron vinyliminium complexes. *Chemistry – A European Journal, 25*(65), 14801-14816.

Romanski, S., Kraus, B., Schatzschneider, U., Neudörfl, J.-M., Amslinger, S., & Schmalz, H.-G. (2011). Acyloxybutadiene iron tricarbonyl complexes as Enzyme-Triggered CO-Releasing molecules (ET-CORMs). *Angewandte Chemie International Edition, 50*(10), 2392-2396.

Romão, C. C., Blättler, W. A., Seixas, J. D., & Bernardes, G. J. L. (2012). Developing drug molecules for therapy with carbon monoxide. *Chemical Society Reviews, 41*(9), 3571-3583.

Romão, C. C., & Vieira, H. L. A. (2014). Metal carbonyl prodrugs: CO delivery and beyond. In *Bioorganometallic Chemistry* (pp. 165-202).

Rosenberg, B., Van Camp, L., & Krigas, T. (1965). Inhibition of cell division in escherichia coli by electrolysis products from a platinum electrode. *Nature, 205*(4972), 698-699.

Rosenberg, B., VanCamp, L., Trosko, J. E., & Mansour, V. H. (1969). Platinum compounds: A new class of potent antitumour agents. *Nature, 222*(5191), 385-386.

Rosenbuch, P., & Welcman, N. (1972). Organoselenium derivatives of metal carbonyls. Part II. Dimeric and monomeric derivatives of iron carbonyl. *Journal of the Chemical Society, Dalton Transactions*(18), 1963-1966.

Russell, B., Chalfein, F., Prasetyorini, B., Kenangalem, E., Piera, K., Suwanarusk, R., . . . Price, R. N. (2008). Determinants of in vitro drug susceptibility testing of plasmodium vivax. *Antimicrobial Agents and Chemotherapy, 52*(3), Article#1040.

Salla, C. A. M., Braga, H. C., Heying, R. d. S., Martins, J. S., Quirino, W. G., Legnani, C., . . . Bechtold, I. H. (2017). Photocurrent response enhanced by spin-orbit coupling on ruthenium(II) complexes with heavy atom ligands. *Dyes and Pigments, 140*, 346-353.

Schadewaldt, H. (1975). [Introduction of atebrine into materia medica]. *Dtsch Med Wochenschr, 100*(50), 2583-2585.

Schatzschneider, U. (2010). Photoactivated biological activity of transition metal complexes. *European Journal of Inorganic Chemistry, 2010*(10), 1451-1467.

Schatzschneider, U. (2011). PhotoCORMs: Light-triggered release of carbon monoxide from the coordination sphere of transition metal complexes for biological applications. *Inorganica Chimica Acta, 374*(1), 19-23.

Schermer, E. D., & Baddley, W. H. (1971). Tellurium and selenium derivatives of π-cyclopentadienyliron dicarbonyl. *Journal of Organometallic Chemistry, 27*(1), 83-88.

Schlawe, D., Majdalani, A., Velcicky, J., Hessler, E., Wieder, T., Prokop, A., & Schmalz, H. G. (2004). Iron-containing nucleoside analogues with pronounced apoptosis-inducing activity. *Angewandte Chemie International Edition, 43*(13), 1731-1734.

Siddik, Z. H. (2003). Cisplatin: Mode of cytotoxic action and molecular basis of resistance. *Oncogene, 22*(47), 7265-7279.

Siegel, R. L., Miller, K. D., & Jemal, A. (2020). Cancer statistics, 2020. *CA: A Cancer Journal for Clinicians, 70*(1), 7-30.

Silakari, O., & Singh, P. K. (2021). Chapter 14 - ADMET tools: Prediction and assessment of chemical ADMET properties of NCEs. In O. Silakari & P. K. Singh (Eds.), *Concepts and Experimental Protocols of Modelling and Informatics in Drug Design* (pp. 299-320): Academic Press.

Slater, A. F. G., & Cerami, A. (1992). Inhibition by chloroquine of a novel haem polymerase enzyme activity in malaria trophozoites. *Nature, 355*(6356), 167-169.

Spengler, G., Gajdács, M., Marć, M. A., Domínguez-Álvarez, E., & Sanmartín, C. (2019). Organoselenium compounds as novel adjuvants of chemotherapy drugs-A promising approach to fight cancer drug resistance. *Molecules, 24*(2).

Stubbe, J., & Kozarich, J. W. (1987). Mechanisms of bleomycin-induced DNA degradation. *Chemical Reviews, 87*(5), 1107-1136.

Stubbe, J., Kozarich, J. W., Wu, W., & Vanderwall, D. E. (1996). Bleomycins: A structural model for specificity, binding, and double strand cleavage. *Accounts of Chemical Research, 29*(7), 322-330.

Sullivan, D. J., Jr., Gluzman, I. Y., Russell, D. G., & Goldberg, D. E. (1996). On the molecular mechanism of chloroquine's antimalarial action. *Proceedings of the National Academy of Sciences, 93*(21), 11865-11870.

Tan, H. W., Mo, H.-Y., Lau, A. T. Y., & Xu, Y.-M. (2018). Selenium species: Current status and potentials in cancer prevention and therapy. *International journal of molecular sciences, 20*(1), 75.

Trachootham, D., Alexandre, J., & Huang, P. (2009). Targeting cancer cells by ROS-mediated mechanisms: A radical therapeutic approach? *Nature Reviews Drug Discovery, 8*(7), 579-591.

Umezawa, H., Maeda, K., Takeuchi, T., & Okami, Y. (1966). New antibiotics, bleomycin A and B. *The Journal of Antibiotics, 19*(5), 200-209.

Urban, B. C., Ing, R., & Stevenson, M. M. (2005). Early interactions between blood-stage plasmodium parasites and the immune system. *Current Topics in Microbiology and Immunology, 297*, 25-70.

Üstün, E., Özgür, A., Coşkun, K. A., Demir, S., Özdemir, İ., & Tutar, Y. (2016). CO-releasing properties and anticancer activities of manganese complexes with imidazole/benzimidazole ligands. *Journal of Coordination Chemistry, 69*(22), 3384-3394.

Valente, A., Santos, A. M., Côrte-Real, L., Robalo, M. P., Moreno, V., Font-Bardia, M., . . . Garcia, M. H. (2014). New iron(II) cyclopentadienyl derivative complexes: Synthesis and antitumor activity against human leukemia cancer cells. *Journal of Organometallic Chemistry, 756*, 52-60.

Vangapandu, S., Jain, M., Kaur, K., Patil, P., Patel, S. R., & Jain, R. (2007). Recent advances in antimalarial drug development. *Medicinal Research Reviews, 27*(1), 65-107.

Verbaanderd, C., Maes, H., Schaaf, M. B., Sukhatme, V. P., Pantziarka, P., Sukhatme, V., . . . Bouche, G. (2017). Repurposing drugs in oncology (ReDO)-chloroquine and hydroxychloroquine as anti-cancer agents. *Ecancermedicalscience, 11*, 781-781.

Verma, A., Hirsch, D. J., Glatt, C. E., Ronnett, G. V., & Snyder, S. H. (1993). Carbon monoxide: A putative neural messenger. *Science, 259*(5093), Article#381.

Volti, G. L., Sacerdoti, D., Sangras, B., Vanella, A., Mezentsev, A., Scapagnini, G., . . . Abraham, N. G. (2005). Carbon monoxide signaling in promoting angiogenesis in human microvessel endothelial cells. *Antioxidants & Redox Signaling, 7*(5-6), 704-710.

Wachter, J. (1989). Synthesis, structure and reactivity of sulfur-rich cyclopentadienyl-transition metal complexes: Sulfur chemistry from an organometallic point of view. *Angewandte Chemie International Edition in English, 28*(12), 1613-1626.

Wallace, D. J. (1989). The use of quinacrine (Atabrine) in rheumatic diseases: A reexamination. *Semin Arthritis Rheum, 18*(4), 282-296.

Wei, C., Goh, L. Y., & Sinn, E. (1988). Chemistry of [CpCr(CO)3]2. An insertion mechanism for the formation of Cp2Cr2(CO)5Se2 and Cp2Cr2(CO)4Se2 from Cp2Cr2(CO)4Se. Carbonylation and crystal structure of Cp2Cr2(CO)4Se2. *Organometallics, 7*(9), 2020-2026.

Weinberg, E. D. (1999). Development of clinical methods of iron deprivation for suppression of neoplastic and infectious diseases. *Cancer Investigation, 17*(7), 507-513.

Westrip, S. (2010). publCIF: Software for editing, validating and formatting crystallographic information files. *Journal of Applied Crystallography, 43*(4), 920-925.

Wilkie, C. A., & Huettl, B. (1989). The thermolysis of dicarbonylcyclopentadienyliron dimer: The formation of biferrocene. *Applied Organometallic Chemistry, 3*(2), 157-163.

Wirth, M., Zoete, V., Michielin, O., & Sauer, W. H. B. (2013). SwissBioisostere: A database of molecular replacements for ligand design. *Nucleic Acids Research, 41*(D1), D1137-D1143.

Woerdenbag, H. J., Moskal, T. A., Pras, N., Malingre, T. M., el-Feraly, F. S., Kampinga, H. H., & Konings, A. W. (1993). Cytotoxicity of artemisinin-related endoperoxides to Ehrlich ascites tumor cells. *Journal of Natural Products, 56*(6), 849-856.

Wong, R. C. S., Ooi, M. L., Chee, C. F., & Tan, G. H. (2005). A facile reaction of bibenzyl trisulfide with [(η5-C5H5)Cr(CO)3]2: formation of a thiolato-bridged dichromium complex of [CpCr(CO)2(SBz)]2 (Bz=PhCH2–). *Inorganica Chimica Acta, 358*(4), 1269-1273.

Yap, N. J., Goh, X. T., Koehler, A. V., William, T., Yeo, T. W., Vythilingam, I., . . . Lim, Y. A. L. (2017). Genetic diversity in the C-terminus of merozoite surface protein 1 among plasmodium knowlesi isolates from Selangor and Sabah Borneo, Malaysia. *Infection, Genetics and Evolution, 54*, 39-46.

Yi, L., & Su, Q. (2013). Molecular mechanisms for the anti-cancer effects of diallyl disulfide. *Food and Chemical Toxicology, 57*, 362-370.

Yip, C. H., Taib, N. A., & Mohamed, I. (2006). Epidemiology of breast cancer in Malaysia. *Asian Pacific Journal of Cancer Prevention, 7*(3), 369-374.

Zoete, V., Cuendet, M. A., Grosdidier, A., & Michielin, O. (2011). SwissParam: A fast force field generation tool for small organic molecules. *Journal of Computational Chemistry, 32*(11), 2359-2368.

Zoete, V., Daina, A., Bovigny, C., & Michielin, O. (2016). SwissSimilarity: A web tool for low to ultra high throughput ligand-based virtual screening. *Journal of Chemical Information and Modeling, 56*(8), 1399-1404.